**CALVAL-TP**
**CLS.DOS/NT/05.240**
**Version : 1rev1, January, 6th 2006**
**Nomenclature : SALP-RP-MA-EA-21315-CLS**

**Ramonville, January, 6th 2006**

# TOPEX/Poseidon validation activities

**13 years of T/P data (GDR-Ms)**

| | AUTHORS | COMPANY | DATE | INITIALS |
|---|---|---|---|---|
| WRITTEN BY | M.Ablain<br>S.Philipps | CLS<br>CLS | | |
| APPROVED BY | J.Dorandeu | CLS | | |
| QUALITY VISA | M.Destouesse | CLS | | |
| APPLICATION AUTHORISED BY | N.Picot | CNES | | |

CLS - 8-10 Rue Hermès - Parc Technologique du Canal - 31520 Ramonville St-Agne - FRANCE
Telephone 33 5 61 39 47 00 / Fax 33 5 61 75 10 14

## DISTRIBUTION LIST

| COMPANY | NAMES | COPIES |
|---|---|---|
| CLS/DOS | M.ABLAIN | 1 electonic copy |
| | J.DORANDEU | 1 electonic copy |
| | S.PHILIPPS | 1 electonic copy |
| | V.ROSMORDUC | 1 electonic copy |
| DOC/CLS | DOCUMENTATION | 1 electonic copy |
| CNES | N.PICOT | 1 copy + 1 electonic copy |
| CNES | D.SCHOLLER | 1 copy + 1 electonic copy |
| CNES | J.LAMBIN | 1 electonic copy |
| CNES | S.COUTIN-FAYE | 1 electonic copy |
| CNES | P.SNINI | 1 electonic copy |
| CNES | J.NOUBEL | 1 electonic copy |

## CHRONOLOGY ISSUE

| Control Initials | ISSUE | DATE | REASON FOR CHANGE |
|---|---|---|---|
| | 1.0 | December, 14th 2005 | Creation |
| | 1.1 | January, 6th 2006 | Revision |
| | | | |

# LIST OF ACRONYMS

| | |
|---|---|
| TBC | To Be Confirmed |
| | |

# List of Tables

# List of Figures

# Contents

# APPLICABLE DOCUMENTS / REFERENCE DOCUMENTS

# 1 Introduction

This document presents the synthesis report concerning validation activities of TOPEX/Poseidon under SALP contract (N° 03/CNES/1340/00-DSO310 Lot 2.C) supported by CNES at the CLS Space Oceanography Division.

Since the beginning of the mission, TOPEX/Poseidon data have been analyzed and monitored in order to assess the quality of AVISO M-GDR products (AVISO handbook, 1996 [2]) for oceanographic applications.

This report is basically concerned with long-term monitoring of both instrumental and geophysical parameter statistics, system and algorithm performances, homogeneity between TOPEX and Poseidon altimeters, for more than 13 years of data. Overall results from Sea Surface Height (SSH) analysis (Sea Level Variability (SLA) and Mean Sea Level (MSL) estimations) are also reported, as they are the main objectives of the mission.

T/P and ERS-2 Cross-calibration results are also presented. Indeed, the two altimeter series can be compared on the long term. These results are obtained from OPR-2 data (CERSAT User Manual [20]) and are derived from data quality assessment and intercalibration activities conducted at CLS, under IFREMER/CERSAT contract.
The comparisons with Jason-1 and Envisat measurements are not presented here. These results are included in specific reports to, as part of the CNES/SSALTO activities. However a study about the mean sea level comparisons between T/P, Jason-1, Envisat and Geosat Follow-on has been presented in this document.

The scientific mission of TOPEX/Poseidon is finished since the 9th October 2005, due to an anomalous behavior followed by stalling of the pitch reaction wheel. Despite of several attempts to restart the wheel, it continues to stop working after a short warm-up phase. In consequence the satellite is currently in a sun-pointing safe mode on two-wheel control.

TOPEX/Poseidon was launched on 10th August 1992 as a 3 year prime mission. The first 10 cycles served to calibrate the instruments.
The Side-B TOPEX altimeter has been switched on since February 1999 (cycle 236), because Side-A Point Target Response (PTR) changes made the altimeter measurement progressively degrading (Hayne and Hancock, 1998 [27]). It is thus important to compare measurements from A and B TOPEX altimeters in terms of biases, drifts and performances.
Moreover, the 15th of August 2002 (cycle 365), a maneuver sequence was conducted over a period of about 30 days to move T/P to the new Tandem Mission orbit at one half the TP/Jason-1 track spacing to the West of Jason-1. As a result, the T/P orbit is not repetitive from cycle 365 (pass 111 included) to cycle 368 (pass 172 included) and no nominal track is available during this period.
The DORIS instrument was switched off since an incident on 01, November 2004. Since then, all the POE requirements were met using lasernet tracking data. Only bent ionospheric correction is available.

After the end of the T/P mission and the successful launch of Jason-1, a synthesis study about the whole T/P mission seems particularly useful. More than 13 years of T/P data represent the reference altimeter mission, with the objective of continuous SSH observations for the long term. All results (except data coverage analysis) are obtained after data selection corresponding to editing criteria described in Le Traon et al., 1994 [36]. However, T/P data have been updated with new corrections (applied on Jason-1 products), but with no

change in the threshold criteria:

- Combined MOG2D (high frequencies of MOG2D model + low frequencies of Inverse Barometer) instead of only Inverse Barometer
- Non-parametric sea state bias used instead of BM4 for TOPEX (provided by Gaspar and al., 2002 [23], [35])
- GOT00V2 tidal correction used instead of GOT99 tidal.
- Taking account of S1, S2 waves for oceanic tidal GOT 2000 and for dry troposphere (ECMWF,cartesian grid)

The impact of the new geophysical parameters on the crossover performances is discussed in section 8.

Moreover a new approach is used to take into account the interpolation anomalies of the TMR correction (section 2.2.4) by using FLG_TMR_BAD, a parameter which indicates the interpolation quality in the M-GDR files.

This document is structured as follows: First, the number of edited measurements, for each criterion, is analyzed as a function of time. Then a statistical monitoring of different parameters is achieved. Crossover analysis allows estimations of system performances and comparisons of redundant corrections. Finally repeat-track analysis allows performing MSL estimations, to compute the relative bias between TOPEX and Poseidon altimeters and to estimate the ocean variability.

# 2 Missing and edited measurements

## 2.1 Missing measurements

Missing measurements relative to the nominal track have been monitored during the last years. It allows detection of coverage anomalies, particularly due to altimeter problems.
The number of missing measurements over ocean has been plotted on figure 1 from cycle 10) to cycle 481. This figure also includes events as Single Event Upsets (SEU) or altimeter tests, appearing as isolated peaks of missing measurements. Notice that the number of missing measurements is not computed from cycle 365 to 368 because no reference track can be used during the T/P orbit change.

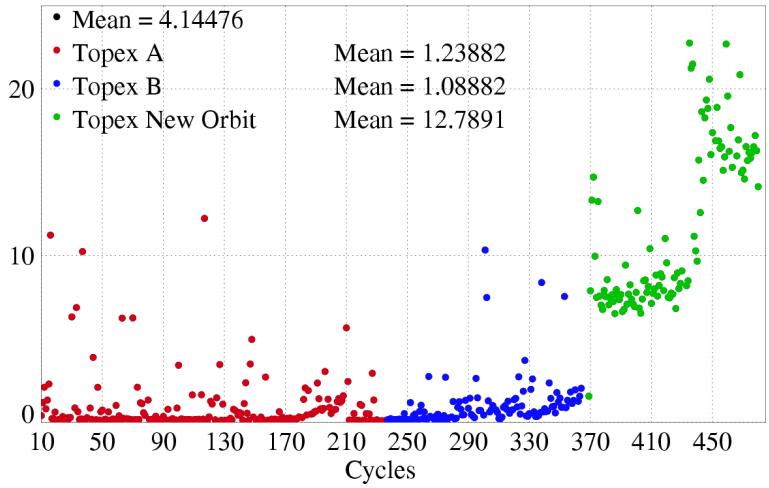


Figure 1: *Percentage of missing measurements relative to a nominal track*

The figure shows a first large increase of the number of missing measurements until cycle 212. From cycle 178 to cycle 212, one of the three tape recorders onboard the satellite (B tape recorder) exhibited anomalous behavior and caused data losses. Then it was decided to not use this tape recorder, switching to a 2-tape recorder functioning mode. Unfortunately, short missing portions of tracks began again to be detected in missing measurements plots (AVISO/CALVAL report, cycle 267 [3]) and the A tape recorder was identified as the cause of these failures (T/P daily status [52]). In order to ensure a proper data acquisition, it was decided to conduct some engineering tests on tape recorder B (TR-B). It has been demonstrated that the unit will operate well within a certain range of tape speeds. This could enable data storage for a two to four hour period on this recorder (T/P daily status [53]). Nevertheless, tape recorder functioning has continued to degrade. Tape recorder A (TR-A) operations were modified on July 2001 (T/P daily status [54]) as it was previously the case for TR-B. In September 2001, after performance of TR-B had degraded to the point that it could no longer be used in a normal operation mode, it was decided not to use it (T/P daily status [55]).
Then TR-B was again used in low tape speed mode, but other degradations on both TR-A and B (see above) has caused the number of missing measurements remain at a higher level during the year 2001. However, in the worst case of cycle 210, the number of missing measurements does not exceed 1.3 % of valid data.
From about cycle 340 onward, the number of missing measurements rises slightly up to the same level as during cycles 190-210. This is due once again to degradations of tape recorders. But from September 2002 (cycle 370 onward), more significant anomalies with tape recorders are observed. As a result, a lot of data

gaps are present, especially in the Indian Ocean and in the Pacific Ocean close to the South America. From cycle 370 to 375, the number of missing measurements increases up to 14 %, and between 375 and 400, it remains almost stable between 7% and 8%. From cycle 400 to 444, the tape recorder performances has continued to decline. Thus it was decided on cycle 444 to remove from service the tape recorder. Science data recovery requirements will now be met through increased TDRSS (Data relay Satellite System) real-time contacts.
Notice that no data is available for cycle 118, 430 and 431 due to 2 safe hold modes. These missing measurements have not been taken into account in the figure 1 and in the global percentage of missing measurements.

## 2.2 Edited measurements

### 2.2.1 Editing criteria definition

The editing criteria are divided into 3 parts. First, the quality criteria concern the flags. Secondly, threshold criteria are applied on altimeter, radiometer and geophysical parameters. Moreover, a spline criterion is applied to remove the remaining spurious data. These criteria are also defined in AVISO and PODAAC User handbook for the GDR product.

#### 2.2.1.1 Quality Flags

Quality flags are used to remove measurements polluted by the presence of ice or land. Since the radiometer land flag was not always reliable (probably due to interpolation problems with the TMR), it is replaced by the flag distance from coast.

#### 2.2.1.2 Thresholds

Editing criteria (Le Traon, 1994 [36]) have been used to select valid measurements over ocean. For each criterion, the percentage of edited measurements (relative to the total number of present measurements) has been monitored. This allows us to detect trends in the number of removed data, which could come from instrumental, geophysical or algorithmic changes.
The threshold criteria applied to the different parameters are described in the table 1.

| Parameter | Min thresholds | Max thresholds | mean removed |
|---|---|---|---|
| Sea surface height | $-130\ m$ | $100\ m$ | 0.18% |
| number measurements of range | 10 | $Not\ applicable$ | 0.33% |
| standard deviation of range | 0 | $0.2\ m$ | 1.13% |
| Off nadir angle | $0\ deg$ | $0.4\ deg$ | 3.52% |
| Dry troposphere correction | $-2.5\ m$ | $-1.9\ m$ | 0.00% |
| MOG2D and inverted barometer correction | $-2.0\ m$ | $2.0\ m$ | 0.001% |
| TMR wet troposphere correction | $-0.5m$ | $-0.001\ m$ | 0.97% |
| Ionosphere correction | $-0.4\ m$ | $0.04\ m$ | 0.66% |
| Significant waveheight | $0.0\ m$ | $11.0\ m$ | 0.13% |
| Sea State Bias | $-0.5\ m$ | $0.0\ m$ | 0.28% |
| Ku-band Sigma0 | $7\ dB$ | $30\ dB$ | 0.30% |

.../...

| Parameter | Min thresholds | Max thresholds | mean removed |
|---|---|---|---|
| Ocean tide | $-5.0\ m$ | $5.0\ m$ | 0.14% |
| Earth tide | $-1.0\ m$ | $1.0\ m$ | 0.00% |
| Pole tide | $-15.0\ m$ | $15.0\ m$ | 0.00% |

Table 1: *E*diting criteria

### 2.2.2 Monitoring of quality flags

#### 2.2.2.1 Distance from coast

The percentage of edited measurements using the 25 km distance to coast flag is plotted as a function of the cycle number in figure 2. The mean percentage is close to 4.6% with a small annual signal.
The decrease by 0.5% of edited measurements between cycle 365 and 368 is a result of the orbit change. Since cycle 370, more and more data gaps appeared due to the problems of the tape recorders. Since cycle 444, data are transmitted in real-time by TDRSS, thus increasing data gaps. As a consequence, the percentage of measurements edited by coast distance varies as the satellite coverage changes.

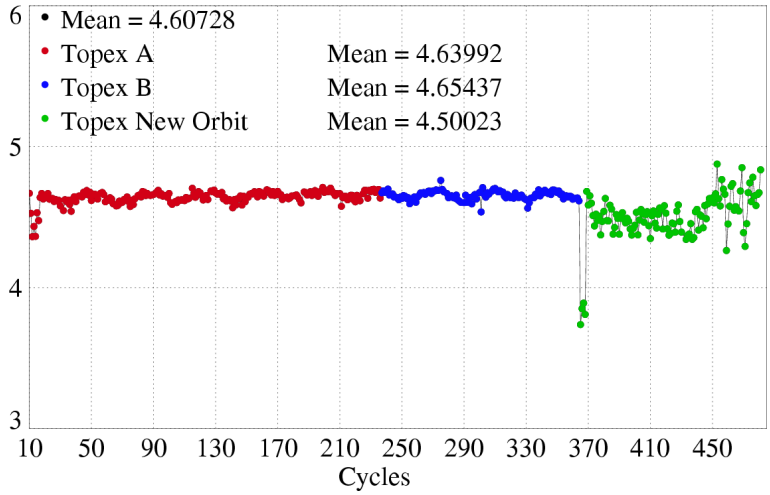


Figure 2: *Percentage of missing measurements edited by coast distance flag*

#### 2.2.2.2 Ice flag

The same kind of plot has been performed for the ice flag (figure 3). It shows no anomalous trend but a dominant annual cycle : the maximum number of points over ice is reached during the northern fall.
The ice flag edited measurements are plotted in Figure 4 for one cycle.

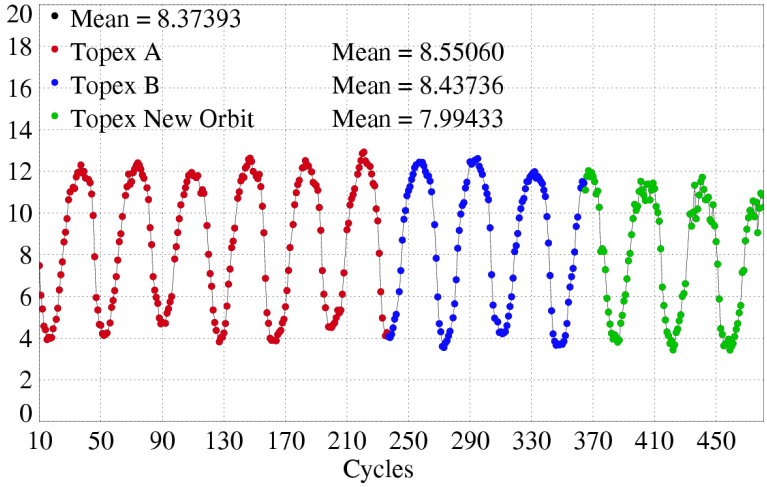


Figure 3: *Percentage of missing measurements edited by ice flag*

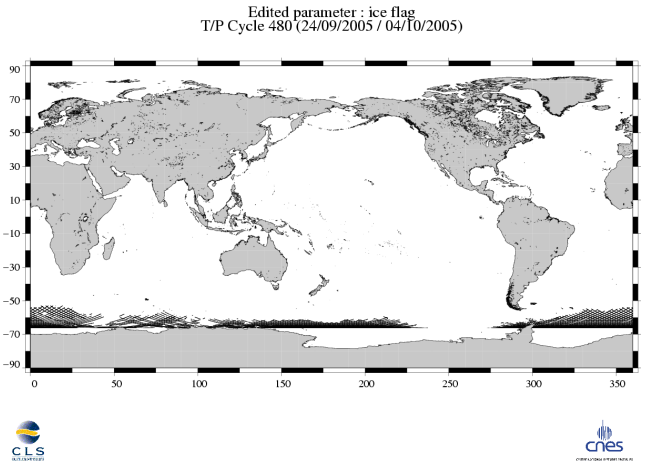


Figure 4: *Map of edited measurements by ice flag criterion on cycle 480*

### 2.2.3 Monitoring of threshold criteria

#### 2.2.3.1 Global monitoring

Instrumental parameters have also been analyzed from comparison with thresholds, after having applied flagging quality criteria (land and ice flag). Notice that no measurements are edited by the following corrections : dry troposphere correction, MOG2D correction (including inverted barometer), equilibrium tide, earth tide pole tide and earth tide pole tide.
The percentage of measurements edited using each criterion has been monitored on a cycle per cycle basis (figure 5). The mean percentage of edited measurements is about 4.0% from cycle 10 to cycle 369. The percentage increases to about 8.9% from cycle 370 onward due to the radiometer wet tropospheric correction (see section 2.2.4).
The percentage of edited measurements is higher than 10% from cycle 433 to 437, as well as after cycle 444. For the period between cycle 433 to 437, this is due to a pitch wheel event linked to the T/P safehold mode occurred from cycle 430 to 432 (see electronic communication : T/P Daily Status (26/07/2004). Consequently, the satellite had a strong mispointing during this period and the altimeter measurements were impacted. The increase of edited measurements for cycle 445 and onward is due to the radiometer wet tropospheric correction (see section 2.2.4).
Besides, an annual cycle is visible due to the seasonal sea ice coverage in the northern hemisphere. Indeed most of northern hemisphere coasts are without ice during northern hemisphere summer. Consequently some of these coastal measurements are edited by the thresholds criteria in summer instead of the ice flag in winter. This seasonal effect visible in the statistics is not balanced by the southern hemisphere coasts due to the shore distribution between both hemispheres.

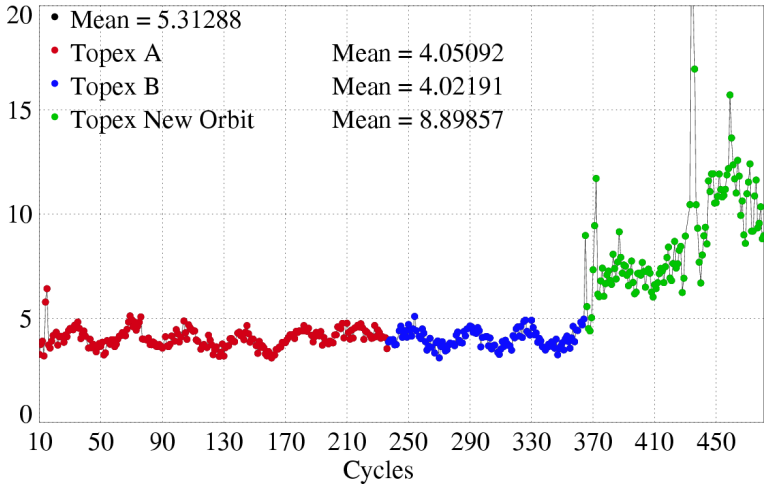


Figure 5: *Cycle per cycle percentage of edited measurements by threshold criteria*

#### 2.2.3.2 Number and standard deviation of elementary TOPEX altimeter measurements

Figure 6 and figure 7 respectively show the percentage of removed measurements due to the number and the standard deviation of elementary TOPEX altimeter measurements.
The number of edited points due to too few ($< 5$) 10-Hz elementary measurements increases from around cycle 150 to the last Alt-A cycle (235). This reveals altimeter changes, and can be attributed to observed modifications in the Alt-A PTR.
In the first Alt-B cycles, high variations are observed in the percentage of edited measurements due to this criterion. Then the value abruptly decreases to the same level as the one obtained in the first Alt-A cycles. This could be explained by land/sea transition problems detected in the first Alt-B cycles with non negligible portions of passes impacted (Dorandeu et al., 2001 [17]). During the first Alt-B cycles, some small differences in the Side-B noise signal caused the Alt-B not to recognize it has lost the signal as quickly as Alt-A (David Hancock, internet communications [24] and [25]). Flight tracker software and parameters were the same for both Side-A and Side-B, whereas different tuning of Alt-B parameters should have been performed.
During cycle 256 (Poseidon cycle), a safe-hold incident occurred on the TOPEX/Poseidon platform with the result that the TOPEX altimeter was powered off during most of this cycle. This event seems to have made the Alt-B characteristics evolve, according to the number of edited measurements after the incident. Indeed after cycle 256, such land/sea transitions problems do not occur anymore (Hayne and Hancock 2000 [28]). Note that the percentage of edited measurements is higher than usual for cycles 365, 366 and 368. This might be due to the maneuvers to change the T/P orbit. Then the value remains stable with the new T/P orbit from cycle 369 onward, at the same level as in the beginning of the mission.
Approximately the same behavior is noticed for the standard deviation of 10 Hz elementary measurements (Figure 7): increase of Alt-A edited measurements after cycles 130-150, high values for the first Alt-B cycles, then lower values after the platform safe-hold. An annual signal is observed due to ice seasonal variations.
As previously, the percentage of edited measurements is higher than usual from cycle 433 to 437 : this is due to a strong mispointing as a result of a pitch wheel event (see section 2.2.3.1).

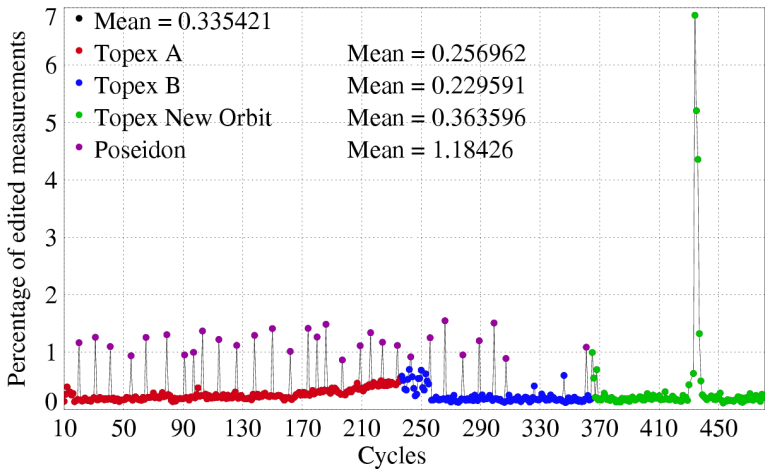


Figure 6: *Number of TOPEX edited measurements due to too low ($< 5$) number of valid 10Hz-elementary measurements*

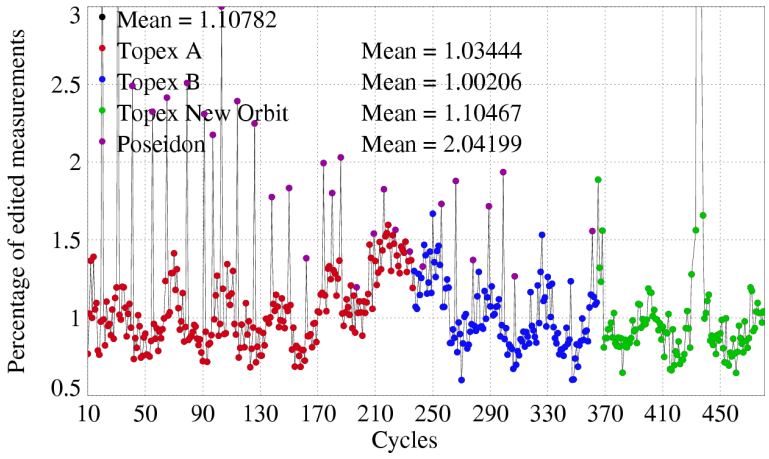


Figure 7: *Number of TOPEX edited measurements due to too high (> 100 mm) RMS of 10-Hz elementary measurements*

#### 2.2.3.3 Significant Wave Height

Significant Wave Heights higher than 11 m are removed during the editing process. The number of edited measurements using this criterion has been plotted on Figure 8. The Alt-A SWH has increased from early in the mission, as it was first detected by Queffeulou (1998) [47] in his comparison of TOPEX and ERS SWH. This instrumental problem has been described in (Hayne and Hancock, 1998 [28]): the Point Target Response (PTR) changes account for most of the increase in the TOPEX SWH estimate. Though low values of SWH are more impacted than high values, it explains why more data are edited in the last Alt-A cycles. With Alt-B, the number of edited measurements due to SWH value recovers the same level as Alt-A in the beginning of the mission. Notice that Alt-B land/sea transition problems from cycle 236 to cycle 255 are less sensitive for this criterion, since SWH values are set to zero for these anomalous measurements. Note that slightly higher percentages of edited measurements are obtained from cycle 365 to 368, probably due to the maneuvers to change the T/P orbit.
As previously, for the number and standard deviation of elementary altimeter measurements, the percentage of edited measurements is higher than usual from cycle 433 to 437 : this is due to a strong mispointing as a result of a pitch wheel event (see section 2.2.3.1).

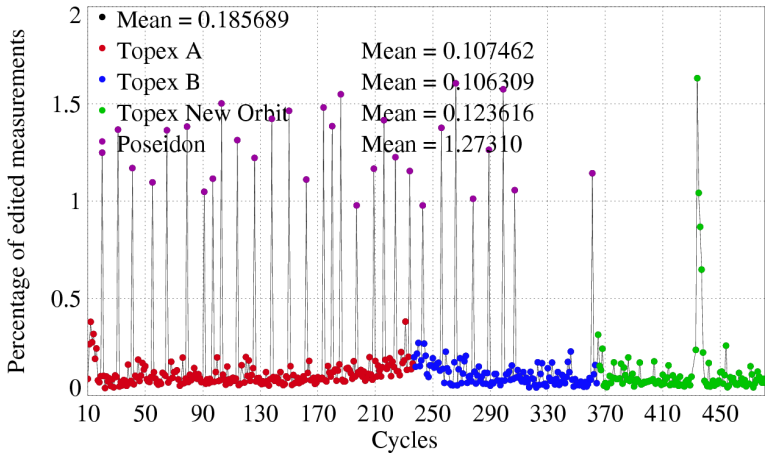


Figure 8: *Number of TOPEX edited measurements due to too high values of SWH (SWH > 11 m)*

#### 2.2.3.4 Backscatter coefficient

The same kind of statistical monitoring has been performed for the Ku-band Backscatter Coefficient (Ku Sigma0) (Figure 9) : it shows again a particularly high number of edited measurements during Alt-B land/sea transition failures, because the Sigma0 parameter is set to a default value in the M-GDR product during these events. Like for the other altimeter criteria, more anomalous Sigma0 values are detected during the T/P orbit transitions (cycles 365-368) and as a result of a pitch event between cycles 433 and 437. During cycles 475 and 476 (see TOPEX/POSEIDON MGDR Quality Assessment Report [56], [57]), more Sigma0 values than usual were edited, as they were below threshold. This seems often to be the case after data gaps, as the AGC temperature correction produces bad values (see Phil Callahan, internet communication [11]).

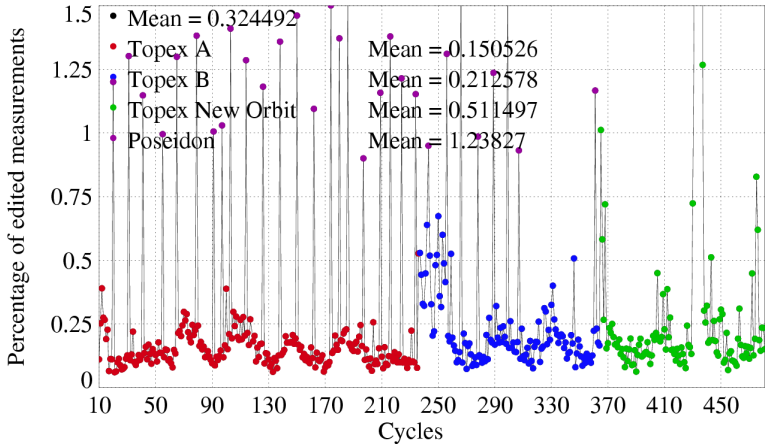


Figure 9: *Number of edited measurements due to invalid Sigma0 values*

### 2.2.4 TMR wet troposphere correction

The number of edited measurements using the radiometer wet tropospheric correction criterion is plotted on Figure 10. It is correlated with the number of missing measurements. Indeed, data gaps cause anomalous values of brightness temperatures and wet correction at the altimeter time tag, because of bad interpolation in the TMR processing, when data are missing. This explains why the number of edited measurements due to the wet troposphere criterion increases during tape recorder problems.

The first anomalies appear between cycle 190 and 210 with a percentage of edited measurements about several times higher than usual (up to 0.7 % instead of less than 0.1%). As mentioned previously, one of the three tape recorders onboard the satellite (B tape recorder) exhibited anomalous behavior and caused data losses. Then, during year 2001, some cycles exhibit a percentage of edited measurements just below 1%. This is due to other degradations on both TR-A and B (see section 2.1). But the more important anomalies appear from cycle 370 onward. Indeed the percentage of edited measurements reaches 7% on cycle 372, then remains relatively stable, around 3-5%. These significant figures can still be explained by tape recorder failures occurring more often than in the past. For cycle 445 and ongoing, the percentage of edited measurements reaches 8%. This can be explained by the large data gaps caused by the shutdown of the tape recorders.

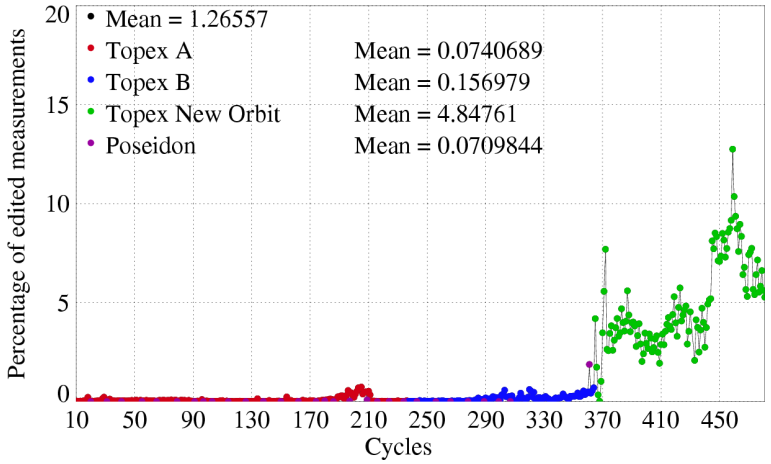


Figure 10: *Number of edited measurements due to invalid TMR wet troposphere correction values*

Despite the comparison to thresholds, some bad TMR corrections were still present in the selected dataset. Thus, now the parameter FLG_TMR_BAD, present in the M-GDR files, is used to remove all measurements which had interpolation problems due to data gaps. Figure 11 shows the percentage of measurements edited by this parameter. The percentage of edited measurements is very small as long as there are little data gaps, and increase to 4-6% for the period where tape recorders are more often malfunctioning (cycle 370 to 444). Finally, after stopping of the tape recorders which led to more data gaps, the percentage of edited measurements increases to 8-10%.

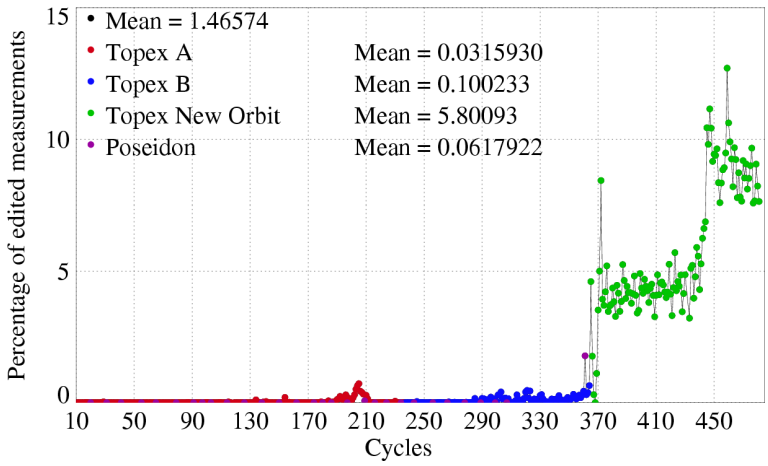


Figure 11: *Number of edited measurements due to TMR_BAD flag*

# 3 Statistical monitoring

## 3.1 Background

Both mean and standard deviation of T/P data main parameters have been monitored since the beginning of the mission. In particular, it is important to analyze the differences between corrections of the same type as a function of time, and to estimate the differences between Alt-A and Alt-B TOPEX altimeters. Only valid points (according to editing criteria) are used to analyze the behavior of these parameters over a long time series.

## 3.2 Comparison of CNES and NASA orbits

Figure 12 displays comparisons between the two types of the radial components of the GDRM precise orbits. The mean and the standard deviation of (CNES orbit-NASA orbit) differences are plotted as a function of the cycle number.
The cycle mean of the difference remains almost constant (about 5 mm) until around cycles 120-130. Then, a trend is observed up to cycle 246. Finally the mean difference returns to lower values after cycle 247. The differences are particularly low after cycle 320.

Different strategies have been applied by the two entities in terms of reference frame: in the NASA processing, horizontal velocities have been accounted for to allow station positions evolving with time, while the CNES processing, estimating at the beginning of 1996 that horizontal velocities were not sufficiently well known, chose to work with a fixed reference frame during a given period (with the open possibility to change the reference frame in accordance with oceanographic requirements). From cycle 247 to cycle 320, the ITRF97 set of station coordinates has been taken into account in the CNES orbit computation, explaining the jump on cycle 247. Following the recommendation of the Miami SWT POD meeting, the reference frame was again switched from ITRF97 to ITRF2000 starting with cycle 320. Advantage of this transition was also taken to turn on the albedo model in the CNES orbit calculation. This reduces the mean radial differences between CNES and NASA orbits (Berthias, 2001 [4]).

The non homogeneity of the terrestrial reference frames explains the trend detected in the difference between the two orbits (Morel et al., 1998 [42]). It can be roughly expressed as a z-axis coordinate drift between the two orbits (Dorandeu, 1998 [14]). Note that global (that is, with no land/sea mask applied) differences between the two orbits would not lead to such a result since northern and southern hemispheres should compensate each other. In our analysis, only ocean data are considered and the Southern hemisphere is thus more sampled. The actual impact of orbit differences in terms of Mean Sea Level (MSL) estimation will be analyzed in the dedicated MSL section (section 6.2.2).

The same features can also be noticed in the standard deviation of the difference. While it was less than 1.5 cm RMS during the first 3 years, it raised through the 3 following years, up to 2.5 cm RMS around cycle 220. One part of this greater value can be attributed to the z-axis coordinate drift between the two orbits. Indeed, after the ITRF97 set of coordinates is used in the CNES orbit calculation, the standard deviation of the differences between the two orbits ranges again between 1 and 2 cm RMS. The particular value of cycle 256 is mainly due to some NASA orbit degradation (after the satellite safe hold mode). After the use of both ITRF2000 reference frame and albedo model in the CNES orbit, differences between the two orbits are now reduced to less than 1.5 cm rms.

From cycle 360 onward, ITRF2000 reference frame has been applied on NASA orbit and the two orbits have been particularly consistent in their mean difference.

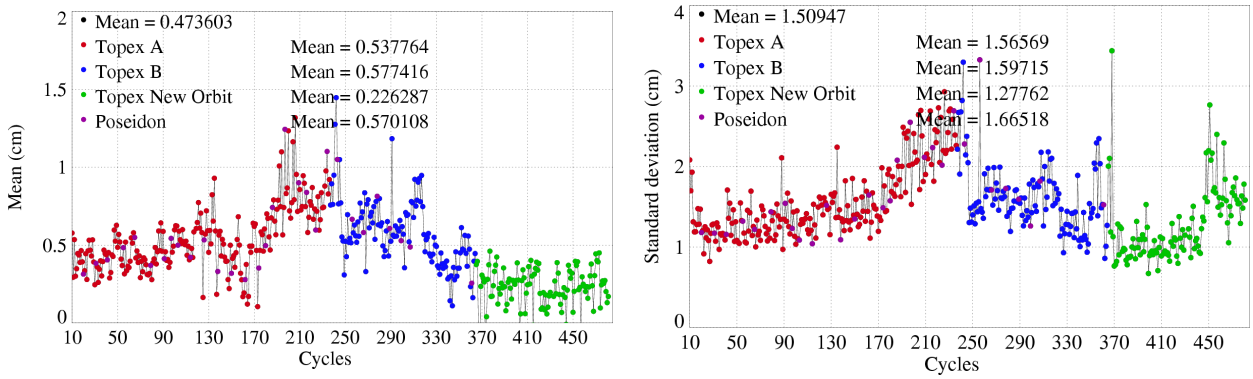


Figure 12: *Cycle mean (left) and standard deviation (right) of differences between CNES and NASA orbits*

## 3.3 Comparison of tidal models

The GOT00 tidal model has been computed to update the T/P product. Both cycle mean and standard deviation of the (GOT00V2-GOT99) differences are plotted on Figure 13. It shows a very close to zero mean difference. Thus using either of the two models introduces no bias. The standard deviation is about 1.5 cm RMS, with annual variations probably due to seasonal coverage of areas where tide models are less efficient (AVISO/CALVAL yearly report, 1997 [15]). The performances of the two models for correcting T/P altimeter data are analyzed in the dedicated section 4.3.2.

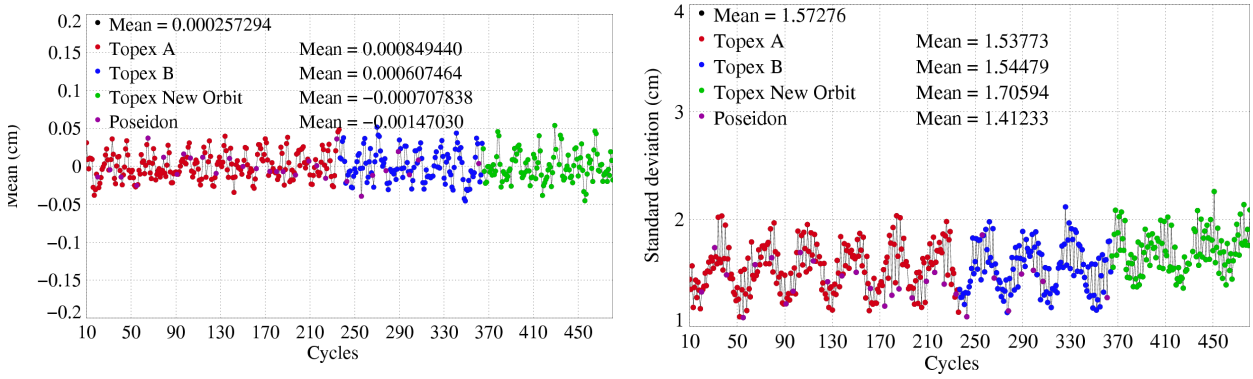


Figure 13: *Cycle mean (left) and standard deviation (right) of differences between GOT00V2 and GOT99 tide model values*

## 3.4 Wet troposphere corrections

### 3.4.1 TMR wet troposphere correction

The mean and the standard deviation of the correction are plotted on figure 14. Apart from large seasonal variations, the long data series allows to notice some general features in the correction, such as instrumental or physical drifts. So the mean correction seems to drift by about 1.2 mm/year from the beginning to early 1997 (cycle 160) (see left figure 14).
On the right figure (14) the long-term (instrumental) drift was corrected using Scharroo, 2004 ([51]). Nevertheless, an increase in the absolute value can be found during the year 1997-1998 (cycles 180 to 220), as well as for the 3 years. These increases are related to a physical change (increase in moisture). The first increase corresponds to the El Niño period, the second is perhaps related to global warming.

The standard deviation evolution (bottom of figure 14) also reveals a particular behavior from mid-1997 to the end of 1998. It also shows an increase over the last years, which is probably related to the increase of the absolute value of the mean wet troposphere correction.

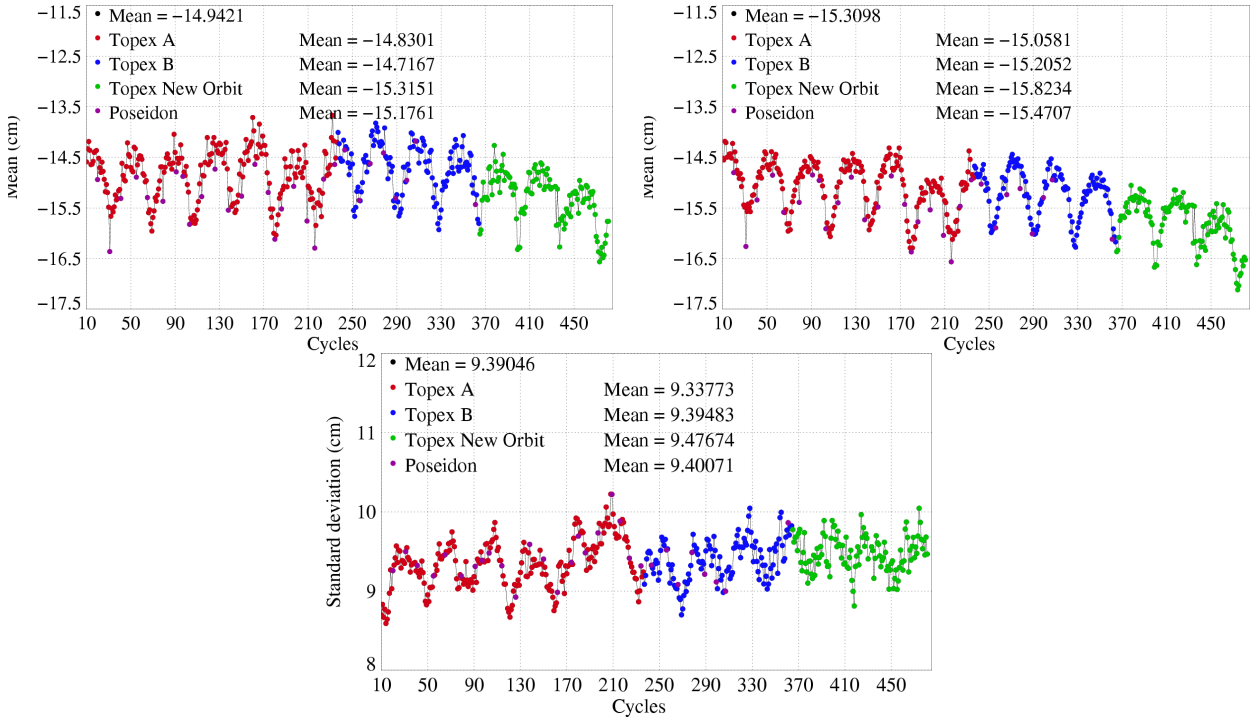


Figure 14: *Cycle mean of uncorrected for long-term drift (left) and corrected for long-term drift (right) TMR wet troposphere correction values. Standard deviation of (uncorrected) TMR wet troposphere correction values (bottom).*

### 3.4.2 TMR brightness temperatures

It is thus interesting to plot the cycle mean of the three TMR brightness temperatures (Figure 15) after removing annual variations. These global averages account for all brightness temperature scales and then potentially reflects any possible trend in either atmospheric or ocean surface parameters, contrary to what has been done by Keihm et al. with their cold data subset. However, figure 15 (top on the left) clearly shows a drift in the 18-GHz channel, consistent to the previously cited study. Drifts can be deduced from 21 and 37 GHz channels, probably also linked to geophysical changes.

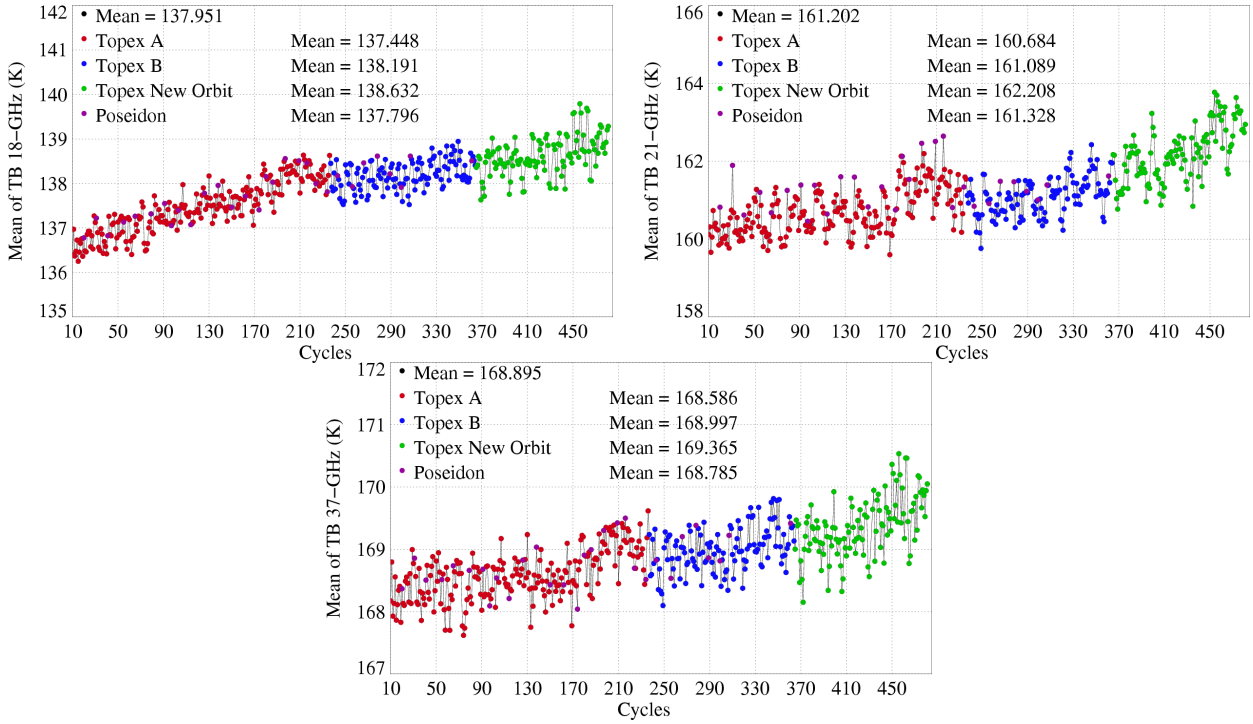


Figure 15: *Cycle means of 18 GHz (top left), 21 GHZ (top right) and 37 GHz (but tom) TMR brightness temperatures. Annual signals have been filtered out*

### 3.4.3 Comparison of TMR and ECMWF wet troposphere corrections

Figure 16 compares the two types of troposphere corrections. Note that for TMR wet troposphere correction, the long term drift is corrected by R.Scharroo (Scharroo et al., 2004 [51]). Significant variations are observed on the long term monitoring of the cycle mean.
The first change that occurred at cycle 82 is due to the assimilation of TOVS data during modeling.
Secondly, a gap is observed at cycle 192 and is due to the improvement of the wet troposphere correction calculation at Météo-France, that allowed to minimize a scale error. After this processing change, the cycle mean difference between TMR and ECMWF corrections is about 0.3.
Then, another gap is observed at cycle 340. The change is due to an improvement of the ECMWF model. After this processing change, the cycle mean difference between TMR and ECMWF corrections is about 11 mm.

These major processing changes in the model correction calculation are also noticed in the standard deviation of the difference between the two corrections. The standard deviation has continuously decreased for the whole T/P mission from about 3-3.5 cm rms at the beginning to 1.5 cm rms at the end, showing the improvements made to the model.

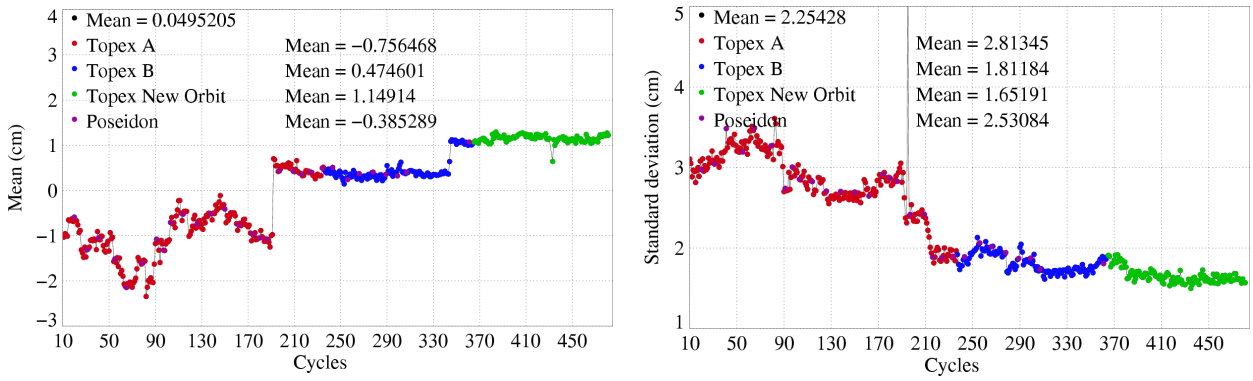


Figure 16: *Cycle mean (left) and standard deviation (right) of differences between TMR and ECMWF wet troposphere corrections*

### 3.4.4 Correction of jumps due to Yaw mode transitions

Irregular variations were observed between the TMR and ECMWF wet troposphere corrections. Yaw mode transitions impacted the TMR correction since the beginning of the mission.

These jumps are now corrected using the scheme shown on figure 17.

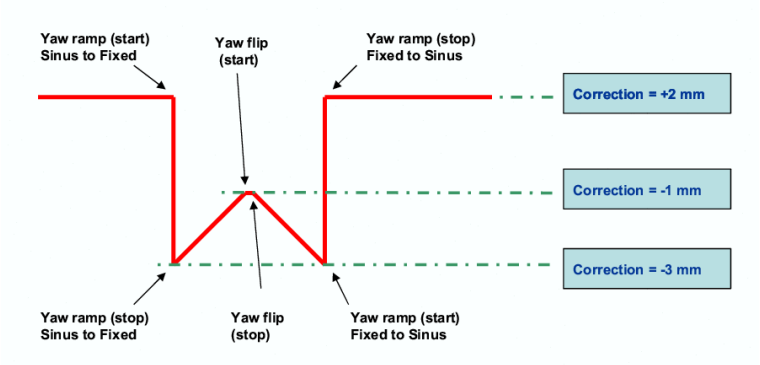


Figure 17: *Adjustment applied to TMR correction to rectify impact of yaw mode transitions.*

The long term monitoring of the daily differences during 18 months (plotted on figure 18) illustrates in black the impact of the "yaw modes", when not corrected. Note that the amplitude of the signal is about 5 mm with a period of 2 months. The line in red shows the difference between TMR and ECMWF wet troposphere correction after applying the jump correction. Note that in both cases the long term TMR drift correction from Scharroo (2004, [51]) was applied.

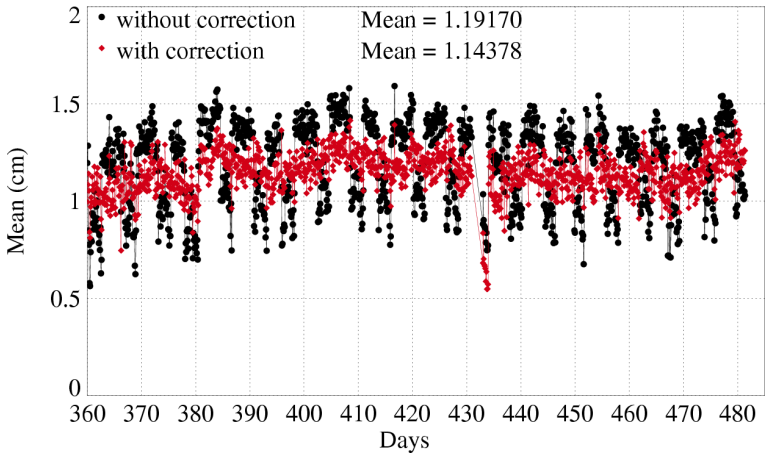


Figure 18: *Daily mean of differences between TMR and ECMWF wet troposphere corrections, with and without jump correction and Scharroo drift correction*

## 3.5 Ionosphere corrections

### 3.5.1 TOPEX dual-frequency ionosphere correction

Cycle by cycle statistics of the dual frequency ionosphere correction are presented on figure 19. Apart from annual variability, the rises and falls in the mean and standard deviation are mainly due to sunspot activity variations. Last years, from 2001, exhibit large solar activity (Blusson, 2002, [5]). This directly impacts the ionospheric correction.

Notice that there is no gap between Alt-A and Alt-B cycle means (before cycle 235 and after cycle 236), as it was one of the goals of the Alt-B calibration phase (AVISO/CALVAL SideB TOPEX altimeter evaluation, 1999 [16]).

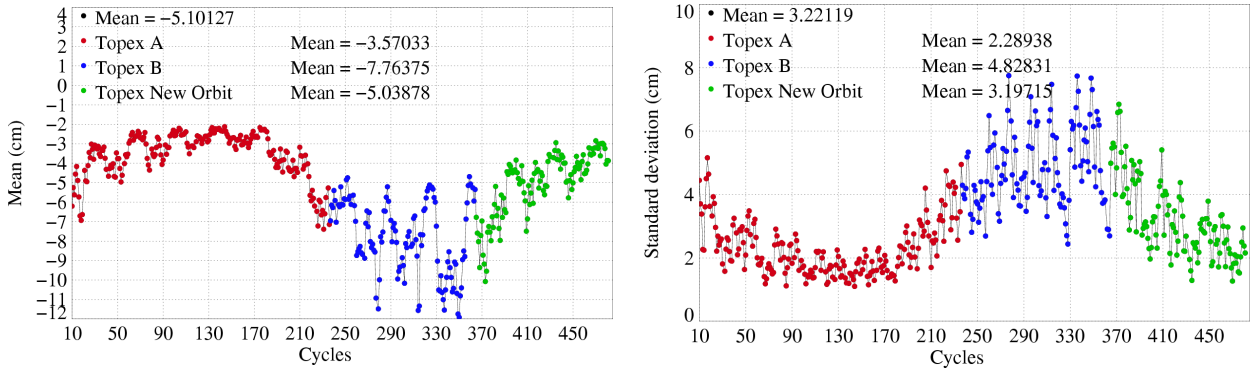


Figure 19: *Cycle mean (left) and standard deviation (right) of TOPEX dual frequency ionosphere correction*

Furthermore, note that the orbit change from cycle 365 onward has no impact on the dual-frequency ionosphere correction. The dual-frequency ionosphere correction is routinely filtered, with a 300 Km wavelength cut-off (low-pass filter), in order to reduce the noise of the correction. Statistics of the difference between before filtering and after filtering are plotted on figure 20. The standard deviation increases until cycle 235 (last Alt-A cycle), from 6.3 to 7.2 mm RMS. It denotes a rising noise of the dual-frequency correction, probably linked to altimeter degradation. After the Alt-B switching on, same values as in the beginning of the mission are obtained for both mean and standard deviation. No trend can be detected in the Alt-B statistics from cycle 236 to cycle 361 (orbit change), thereafter the standard deviation is decreasing.

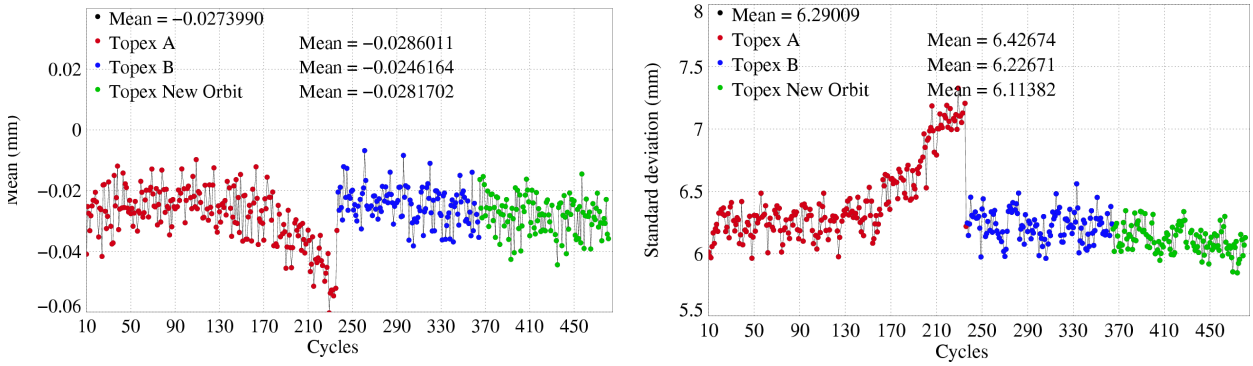


Figure 20: *Cycle mean (left) and standard deviation (right) of differences between raw TOPEX ionosphere values and filtered values (300 km low pass filter)*

### 3.5.2 Comparison of TOPEX dual-frequency and DORIS ionosphere corrections

Both mean and standard deviation of the difference between DORIS and TOPEX dual-frequency corrections are plotted on figure 21. A mean value of about 1 cm is obtained during the first 5 years. But after, the cycle mean difference exhibits larger variations and increases (in absolute value) by about 0.5 cm. The mean difference between TOPEX and DORIS corrections is correlated to the sunspot activity : the mean difference increases when the ionosphere correction increases and conversely. This may be explained by a lower ability of the DORIS correction to retrieve large and quick variations which are more intense in case of high solar activity. The end of the period (after cycle 350) corresponds to the beginning of the solar activity decrease, the two kinds of corrections becoming more consistent.

The standard deviation of the difference is also impacted: it increases by about 1 cm RMS in high solar activity periods, showing that variations between the two corrections are not a simple increasing bias.

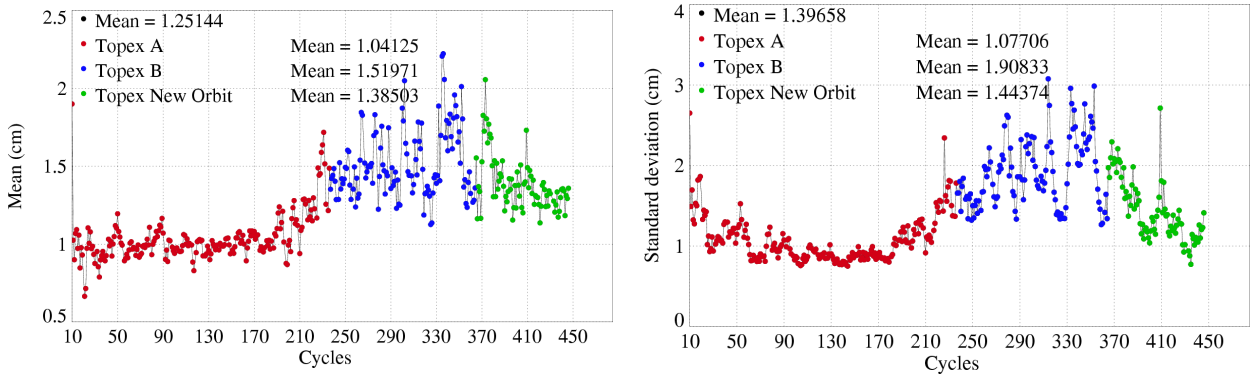


Figure 21: *Cycle mean (left) and standard deviation (right) of differences between DORIS and TOPEX ionosphere corrections*

In order to assess the evolution of the discrepancies between the two corrections, the mean differences have been computed according to several local time intervals of 4 hours. The computation has been performed through the entire mission. Each cycle gives an estimate of the mean difference between DORIS

and TOPEX corrections for every local time interval. Averages each year have been computed and leads to the results plotted in figure 22.
While differences between DORIS and TOPEX corrections remain almost stable in the years 1993 - 1997 for all local times, the differences increase since 1997, particularly for local times ranging from 10 a.m. to 6 p.m. In 2000 and 2001, the mean difference has increased by about 8 mm for local times between 10 a.m. and 2 p.m. In 2004 and 2003, the mean difference has decreased for local times between 6 a.m. and 18 p.m. In 2004, the difference remain almost stable for all local times.
The shape of the increase in the mean difference follows the shape of the Total Electronic Content, as a function of local time. Thus it seems to show that the variations in the mean difference between DORIS and TOPEX corrections are mainly due to the DORIS correction for high solar activity conditions. At global scale, taking all local times into account, this translates into a mean increase of about 0.5 cm of the (DORIS - TOPEX) difference.
It is important to notice that this non constant difference between DORIS and TOPEX ionosphere corrections directly impacts the relative bias between TOPEX Sea Surface Height (SSH) and Poseidon SSH estimations. After the 5 first years, the relative bias between the two altimeters may thus increase and is expected to be 0.5 cm higher in the last cycles than in the first part of the mission. Moreover, seasonal variations as large as 0.5 cm are observed in the (DORIS  TOPEX) ionosphere differences. They also add uncertainties in the relative bias between the two altimeters.
The DORIS instrument was finally switched off on 1st November 2004 (cycle 446).

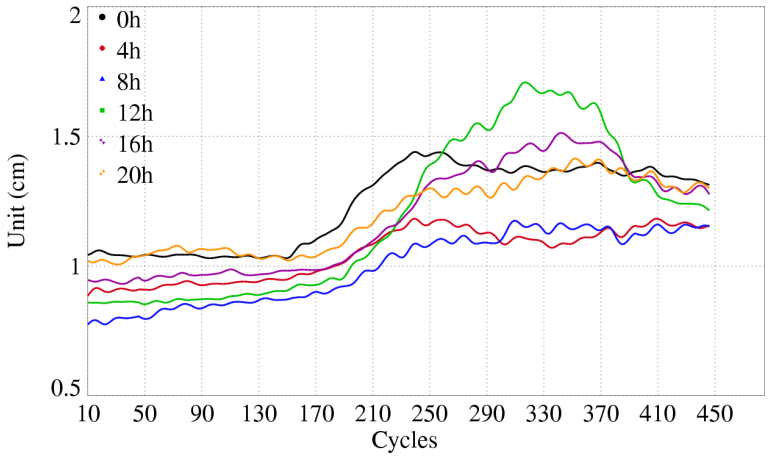


Figure 22: *Differences between DORIS and TOPEX ionosphere corrections as a function of local time*

## 3.6 Significant wave height monitoring

### 3.6.1 Ku-band SWH

The cycle mean of Ku-band SWH is plotted as a function of the cycle number on figure 23. The Alt-A SWH has experienced a large increase (of about 30-35 cm) after approximately cycle 130. Alt-B values (after cycle 236) are consistent to usual values of Alt-A before the change. TOPEX altimeter drifts are responsible of these changes (Hayne et Hancock, 1998 [27]). No trend can be detected from the Alt-B estimates and after the orbit change, through cycles 236-481.
The standard deviation only reflects sea state variations, with higher variability during the austral winter. Alt-B values are consistent with Alt-A.

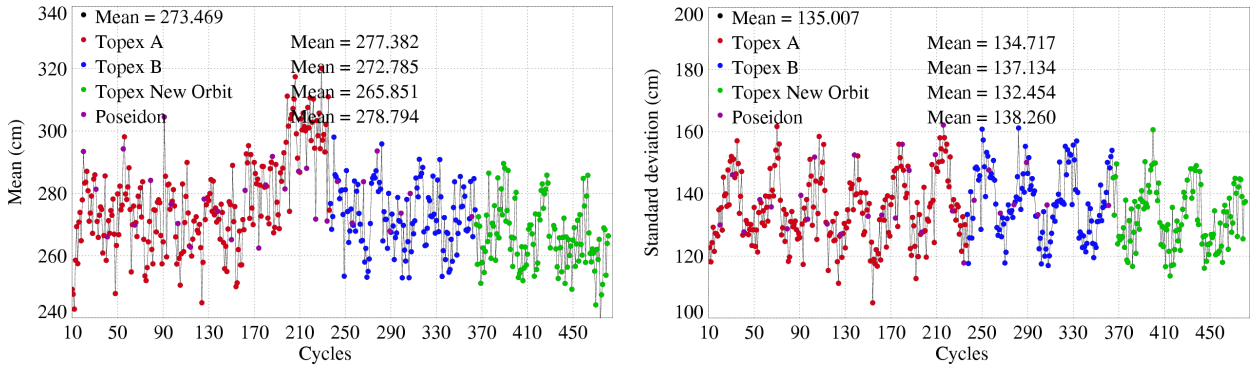


Figure 23: *Cycle mean (left) and standard deviation (right) of Ku-band TOPEX SWH*

### 3.6.2 Comparison of Ku-band and C-band SWH

The difference between the two bands in terms of SWH is represented on figure 24. The figure shows an evolution of the Side-A altimeter from the very beginning of the mission, though the mean difference between the two bands only varies by about 2.5 cm. Alt-B values were first very close to those of last Alt-A cycles, at the end the difference became smaller. The cycle standard deviation also points out this continuous evolution, probably due to Alt-A instrument degradation. The standard deviation of the (Ku C) SWH differences is dramatically reduced on Alt-B cycles which lead to low values, even lower than Alt-A values in the beginning.

Some very slight consistent trend can also be observed in the Alt-B mean difference, but the difference between Ku and C Alt-B SWH measurements do not vary by more than 1 cm in average.

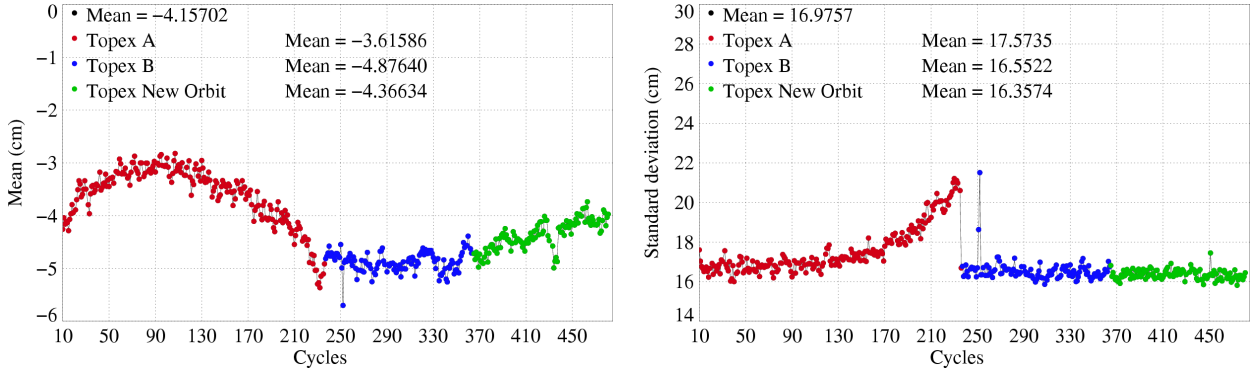


Figure 24: *Cycle mean (left) and standard deviation (right) of differences between Ku-band and C-band TOPEX SWH values*

## 3.7 Backscatter coefficient monitoring

### 3.7.1 Ku-Band Sigma0

Statistics have been computed for the Ku-band Sigma0 (Figure 25). The cycle mean remains more or less constant in the first part of the mission, maybe because the last version of MGDR includes Sigma0 reprocessed values, accounting for updated calibration tables. After cycle 132, higher variability of the parameter is observed, though calibration corrections are routinely applied in the processing (Hayne and Hancock, 1997 [30], Hayne and Hancock, 1999 [31]).

Note that all the results presented in this report are only based on M-GDRs, even though some improvements are now proposed by Hayne and Hancock, 1999 [31] and Hayne and Hancock, 2002 [32] with new calibration tables for both TOPEX Alt-A and Alt-B.

Given the variability of the Ku Sigma0, there is no significant bias between Alt-A and Alt-B. Notice that biases between the two altimeters for both Ku and C bands have been estimated during the Alt-B calibration phase and actually applied to Alt-B data (Dorandeu, 1999 [16]).

After cycle 236 (first Alt-B cycle), Ku Sigma0 variations seem consistent to what was previously observed with Alt-A. However, two reprocessing steps have been necessary during the Alt-B M-GDR operational production. In fact, Sigma0 trends are adjusted to uncorrected values to compute the correction table, so it was not easy to determine a long term correction based on a short Alt-B period of observation:

- The first reprocessing seems to be due to the platform event (at cycle 256) after which the TOPEX Ku band sigma0 mean value experienced an unexplained increase (Hayne and Hancock, 2000 [28]). Cycles 259 trough 265 were reprocessed (Callahan, 2000 [7], Hayne, 2000 [33]). But Cycles 257 and 258 have been left apart from this correction. Another reprocessing was decided on cycle 277-284 (Callahan, 2000 [7]) in order to correct Sigma0 values for errors of about 0.06 dB in Ku band and 0.12 dB in C band. This corresponds to updated correction tables, once again.
- The study from Hayne and Hancock, 2002 [32] shows that the TOPEX first calibration mode (Cal 1) could only provide a basis for correcting the Side B Ku-band Sigma0 in the first cycles. In operational mode, both Ku and C band calibration tables are actually computed from long term trends adjusted on Sigma0 observations.

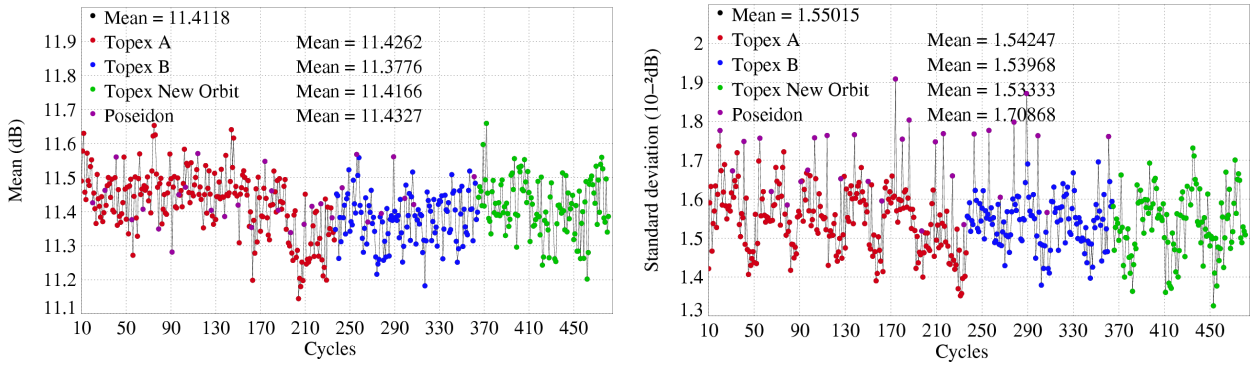


Figure 25: *Cycle mean (left) and standard deviation (right) of Ku-band TOPEX Sigma0 (10-2 dB)*

### 3.7.2 Comparison of Ku-band and C-band Sigma0

Figure 26 shows the cycle mean and standard deviation of the difference between Ku and C bands in terms of Sigma0. The figure accounts for Sigma0 modifications of the calibration tables described above. Cycles 257 and 258 mean values are higher (by about 0.2 dB) because these two cycles have not been corrected in the first reprocessing.

As far as the standard deviation is concerned, the difference between the two bands is now consistent with first values of Alt-A. This parameter had continuously decreased on Alt-A along the mission, maybe due to altimeter changes.

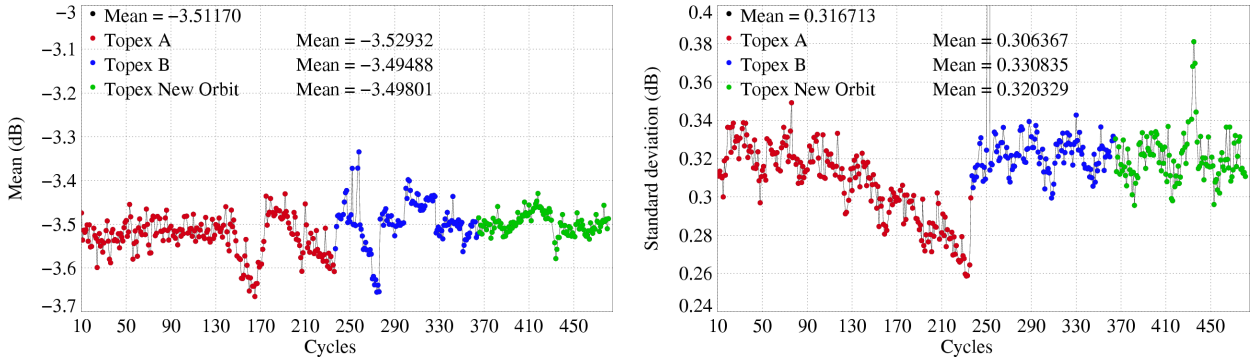


Figure 26: *Cycle mean (left) and standard deviation (right) of differences (10-2 dB) between Ku-band and C-band TOPEX Sigma0 values*

## 3.8 Sea state bias corrections (SSB)

### 3.8.1 BM4 and BM3 SSB

Because of the Sea State Bias (SSB) dependency on SWH (3 or 4-parameter models), both corrections are affected by a downward trend for increasing mean SWH (Figure 27) as it was the case in the last years of TOPEX Alt-A, as mentioned previously. Up to cycle 235, the SWH trend in Alt-A measurements translates into nearly 1 cm in terms of SSB correction. Note that this 1 cm variation creates an unrealistic trend in Mean Sea Level estimations (MSL rise becoming overestimated) due to the SSB correction alone. It also impacts the estimation of the relative bias between TOPEX and Poseidon (also overestimated). But the effect of altimeter drifts on the range itself also adds uncertainty on MSL estimations, and the two effects are partly compensating each other (Hayne and Hancock, 1998 [27]). As the Alt-B SWH values nearly recover those of Alt-A at the beginning of the mission, the Alt-B SSB cycle means also return to the level of first Alt-A cycles.

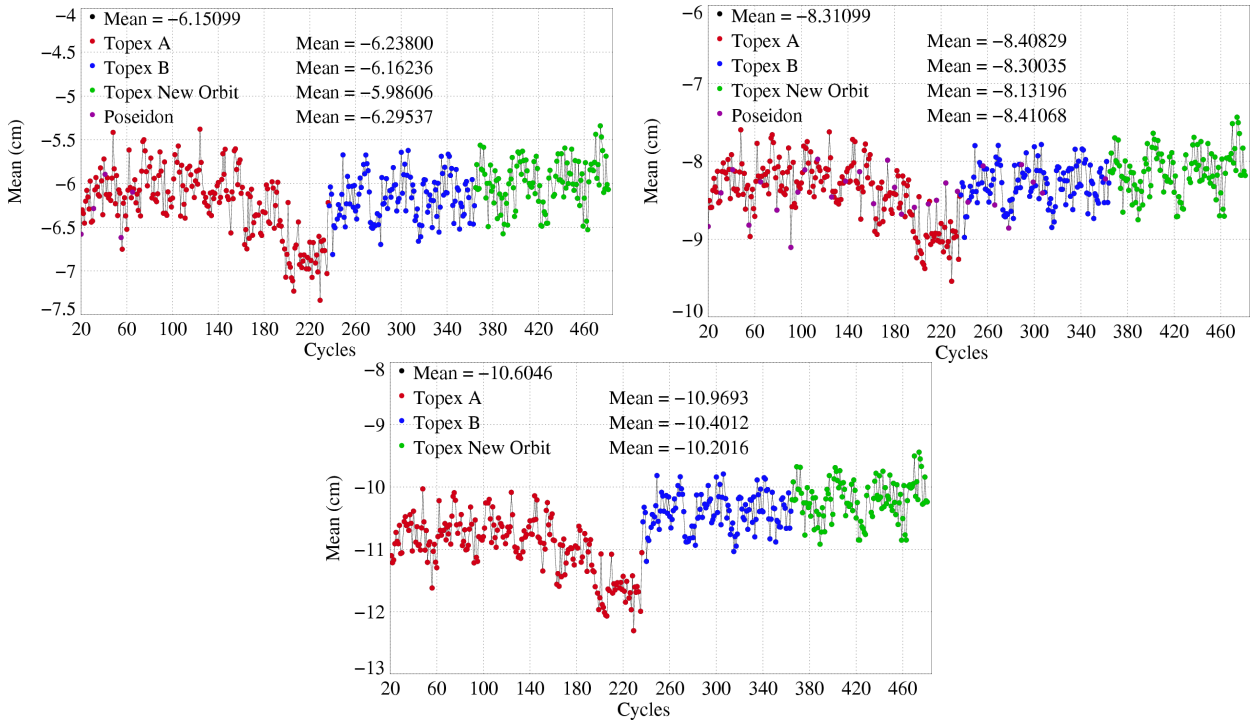


Figure 27: *Cycle means of BM3 SSB (top left), BM4 SSB (top right) and Non Parametric SSB correction (bottom)*

An annual cycle of about 0.3 cm amplitude is present in the cycle mean of the difference between BM4 and NASA BM3 models (Figure 28), because of sea state annual variations differently taken into account by the two models. But no drift can be detected from this figure, and the standard deviation of the difference remains lower than 1 cm RMS.

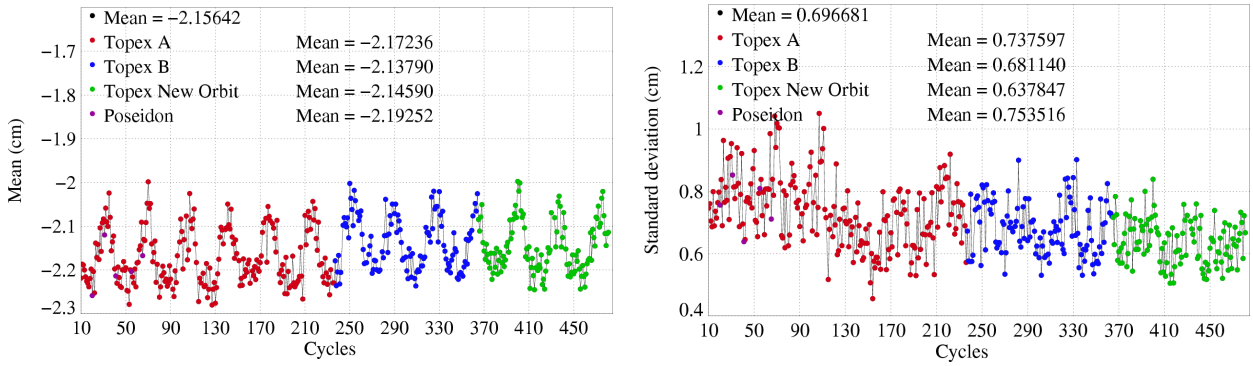


Figure 28: *Cycle mean (left) and standard deviation (right) of differences between BM3 and BM4 SSB corrections*

### 3.8.2 Non Parametric and BM4 SSB

The non-Parametric SSB (Gaspar et al, 2002 [23]) is computed for Alt-A and Alt-B data in order to compare with the BM4 SSB. Note that this Non Parametric SSB is not yet available for Poseidon1 data. The cycle mean of the correction has a similar shape as the BM4 or BM3 SSB (Figure 27). But due to wind and waves differently taken into account by the two models, a bias is observed on the cycle mean of the difference between the two corrections (Figure 29). This bias is about 25 mm during Alt-A period, and about 21 mm in the Alt-B period. It remains stable until the last cycles. It is not the same on the two periods because two different coefficient tables are used for the Non Parametric SSB, one has been computed from TOPEX crossovers on Alt-A period and the other from collinear passes on Alt-B period, while the BM4 SSB has been computed only on Alt-A cycles and is applied on the whole T/P period. Furthermore, the SWH trend observed during the last Alt-A cycles is differently taken into account by the two SSB model and this explains the drift observed on this period leading to a slightly rise of the bias from 25 mm to about 27 mm.

The cycle standard deviation of the difference between the two corrections (Figure 29) has lower values on the Alt-A period (about 7.5 mm) than on the Alt-B period (about 9 mm).

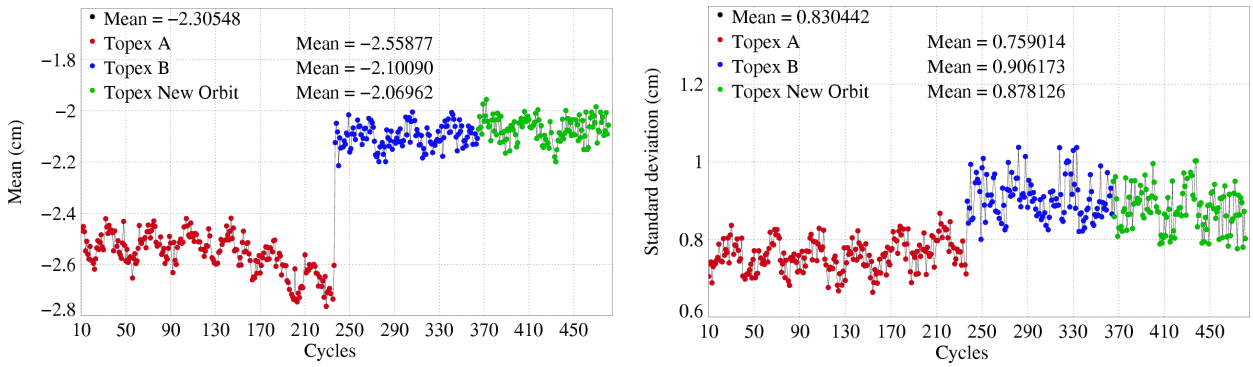


Figure 29: *Cycle mean (left) and standard deviation (right) of differences between BM4 and Non Parametric SSB corrections*

## 3.9 Waveform-deduced off-nadir angle

An estimation of the off-nadir angle is deduced from the shape of the waveforms themselves. Statistics of this parameter are plotted as a function of the cycle number on figure 30. They show an increase of the mean parameter on Alt-A altimeter from cycle 130 to approximately cycle 210, with higher values for cycles 207 and 208. The Alt-A PTR change could be one candidate to explain this mean off-nadir angle rise. A small gap in the mean parameter is observed after cycle 213, which is the first AVISO MGDR cycle accounting for the version 6.3 SDPS software (Callahan, 1998 [6]).
There is no clear evidence of the difference between Alt-A and Alt-B estimations on this figure, even if the first Alt-B cycle (236) seems particular high (maybe due to the time needed by the instrument or the processing to stabilize).
The cycle standard deviation shows a constant value (around seasonal variations) for A1t-A. The anomalous value obtained at cycle 193 is due to a pointing problem during an ASTRA SEU (Callahan 1998 [9] and Hancock, 1998 [26]). Values for Alt-B seem to be about 2.10-3 deg. RMS higher than Alt-A. Cycle 236 leads to the highest value showing that there is much more variability of this parameter for this first Alt-B cycle. Cycle 317 also exhibits a higher cycle standard deviation value for the attitude parameter. This is the result of a clock rollover that occurred during this cycle (Callahan, 2001 [9]). Indeed, even if no significant impact on data quality can be detected, some waveform deduced attitude values between 0.2 and 0.3 degrees are observed during this cycle.
The mispointing values are higher than usual from cycle 433 to 437 due to a pitch wheel event linked to the T/P safehold mode occurred from cycle 430 to 432 (see electronic communication : T/P Daily Status (26/07/2004). Consequently, the satellite had a strong mispointing during this period.

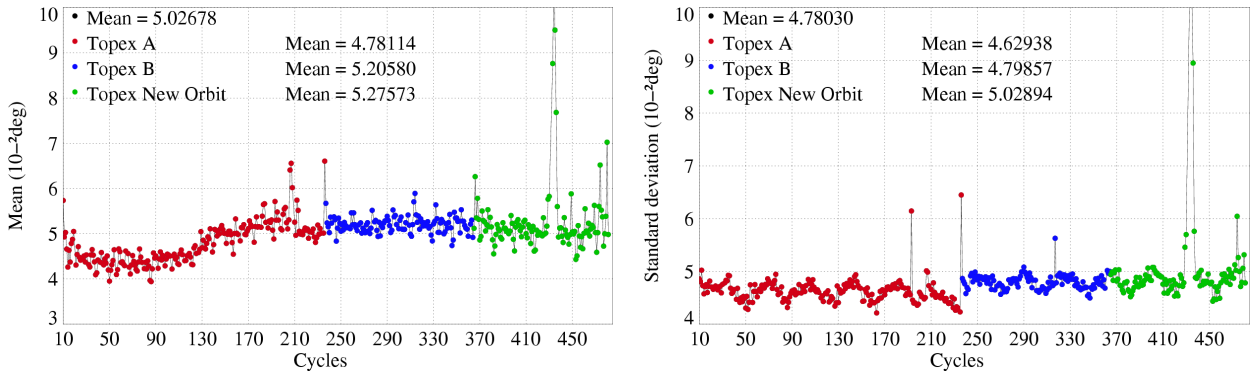


Figure 30: *Cycle mean (left) and standard deviation (right) of waveform-deduced off-nadir angle values*

## 3.10 Cross-Track Distance

It is important that the orbit of the satellite stays within ± 1 km, therefore the cross track distance is monitored. Figure 31 shows, that the orbit is most of the time within the ± 1 km.

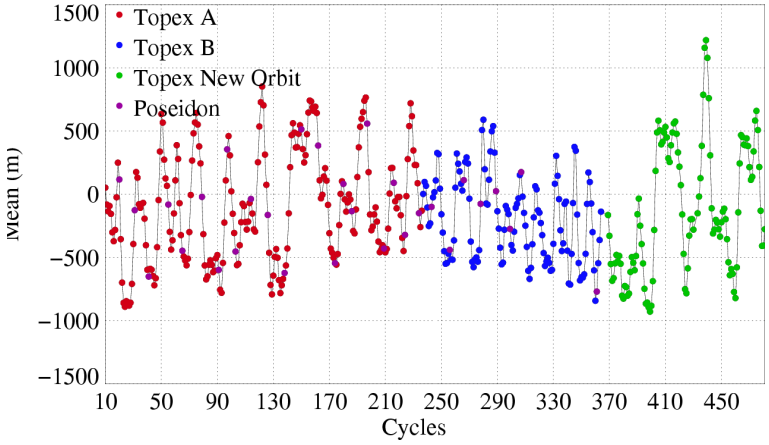


Figure 31: *Mean of Cross-Track distance per cycle.*

# 4 Crossover analysis

Crossover differences are systematically analyzed to estimate data quality and to assess the effectiveness of different corrections applied to Sea Surface Height (SSH). The main SSH calculation, used as a reference, is defined as follows:

$$SSH = Orbit - Altimeter\ Range - \sum_{i=1}^{n} Correction_i$$

with $T/P\ Orbit = NASA\ JGM3\ orbit$ and

$$\begin{aligned}\sum_{i=1}^{n} Correction_i &= Dry\ troposphere\ correction \\ &+ Combined\ MOG2D\ correction\ (high\ frequencies\ from\ MOG2D\ model\ + \\ &\quad low\ frequencies\ from\ inverse\ barometer) \\ &+ Radiometer\ wet\ troposphere\ correction\ (TMR\ corrected\ from\ Scharroo\ 2004). \\ &+ Dual\ frequency\ ionospheric\ correction\ (DORIS\ for\ Poseidon) \\ &+ Non\ Parametric\ SSB\ (BM4\ for\ Poseidon) \\ &+ GOT00.2\ ocean\ tide\ correction\ (with\ consideration\ of\ S1\ wave) \\ &+ Earth\ tide\ correction \\ &+ Polar\ tide\ correction\end{aligned}$$

Except the MOG2D and the GOT00.2 tide correction, all the parameters are extracted from the M-GDR (Aviso User Handbook [2]). The Results presented below are based on a crossover data set from which only SSH differences lower than 30 cm are selected, in order to avoid contamination by spurious measurements, for instance near the coastlines.

## 4.1 Overall results

Data quality can be monitored from the cycle-by-cycle standard deviation crossover differences which are computed using the main analysis defined above. Figure 32 shows the trend in the standard deviation according to the cycle number. Some general features can be deduced from this figure:

- The standard deviation is between 5.5 and 7.5 cm, showing the excellent quality of the data.
- The crossover standard deviation tends to decrease in the first part of the mission.
- An annual cycle appears on this figure, with maximum values of the global crossover standard deviation in summer (northern hemisphere summer).
- The Side-A altimeter problems, detected for example in the Alt-A SWH parameter, seem to have no quantifiable impact on the crossover standard deviation.
- Higher values are obtained from Poseidon cycles, particularly in the last years (cycles 243 to 299).
- The ground track change after cycle 365 seems to have no impact on the crossover standard deviation.

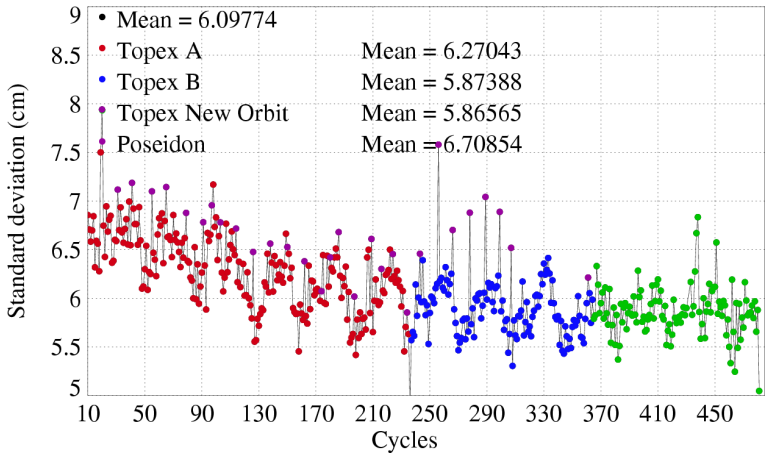


Figure 32: *TOPEX/Poseidon crossover cycle standard deviation, from cycle 11 to cycle 481. Only crossover differences less than 30 cm are selected*

In order to better assess the system performances, the same analysis has been performed selecting deep ocean areas ($oceandepth < -1000m$), with low ocean variability ($< 20cm\ rms$), excluding high latitudes to avoid contamination by ice. The results are plotted on figure 33. The overall standard deviation is lower than 6 cm RMS. No trend and no seasonal signal can be detected, showing the impact of crossover selection and the influence of high latitudes in the previous figure (Figure 32), given the great number of crossovers in these zones.

A dedicated study was performed in a previous annual report (Dorandeu et al., 2001 [17]) to analyze the variance of crossover differences by latitude bins. The study showed that the decreasing trend was particularly located at high latitudes in the Southern hemisphere (below 60S): the crossover variance decreases by about 15 $cm^2$ in these areas which count, on average, for almost $\frac{1}{4}$ of the total number of crossover points. As these zones are known to be the most impacted by atmospheric pressure variations, the same analysis was performed without applying any pressure induced correction (neither dry tropospheric nor inverse barometer corrections were applied). Comparing the two results allowed computing the variance explained by atmospheric corrections at crossovers. The study showed that the variance explained by pressure induced corrections particularly increases for latitudes below 60S, with the same order of magnitude (15 $cm^2$) as the fall in the variance of fully corrected SSH crossover differences.

Thus the decreasing trend in the TOPEX/Poseidon crossover variance seems to be mainly due to pressure corrections, maybe because of improvements in the ECMWF meteorological model (see Figure 16). The impact of these corrections is largely located at high latitudes, explaining why no trend can be detected from crossover analysis excluding these zones. The analysis by latitude bands also showed annual cycles at hemispheric scale essentially located in high latitude areas. In the southern hemisphere, at these latitudes (higher than 40 degrees), the number of crossover points is about 3 times greater than in the northern hemisphere, because of much more ocean surface. This basically explains why an annual cycle appears at global scale, in phase with the southern hemisphere annual cycle.

The quality of Poseidon cycles, showed as violet dots on figure 32, can be compared to that of TOPEX. A difference in the crossover variance is observed between the two altimeters, and this difference tends to increase in the last cycles (except cycle 361). Since among all the corrections used to compute the SSH only the ionospheric correction differs between the two kinds of data, it is interesting to use the DORIS correction

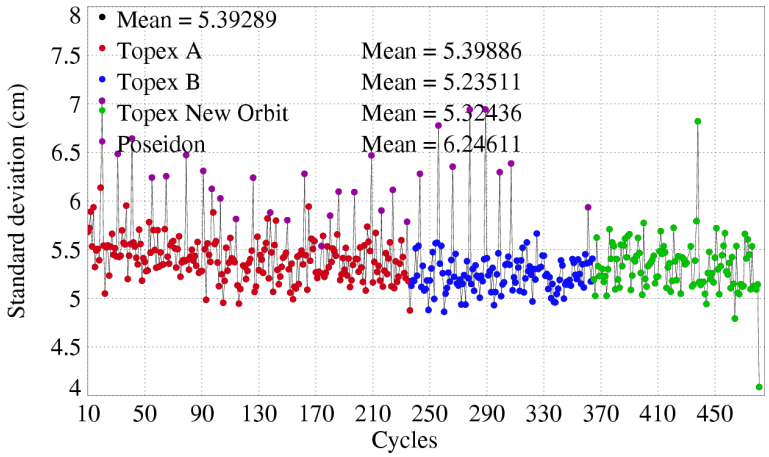


Figure 33: *TOPEX/Poseidon crossover standard deviation, when selecting:latitudes between 50S and +50N; low ocean variability areas (ocean variability* $< 20cm$*); open ocean areas (depth* $< -1000m$*)*

for both altimeters and to compare the results (Figure 34). Using the DORIS ionospheric correction makes the results from TOPEX and Poseidon altimeters much more consistent. Thus it shows that the DORIS ionosphere correction degrades the crossover variability, essentially in the second part of the mission and explains why higher differences are found between TOPEX and Poseidon in the last years (Figure 33). The crossover variances using TOPEX dual frequency and DORIS corrections will be specifically analyzed in the dedicated section 4.5.

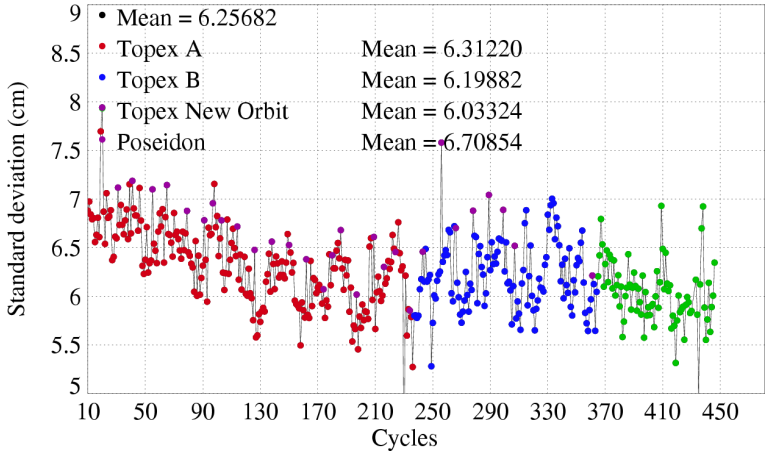


Figure 34: *TOPEX/Poseidon crossover standard deviation when using the DORIS ionosphere correction (same as Figure 32 but with DORIS instead of TOPEX ionosphere correction)*

However, differences of about 2 $cm^2$ remain between TOPEX and Poseidon after applying the same ionosphere correction. It is known that TOPEX data are somewhat filtered due to the altimeter processing (tracker processing instead of retracking), which explains the noise difference with Poseidon (Le Traon et al, 1994 [36]). This can translate into different crossover variance from the two altimeters.

Figure 35 (right) shows the geographical pattern of the crossover standard deviation computed from cy-

cle 11 to cycle 481 and averaged over bins of 4x4 degrees. Please remind that here the MOG2D correction was used. In some high-latitude areas of the northern hemisphere, e.g. the Bering Strait and Hudson Bay, the standard deviation is always high (over 13 cm RMS), probably because of bad ocean tide modeling. Deficient tide models degrade also the results in some coastal areas and enclosed seas. The map also gives "conventional" information on the high variability of the major ocean currents (Gulf Stream, Kuroshio, Confluence zone, Agulhas Current), with higher variability in the western parts of the basins. As a comparison, the left of figure 35 shows the crossover standard deviation from last years report ([1]), where the MOG2D correction was not yet used (but only inverse barometer). The standard deviation of the crossover differences in high latitudes is clearly more important compared to the case when MOG2D is used. This is related to the high pressure variability at high latitudes (Le Traon et al., 1996 [37]) which is imperfectly accounted for in the inverse barometer correction.

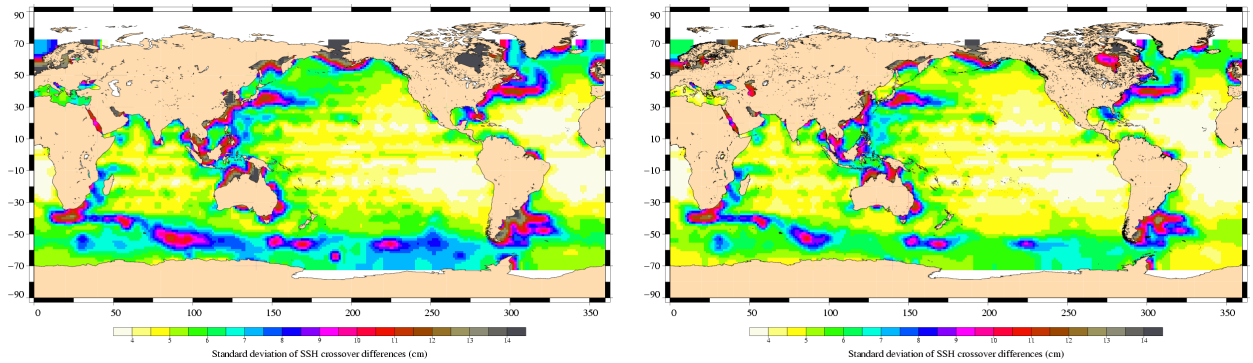


Figure 35: *Geographical pattern (4x4 degree bins) of TOPEX/Poseidon crossover standard deviation (cm), without MOG2D correction from cycles 11 to cycle 444 (left) and with MOG2D correction from cycle 11 to cycle 481.*

From this map, the system accuracy can be estimated: the sea surface height (SSH) variance can be split into a component due to ocean variability, and a component due to residual orbit errors and errors in both instrumental and geophysical altimeter corrections. If there was an area with zero ocean variability, we could derive an estimate of the absolute system performance. Areas of weakest variability (which increase errors due to the system) yield a crossover standard deviation lower than 3-4 cm. Since crossovers are differences between ascending and descending passes, the result needs dividing by 2 to estimate the precision (assuming errors between two crossing passes are not correlated). However, this estimate does not include geographically-correlated orbit error, which cancels out at crossovers. This analysis therefore shows that system precision is better than 3 cm for isolated measurements.

The same type of map can be produced for the averaged crossover differences. In some areas, Figure 36 shows systematic differences between ascending and descending passes, on the order of 3-6 cm, which are probably due to geographically-correlated orbit errors.

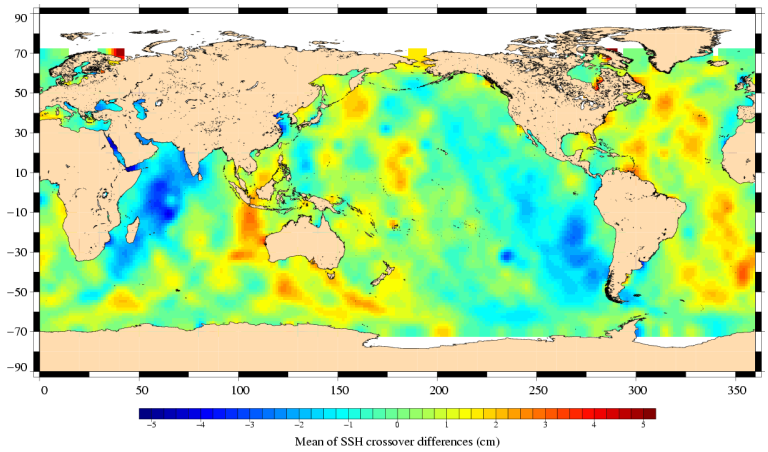


Figure 36: *Geographical pattern (4x4 degree bins) of the mean of crossover differences, from cycle 11 to cycle 481.*

## 4.2 Comparison of NASA and CNES orbits

The two orbit fields present in the M-GDRs can be compared in terms of crossover variance. Computing the cycle by cycle difference between the variance using the CNES orbit and the variance using the NASA orbit leads to the results plotted in figure 37. The CNES orbit globally increases the variance by about 2.1 $cm^2$ relative to the NASA orbit but the degradation is particularly high from cycle 100 to cycle 246. As mentioned before (section 3.2), during this period the DORIS station coordinates have not been updated in the CNES orbit computation. This of course impacts the global orbit quality in the long-term. The difference in crossover variance is clearly reduced since the use of the IRTF97 reference frame for the CNES orbit starting at cycle 247. The CNES orbit performance at crossovers has been even more improved after introducing the ITRF2000 reference frame and the albedo model at cycle 320. The crossover variance difference between NASA and CNES orbits is than very close to zero except during the orbit transition from cycle 365 to cycle 368. Since the last day of cycle 446 (1st November 2004), Doris is switched off. In consequence, the error between the 2 orbits is increasing.

The four plates of Figure 38 respectively show the geographical pattern of the difference in crossover variance between CNES and NASA orbits before cycle 246 (top left), from cycle 247 to cycle 319 (top and right), from cycle 320 to cycle 364 before the orbit change (bottom and left) and after cycle 369 after the orbit change (bottom and right). The 4 periods correspond to the changes in the CNES orbit calculation (ITRF97 at cycle 247, ITRF2000, albedo model at cycle 320 and the orbit change from cycle 365 to 368). The figure shows the improvements made to the CNES orbit calculation by changing the reference frame. From cycle 320 onward, the relative performances of the two orbits are globally balanced and in the last period, after the orbit change, the CNES orbit seems slightly better. Indeed, in order to improve the CNES orbit calculation, the Hill force has been adjusted since September 2002 over a period of 1 day instead of 3 days. Moreover ITRF2000 has been applied in the NASA orbit calculation from cycle 360 onward. As a result, the consistency between 2 orbits is better.

Differences between ascending passes and descending passes have been computed for the two orbits and averaged in geographical bins for the whole T/P mission. The local means are then compared on Figure 39. Systematic differences in the crossover mean, along the satellite track, are as large as 2 cm. These long

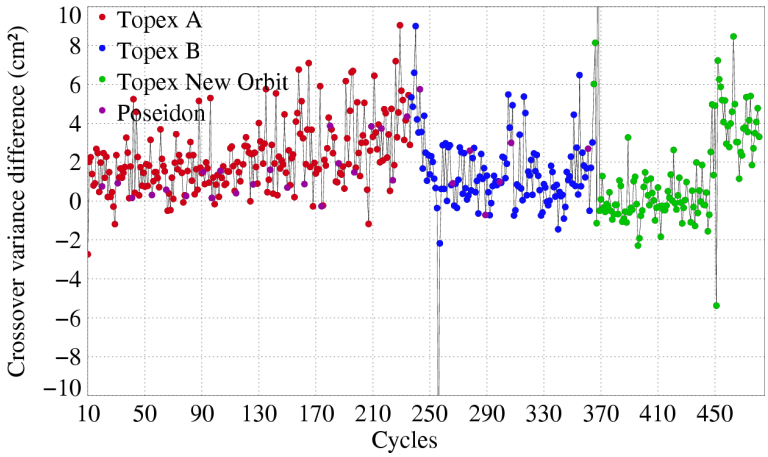


Figure 37: *Gain in crossover variance (cm2) when using NASA orbit rather than CNES orbit*

wavelength signals may be due to geographically correlated orbit errors.

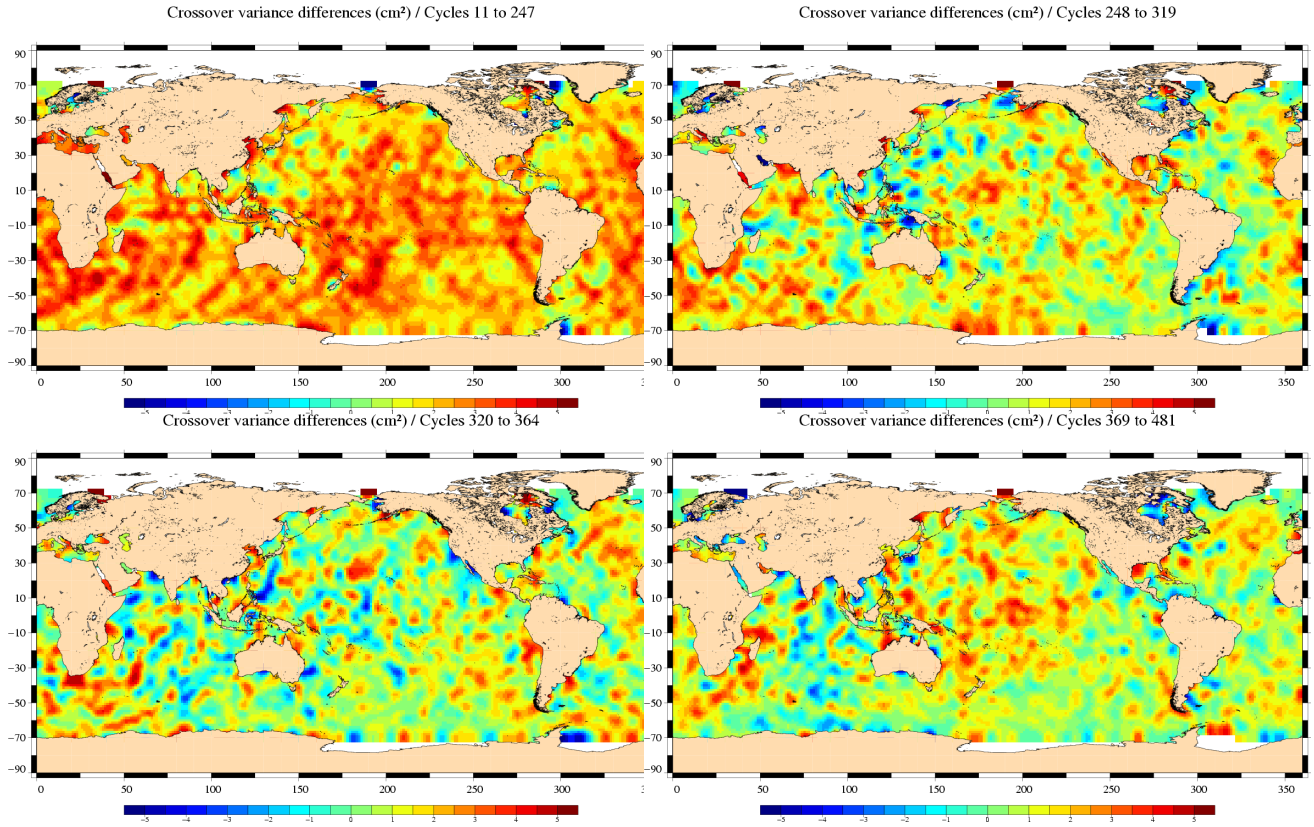


Figure 38: *Difference in crossover variance (cm2) when using NASA orbit rather than CNES orbit, before use of the ITRF97 set of coordinates in the CNES orbit (top left), with the use of ITRF97 (top right) and with ITRF2000 before (bottom left) and after the orbit change (bottom right)*

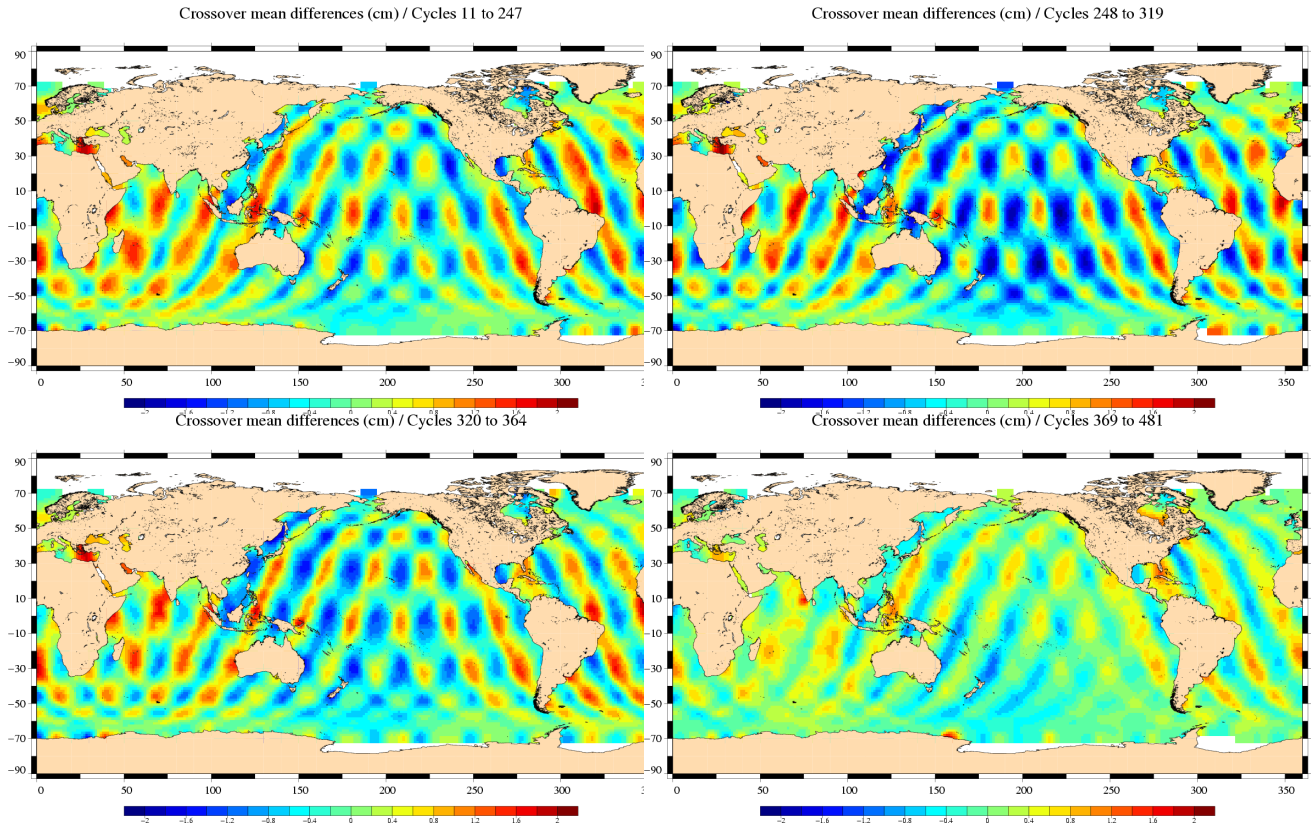


Figure 39: *Difference in crossover means obtained when using NASA and CNES orbits*

## 4.3 Comparison of tidal models

### 4.3.1 CSR3.0 and FES95.2

Since no changes have been made to the tidal models used in the M-GDRs, no difference relative to the results presented in the T/P annual report from 2001 (Dorandeu et al., 2001 [17]) are expected. One should thus refer to this previous report for a comparison of CSR3.0 and FES95.2 performances at crossovers.

### 4.3.2 GOT99 and CSR3.0

Results of crossover variance difference when using the GOT99 tidal correction rather than the CSR3.0 tidal correction are presented in the T/P annual report from 2004 (Ablain et al., 2005 [1]).

### 4.3.3 GOT00V2 and GOT99

Figure 40 shows the crossover variance difference when using the GOT00.2 tidal correction rather than the GOT99 tidal correction. The GOT00.2 tidal correction yields the best performances particularly near to the coasts (Figure 40) and in semi-enclosed seas, but the improvements provided by this model are also significant in deep ocean areas. These improvements come essentially from two sources: Firstly, to develop GOT00V2 not only TOPEX/Poseidon data were used, but also ERS2 data (which can sample nearer the coast than TOPEX). Secondly, a longer time period was used to develop the GOT00V2 model (see Ray,1999 [45]).

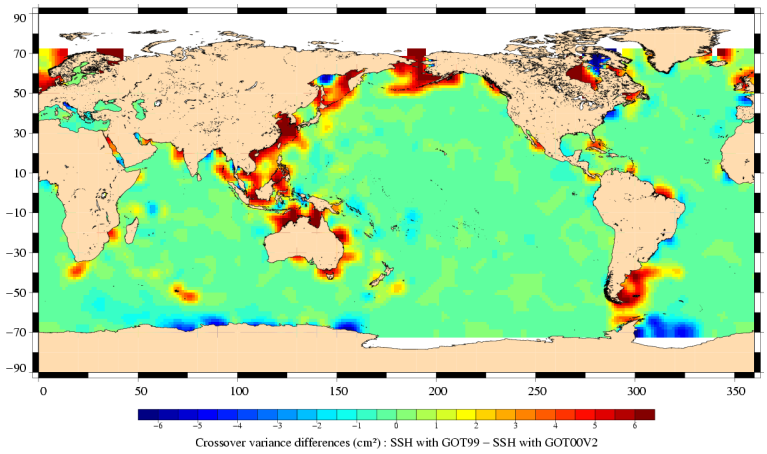


Figure 40: *Gain in crossover variance (cm2) when using the GOT00V2 tidal correction rather than the GOT99 tidal correction*

## 4.4 Comparison of radiometer (TMR) and model (ECMWF) wet troposphere corrections

Figure 41 shows the crossover variance difference when using the TMR correction rather than the ECMWF troposphere model. The variance difference is about 4 $cm^2$. But the improvements made to the model (see section 3.4.3) result in a decreasing variance relative to the TMR correction. A gain in crossover variance of about 2 $cm^2$ is obtained in the last cycles by the ECWMF model relative to the first part of the mission.

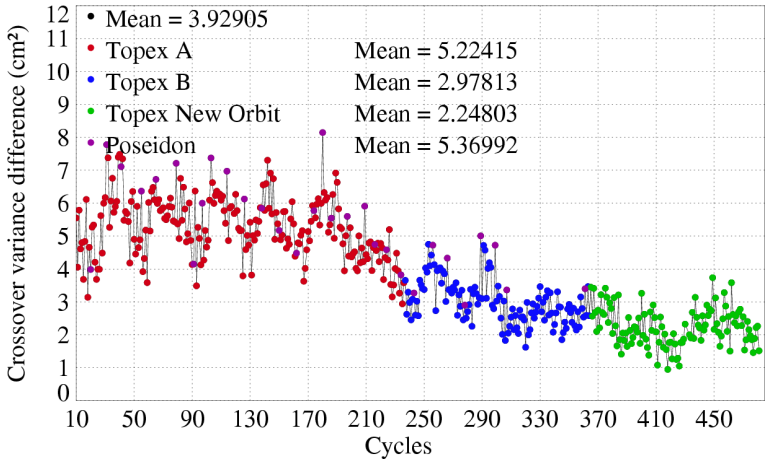


Figure 41: *Gain in crossover variance (cm2) when using the TMR wet troposphere correction rather than the ECMWF correction*

The gain in variance when using the TMR correction rather than the ECMWF correction is higher in the wettest areas (Figure 42).

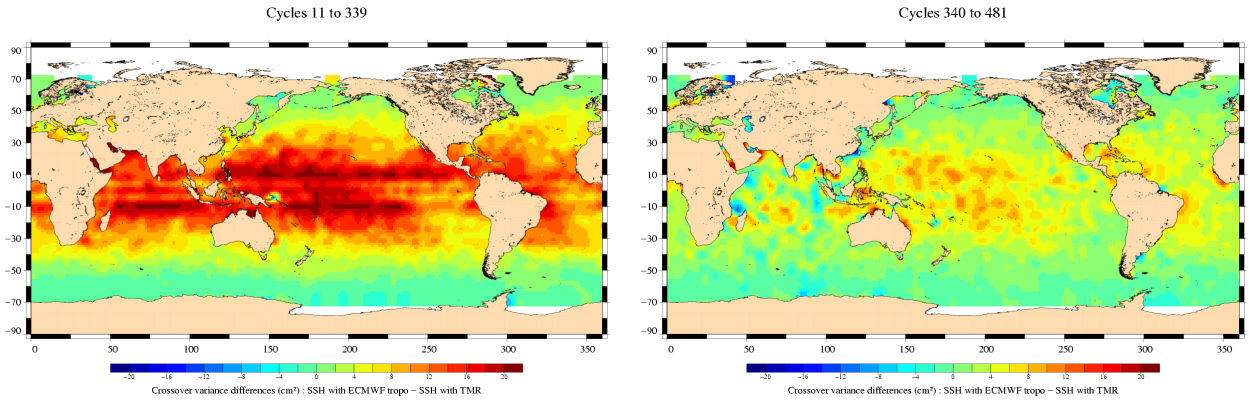


Figure 42: *Gain in crossover variance (cm2) when using the TMR wet troposphere correction rather than the ECMWF correction*

## 4.5 Comparison of Topex dual-frequency and Doris ionosphere corrections

Taking the dual-frequency ionosphere correction as a reference and using only TOPEX crossover points, the same type of analysis as above has been achieved. The dual frequency ionosphere correction was first filtered using a low-pass Lanczos filter and a cutoff wavelength of 300 km.

The crossover variances difference when using the TOPEX (dual-frequency) ionosphere correction rather than the DORIS correction is shown on Figure 43. Over the whole period the difference is nearly 2 $cm^2$ (Figure 43 on the left). Thus, the dual frequency correction yields the best performances, particularly in the year 2001, when the solar activity reaches its maximum over the TOPEX/Poseidon mission. Between cycles 290 and 370, the difference between DORIS and TOPEX crossover variances is as large as 5 $cm^2$. It explains the major part of the greater variance obtained with Poseidon data relative to TOPEX in this period. In the last years, solar activity has decreased, so has the difference between DORIS and TOPEX crossover variance.

The results are clearly degraded by the use of the DORIS correction around the geomagnetic equator (Figure 43 on the right). In these areas the DORIS correction poorly retrieves the equatorial ionosphere spikes and often lowers the crest of them. But in some high SWH areas, up to 1-2 $cm^2$ of variance is added by the dual frequency correction relative to DORIS. Instrumental drifts and losses of accuracy in Alt-A SWH estimation may also impact the results.

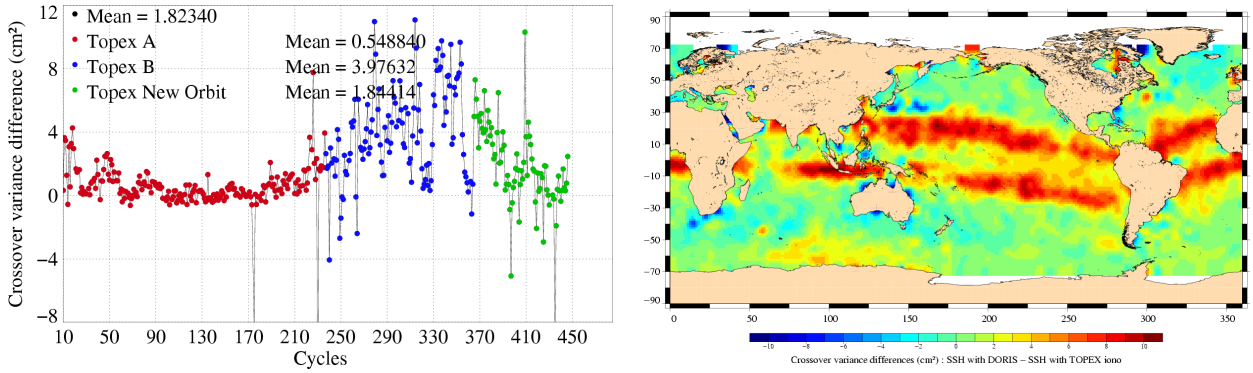


Figure 43: *Difference in terms of crossover variance (cm2) when using the TOPEX ionosphere correction rather than DORIS*

Figure 44 compares the crossover mean differences obtained using DORIS and TOPEX ionosphere corrections. The figure thus compares differences between ascending and descending passes computed respectively with DORIS and TOPEX corrections. Using only Alt-A measurements (i.e. cycles 11 to 235), a slight difference on the order of a few millimeters is observed between the two hemispheres. The same type of map is obtained when comparing the BENT model and the dual-frequency correction (not shown here). One hypothesis could be that the altimeter processing causes this kind of behavior, due to hemispheric corrections.

When using only Alt-B measurements (i.e. cycles 236 to 481), the results are dramatically different. On the one hand, differences are much more contrasted maybe because of the high solar activity through the considered period. On the other hand, differences at hemispheric scale are from the opposite relative to

those obtained with Alt-A. Therefore this change seems to be due to the altimeter processing.

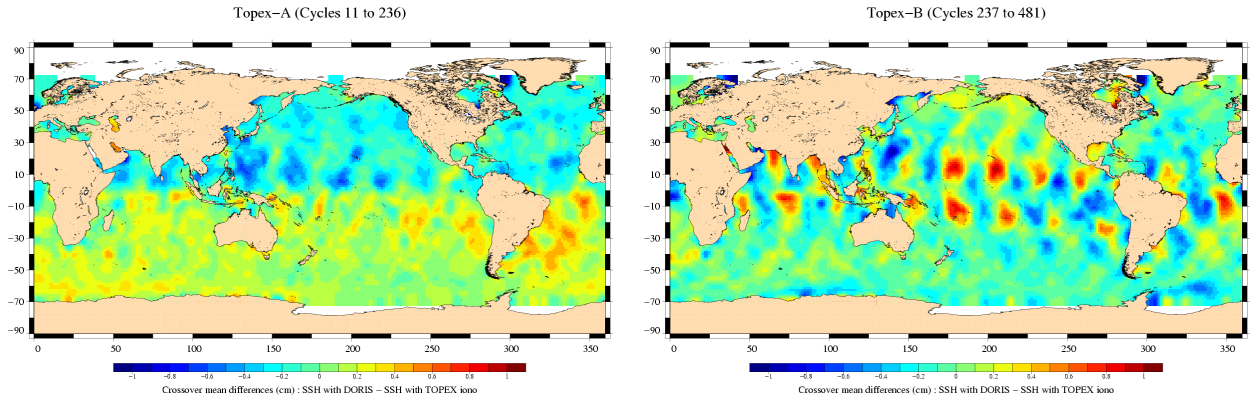


Figure 44: *Comparison of mean crossover differences obtained when using DORIS and TOPEX ionosphere corrections (DORIS  TOPEX), with Alt-A cycles (left) and Alt-B cycles (right)*

## 4.6 Comparison of sea state bias corrections (SSB)

### 4.6.1 BM4 and Non-Parametric SSB

The four-parameter (Gaspar et al., 1994, [22]) and the Non-Parametric (Gaspar et al., 2002, [23]) Sea State Bias (SSB) corrections have been compared in terms of crossover variance (Figure 45 bottom), only for TOPEX data, since the Non-Parametric SSB is not available for Poseidon. The BM4 SSB has been computed using only Alt-A cycles contrary to the Non-Parametric SSB which uses two different coefficient tables: the first has been computed on the Alt-A period and the second on the Alt-B period. This explains the significant difference of performance between the two SSB models from cycle 237 onward (Alt-B cycles).

The geographical pattern of the gain in variance using non parametric model rather than BM4 is presented on Figure 45 with two maps in order to distinguish Alt-A cycles (on the left) from Alt-B cycles (on the right). The significant gain obtained on Alt-B cycles is clearly visible in regions where large waves are usually observed, at latitudes higher than 30 degrees.

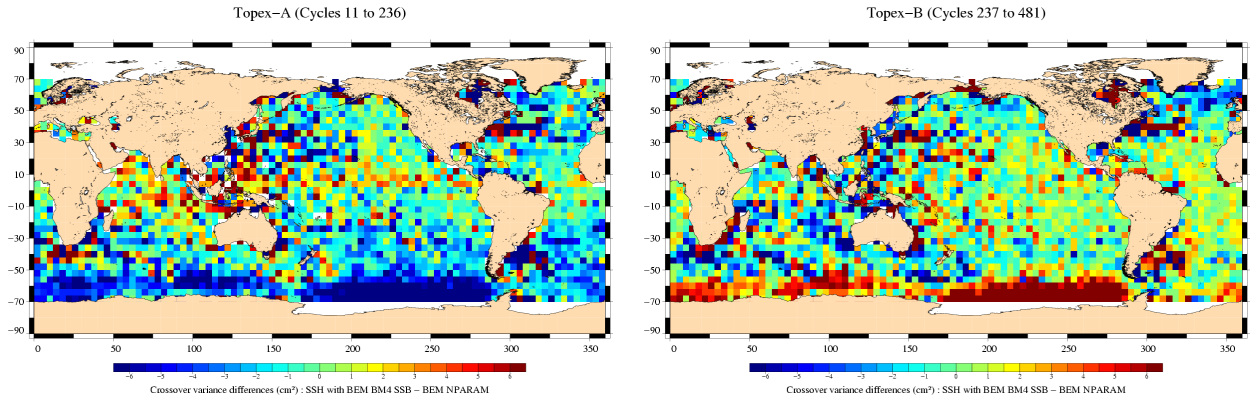


Figure 45: *Gain in crossover variance (bottom) when using non-parametric SSB correction rather than BM4 SSB with Alt-A cycles (left) and Alt-B cycles (right)*

# 5 Topex/Poseidon / ERS cross-calibration

ERS OPR ([20]) produced by CERSAT (French Processing and Archiving Facility for ERS-1 and ERS-2) at IFREMER have been used to achieve this study. ERS-1 and ERS-2 OPR data quality assessment and cross-calibration relative to TOPEX/Poseidon are routinely performed at CLS under IFREMER contract. Dual crossovers are computed from TOPEX/Poseidon M-GDR data and ERS data allowing comparisons of both altimeter and radiometer parameters.
For more informations, the ERS-2 annual report from 2005 about calval activities is available at: http://www.jason.oceanobs.com/documents/calval/validation_report/tp/annual_report_e2_2005.pdf.

## 5.1 SWH cross-calibration

Both ERS-1 and ERS-2 data sets have been used to compute statistics of the differences between TOPEX/Poseidon and ERS SWH estimations (figure 46). Only SWH crossover differences with a maximum time lag of 1 hour are selected to limit sea state variability. The differences are then averaged over 12 TOPEX cycles to get homogeneous sampling. This could not be done with Poseidon for which the mean is computed over only 1 cycle, explaining the noisier (ERS-Poseidon) differences.
For ERS-1 and TOPEX/Poseidon comparisons, phases C ($1^{st}$ 35-day repeat mission, October 1992 - December 1993) and G ($2^{nd}$ 35-day repeat mission, March 1995 - June 1996) of ERS-1 have been reprocessed in version 6, phases E-F (geodetic mission, April 1994 - March 1995) are still in version 3. The differences obtained between the three time series can be explained by the following reasons: a bias of 12 cm is obtained between version 6 and version 3 (the two last time series), and the mean SWH is impacted in the long-term by the IF filter drift (Mertz et al., 2002 [41]).
The Side-A TOPEX SWH drift is clearly evidenced on figure 46, since differences between ERS-2 and Poseidon remain almost constant during the same period. A variation as large as 35 cm in the Alt-A SWH can be deduced from these results. The gap between Alt-A and Alt-B can also be easily estimated and it is confirmed by the results of TOPEX-alone statistical monitoring (Figure 23). Notice that the Alt-B SWH mean level is about 5 cm lower than the one of Alt-A around cycles 110-120.
The last Alt-B estimates seem steadier than the Alt-A estimations, even though around cycles 270 and 310, the mean differences relative to ERS-2 can increase to about 8 cm. These variations can be attributed to ERS-2 since during cycles 60 to 62, many problems occurred to ERS-2. From figure 46, no trend can be detected in (ERS - Poseidon) SWH differences.

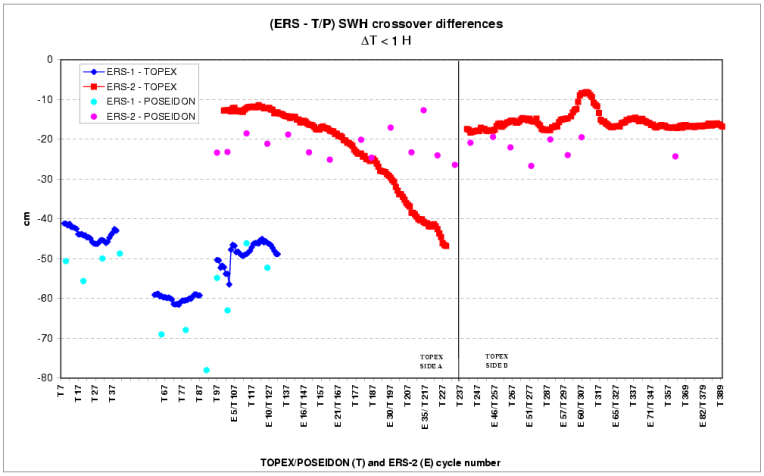


Figure 46: *Differences of SWH at 1 hour crossovers between ERS and TP. Except for Poseidon, each point is obtained averaging differences over 12 TOPEX cycles*

## 5.2 Sigma0 cross-calibration

Sigma0 differences between ERS and TOPEX (Ku band) measurements have also been processed as described above and plotted on figure 47. Major variations in the (ERS-2 - TOPEX) mean differences up to TOPEX cycle 270 seem to be due to TOPEX and can be correlated to what is observed in the Sigma0 statistical monitoring (figure 25). For instance, the increasing mean difference between ERS-2 and TOPEX backscatter coefficients form cycle 160 to cycle 220 can be attributed to TOPEX, since this variation is also observed in the TOPEX-alone trend. After cycle 270, one should be less confident on ERS-2 Sigma0 estimations. In fact, large drops in ERS-2 Sigma0 occurred during the year 2000 (Dorandeu et al., 2000 [18]). Although the ERS-2 Sigma0 drops have been corrected in the results presented on figure 47, according to the recommendations from this study, large degradation in the ERS-2 measurement due to mispointing explains the bell shape observed in (ERS-2 - T/P) differences between cycles 260 and 300. Moreover, many problems occurred in cycles 60 to 62 ERS-2 (Mertz et al., 2002 [39]), leading to a large decrease around cycle 313.

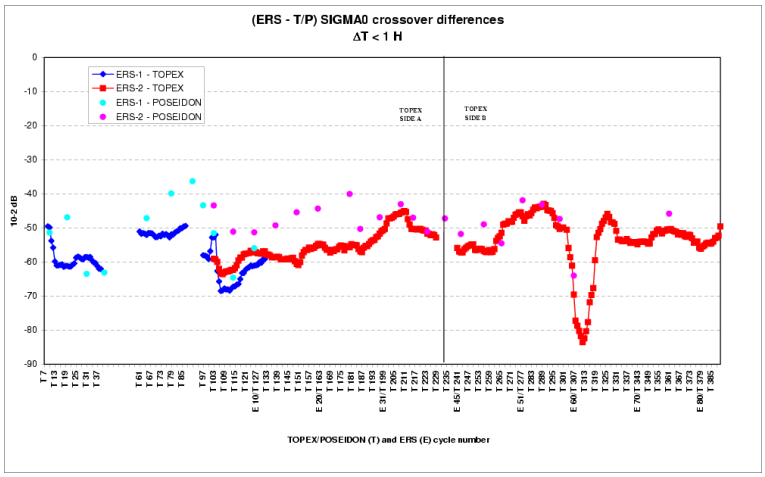


Figure 47: *Differences of Sigma0 at 1 hour crossovers between ERS and TP. Except for Poseidon, each point is obtained averaging differences over 12 TOPEX cycles*

## 5.3 Topex / ERS radiometer cross-calibration

Comparison between the TOPEX microwave radiometer (TMR) and the ERS-2 microwave radiometer (MWR) has been carried out following the method detailed in Stum, 1998 [50]. It consists in comparing the measurements of the two satellites at TP/ERS crossover points with less than 1-hour time lag. Estimates of the differences are made over time periods of 12 TP cycles, to get homogeneous and repeatable sampling of the atmosphere. The mean value of the (TMR - ERS ATSR/M) wet tropospheric correction difference at these crossovers is computed. Studies have been carried out to calculate the drift over time of the TMR path delay (Ruf, 2002 [48]). The data set has been corrected for in this study. Figure 48 shows the (T/P - ERS-2) crossover mean wet tropospheric correction difference versus the series of 12 T/P cycles time periods. The TMR path delay was corrected for the drift in this figure. The abscissa of each reported value is referred to the end of the 12-cycle period (e.g. for the 12-cycle period 2 to 13, the abscissa is 13, and so on). The values obtained for ERS-2 data may not be confident: indeed, a drift appears in the 23.8 GHz brightness temperature (see Obligis et al., 2003, [44]) and may be reevaluated. A new correction was proposed by Scharroo et al., 2004 ([51]) to take into account the gain fall, the drift, and the stop of the drift in April 2000. An evaluation of those corrections is under investigation at CLS and will be presented in the annual report of ERS-2 (Mertz et al., 2005 [40]). The most prominent feature of figure 48 is the increase of the difference after T/P cycle 157 (December 1996). The small oscillations with a one-year time period are probably due to annual variation of the crossovers sampling: during summer, less crossovers with dry atmospheres are sampled, because of the sea ice extension in the Southern hemisphere, and this leads to a higher mean of the T/P-ERS path delay difference.

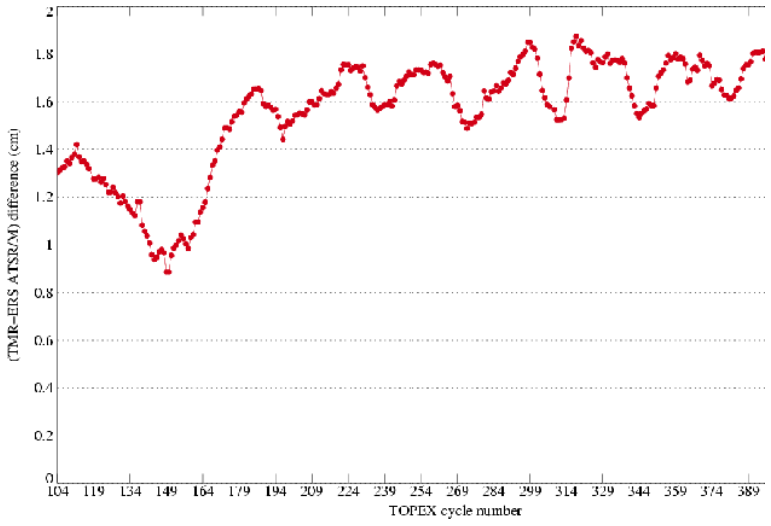


Figure 48: *Differences of Sigma0 at 1 hour crossovers between ERS and TP. Except for Poseidon, each point is obtained averaging differences over 12 TOPEX cycles*

# 6 Repeat-track analysis

This analysis is used to compute Sea Level Anomalies, variability and thus to estimate data quality, but also to determine the trend in the Mean Sea Level (MSL) and the relative bias between Alt-A, Alt-B and POSEIDON altimeters.

A mean profile was estimated from seven years of TOPEX/Poseidon data, to integrate ocean signals over a representative period. This reference point can thus be used to compute Sea Level Anomalies (SLA) until cycle 364. Due to the orbit change between cycles 365 and 368, the T/P orbit is not repetitive and no nominal track is available during this period. Therefore it is not possible to compute SLA. On the new ground track, there are too few repeat cycles to allow computing a significant reference profile. Thus SLA are computed relative to the CLS01 Mean Sea Surface (Hernandez et al, 2001) (CLS01 MSS) also estimated from the same seven years of T/P data.

## 6.1 Ocean variability

The sea-surface variability map for the period covering cycles 11 to 481 (Figure 49) is obtained by geographically calculating the standard deviation of the altimeter residuals relative to the mean profile (or to the MSS).

This variability can be split into a component due to ocean signal itself (notice the very high variability in the area of the major ocean currents) and also into other components including residual orbit errors and errors due to altimeter corrections. In the repeat-track method, most of the orbit error (the component due to errors in the geopotential model) cancels out. The geographical areas with lowest variability yield standard deviation values on the order of 3 to 4 cm, which can be taken as an estimate of the system precision. This analysis therefore confirms the results derived from crossover analysis.

Apart from major currents areas (Gulf Stream, Kuroshio, Agulhas current, Confluence zone, circumpolar current), high variability is observed near the coastlines and in enclosed seas where tidal models are less efficient. Higher variability is also observed near the equator: the "El Niño" and "La Niña" events (eg. 1997-1998) increase the variability in the equatorial Pacific.

The cycle-by-cycle SLA standard deviation has been computed and plotted on Figure 50. It shows the large impact of the 1997 El Niño event increasing the ocean variability by about 1 cm rms at global scale. After 1999, higher variability is obtained because the reference 7-year mean profile does not include all particular ocean signals of the last years. The variability increases in October 2002 due to another "El Niño" situation. In addition, with T/P on its new ground track, one should expect higher SLA variability just because the MSS is less precise outside the nominal track (Hernandez et al).

In terms of measurement quality, this study confirms crossover analysis results: there is no difference between Alt-A and Alt-B. Higher variance is obtained for some very incomplete Poseidon cycles (e.g. cycles 256 and 278).

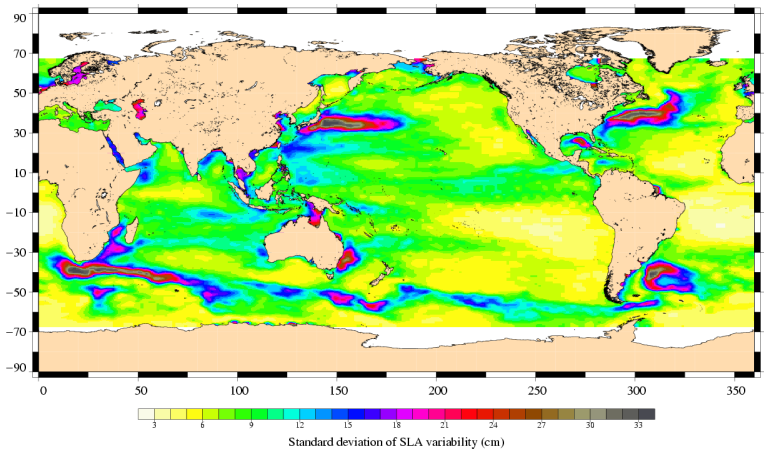


Figure 49: *Map of SLA variability (cm) from collinear analysis of T/P data from cycles 11 to 481.*

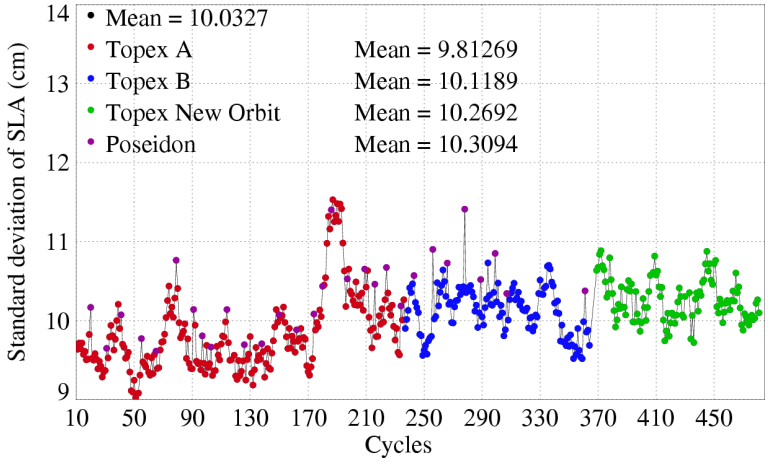


Figure 50: *Cycle per cycle monitoring of SLA variability (cm) from collinear analysis of T/P data from cycles 11 to 481.*

## 6.2 Mean sea level variations

### 6.2.1 Main results

The cycle-by-cycle mean of the residual heights can be used to estimate the trend in the MSL as observed by TOPEX/Poseidon. The value for each cycle is calculated from averaging over 2° by 3° bins, then weighting by latitude to take account of the relative geographical area represented by the bin. Moreover the annual, semi-annual and 60 day variations have been removed.

The relative bias between TOPEX and Poseidon, clearly marked in the last Alt-A cycles, has been taken into account. Furthermore, as already shown in the comparison between TOPEX and DORIS ionosphere corrections (section 3.5.2), the drift between the two corrections has been corrected for on Poseidon cycles.

Based on the studies from several authors (e.g. Ruf, 2000 [49], Kheim et al., 2000 [34]), there is now a consensus among most of SWT members considering that a TMR drift correction should be applied to the TOPEX/Poseidon data for MSL estimations. Therefore, in this study the long term TMR drift correction from Scharroo (2004, [51]) was applied.

Figure 51 shows the cycle-by-cycle MSL estimations from cycle 11 to cycle 481 for Alt-A, Alt-B and Poseidon using the NASA orbit and the MOG2D correction (including inverse barometer correction).

- The last 1997 "El Niño" event leads to an unprecedented MSL rise (since the beginning of the mission), showing that long time series are needed to infer climate change conclusions from MSL estimates at the level of precision of 1 mm/year
- After El Niño, the MSL falls down back, but again rises in the last Alt-A cycles. We know that, via the SSB correction (SWH increase), the impact of the Alt-A instrumental changes on MSL estimations is non-negligible, even though effects on the range measurement tends to compensate the effect of SSB. This may explain the higher MSL for the last Alt-A cycles.
- The Alt-B MSL estimations lead to a gap between 0.5 and 1 cm relative to the last Alt-A cycles, but they seem to be more consistent to Alt-A data before El Niño.

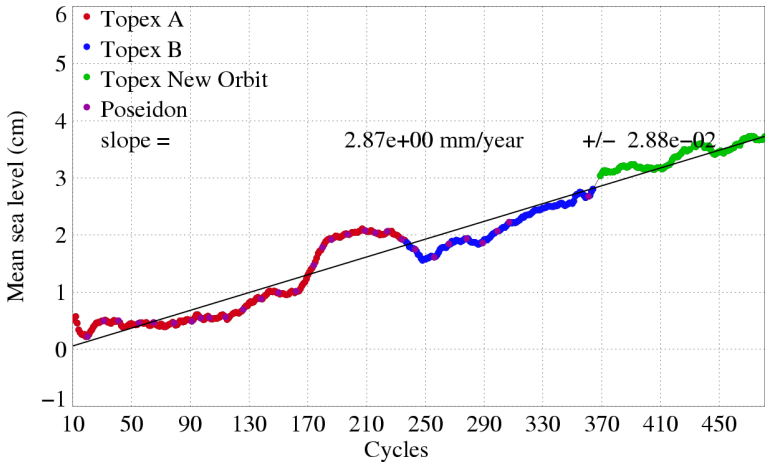


Figure 51: *Mean Sea Level obtained from AVISO M-GDR data (with additive correction). MOG2D correction is applied.*

### 6.2.2 Impact of orbit calculation

As seen before (section 3.2), NASA and CNES terrestrial reference frames used in the precise orbit determination are not the same and cause radial differences at the level of a few millimeters. The impact of these discrepancies has been estimated in terms of Mean Sea Level variations and plotted on Figure 52. Dramatic differences, as large as 1 cm at hemispheric scale, are obtained between the two MSL estimations after cycle 170. As northern and southern hemispheres are not equally sampled, a trend is also observed in global MSL estimations. The figure shows a definite change in differences between the two orbits at cycle 247 when the ITRF97 reference frame was used in the CNES orbit calculation. This led to less difference between the two MSL estimations. As already mentioned, other important changes occurred in the CNES orbit calculation at cycle 320, with the use of the ITRF2000 reference frame and the albedo model. Moreover ITRF2000 has been applied in the NASA orbit calculation from cycle 360 onward. As a result, the consistency between 2 orbits is better. Differences are reduced to very close to zero values at both global and hemispheric scales.

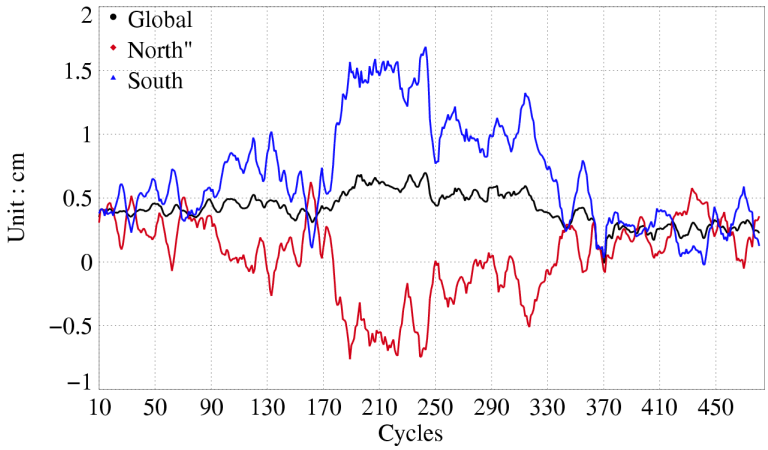


Figure 52: *Difference in MSL estimations using respectively CNES and NASA orbits*

## 6.3 Topex/Poseidon relative altimeter bias

Collinear differences are also used to compute the (TOPEX - Poseidon) relative bias. Each Poseidon cycle is compared to the two adjacent TOPEX cycles, leading to a mean relative bias estimate.
Figure 53 shows the values of the mean (TOPEX - Poseidon) SSH differences as a function of Poseidon cycles. The figure is split into three parts defined by Poseidon data retracking and the switch from Alt-A to Alt-B.

After Poseidon data retracking, the relative bias was about 1 cm higher than before, even though a dedicated bias value had been applied in the AVISO processing to account for the impact of retracking. In addition, the relative bias value has increased during the last Alt-A cycles, maybe due to Alt-A changes.

After the Alt-B switching on, the TOPEX/Poseidon relative bias has been reduced to very low values because of remaining Alt-A/alt-B bias. Moreover, the last estimates are directly impacted by the (TOPEX - DORIS) ionosphere correction difference which leads to overestimate the relative bias by about 0.5 cm in the last cycles.

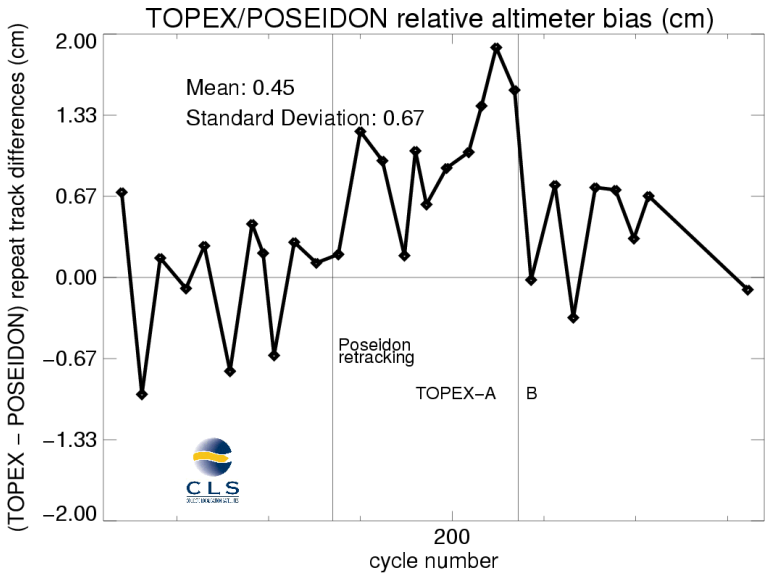


Figure 53: *(TOPEX Poseidon) SSH relative bias from AVISO M-GDRs (no other correction applied)*

## 6.4 Sea level seasonal variations

A short description of major oceanic signals is given here, in order to assess the data quality for oceanographic applications.
The large scale seasonal variations in the surface-topography (e.g. steric effect due to heat flux variations, seasonal and inter-annual variability of the equatorial currents) are clearly evidenced on this figure.
Important inter-annual signals can be observed in the steric effect which is characterized by the contrast between Northern and Southern hemispheres, according to seasons. It is larger, for example, during winter and spring 1996 relative to 1993. Seasonal variations in west boundary currents, and therefore in the associated transports, are also exposed to inter-annual variations: the winter cooling of both Gulf Stream and Kuroshio currents and their extensions is weaker in 1994 and particularly great in 1996 and 1998.

The most important changes are observed in the equatorial band. Though El Niño events have already occurred (e.g. fall 94/winter 95), the 1997 El Niño is the major feature in these regions since the beginning of the mission, because of its amplitude and duration. Due to Kelvin waves eastward propagation, it creates large positive anomalies in the eastern part of the Pacific ocean. Warmer water masses reach the California coasts in summer/fall 1997. At the same time, negative anomalies affect the western part of the basin.

At the end of 1997 and winter 1998, large anomalies are also observed around the equator in the Indian Ocean. After El Niño events, trade winds forcing acts again to create westward propagation of water masses. Surface-topography anomalies, respectively positive and negative at the western and eastern parts of the Pacific, lead to "La Niña" situation in 1999 and 2000. During Summer 2001, eastward propagations seem to begin in the equatorial zone.

At the end of 2002, another El Niño situation occurs. It has been noticed in terms of SLA variability (section 6.1). Then the equatorial Pacific Ocean comes back to La Niña situation in Spring 2003.

The fall figure of 2005 (66 ) is noisier than the other figures, since less cycles are used to create the figure as the mission of TOPEX/Poseidon finished in October 2005.

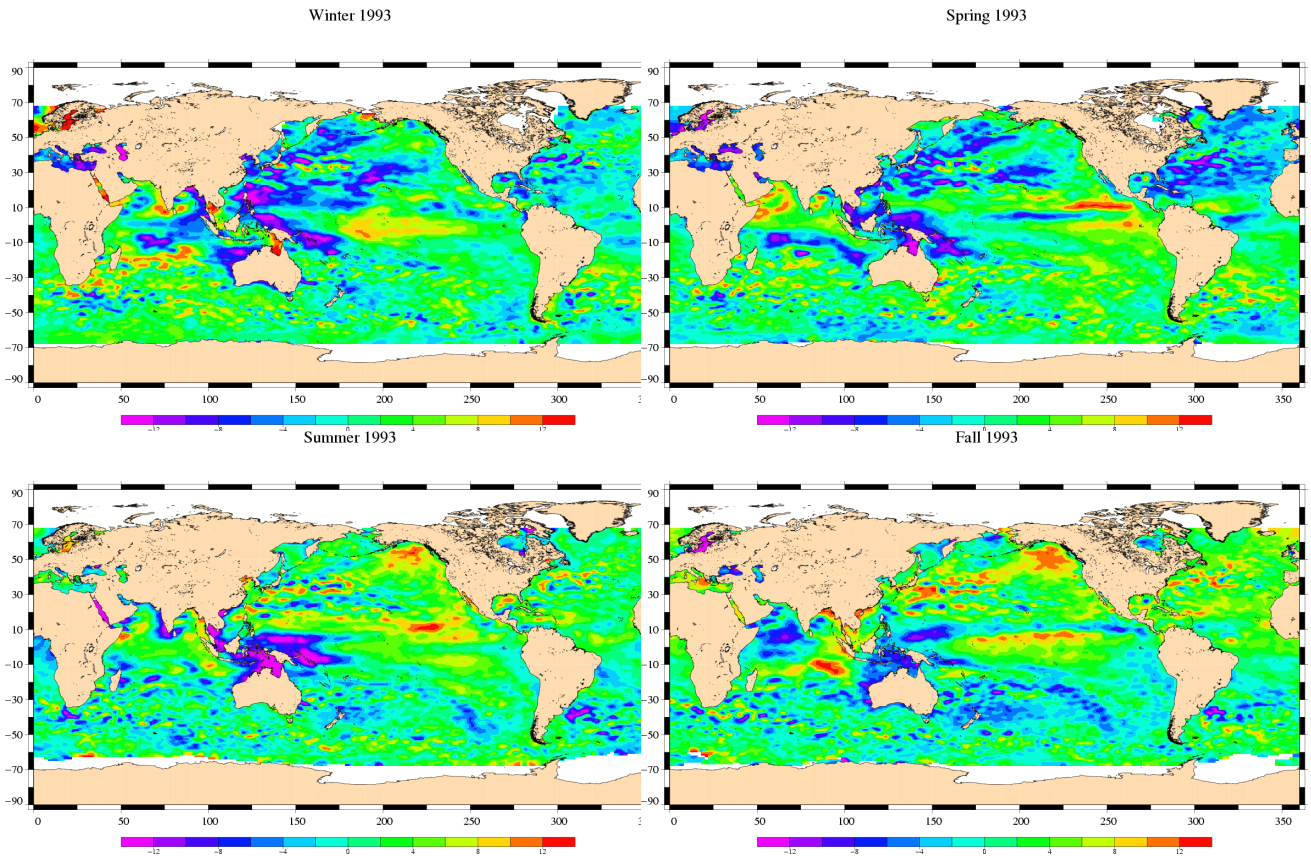


Figure 54: *Seasonal variations of Jason SLA (cm) for year 1993 relative to a MSS CLS 2001*

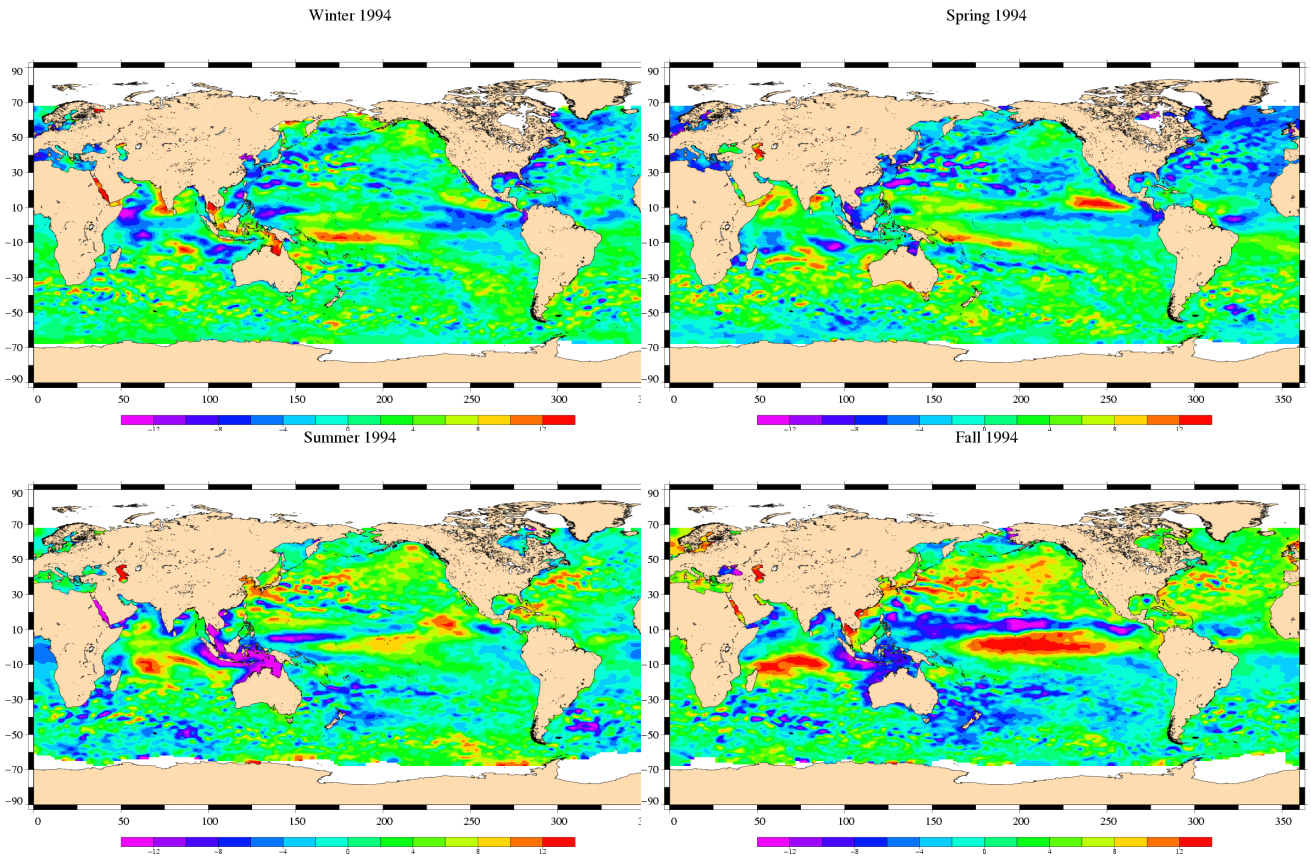


Figure 55: *Seasonal variations of Jason SLA (cm) for year 1994 relative to a MSS CLS 2001*

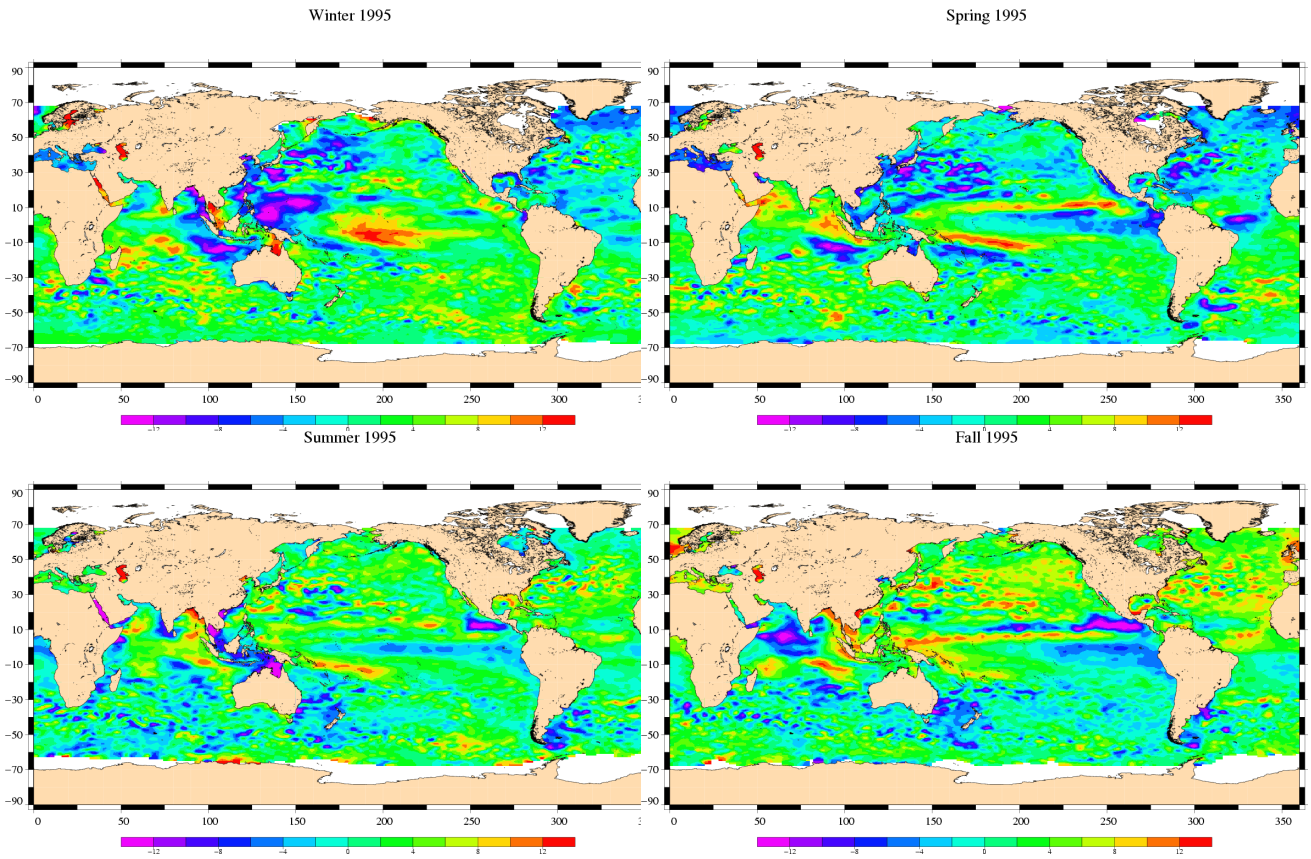


Figure 56: *Seasonal variations of Jason SLA (cm) for year 1995 relative to a MSS CLS 2001*

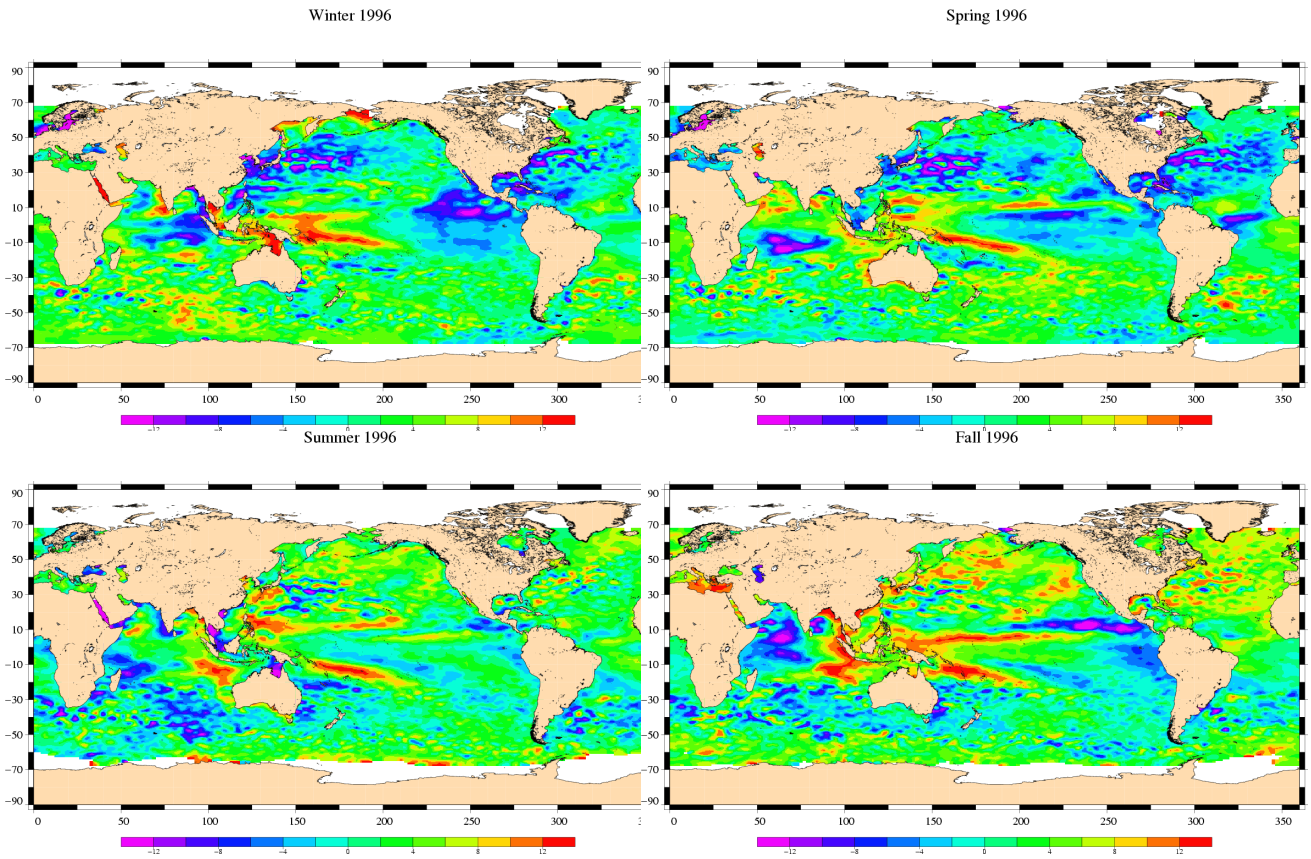


Figure 57: *Seasonal variations of Jason SLA (cm) for year 1996 relative to a MSS CLS 2001*

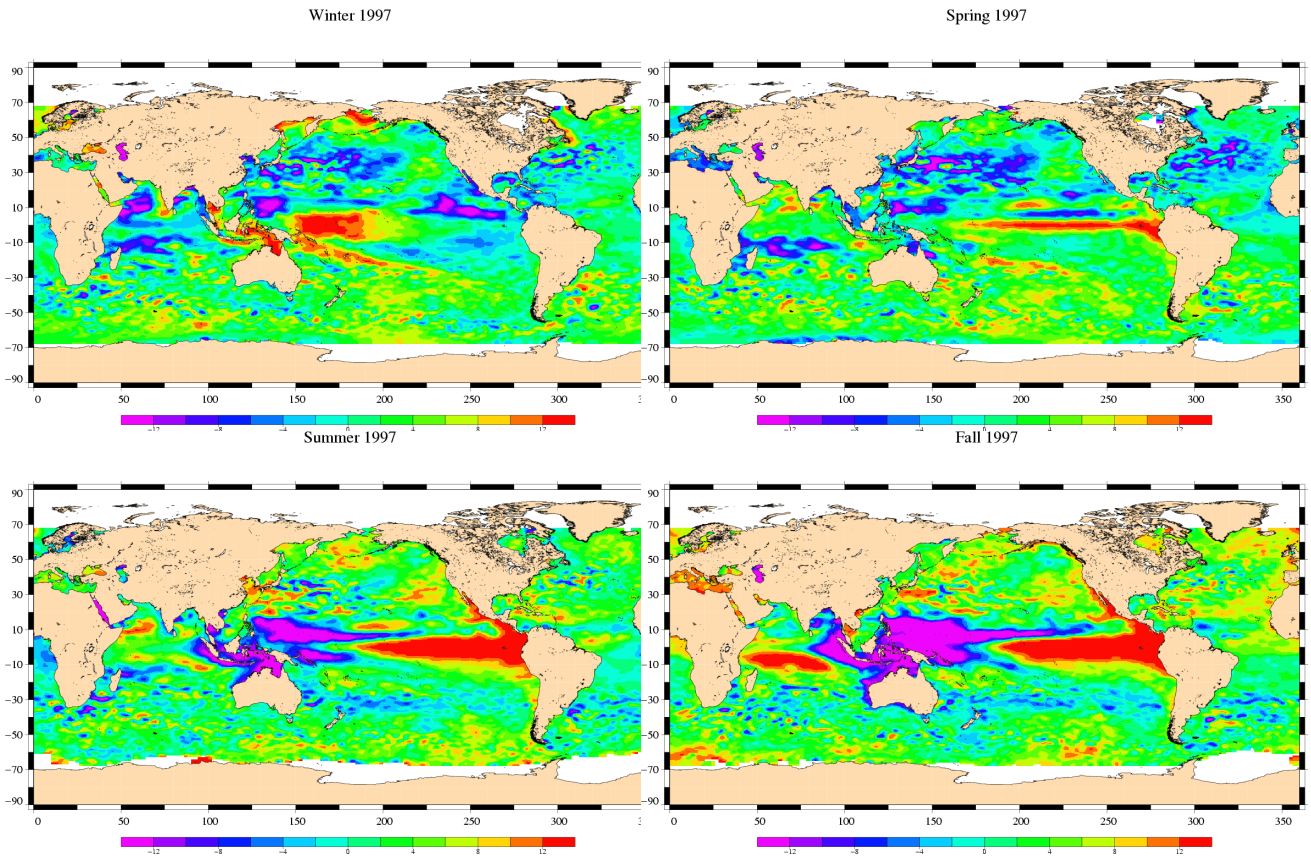


Figure 58: *Seasonal variations of Jason SLA (cm) for year 1997 relative to a MSS CLS 2001*

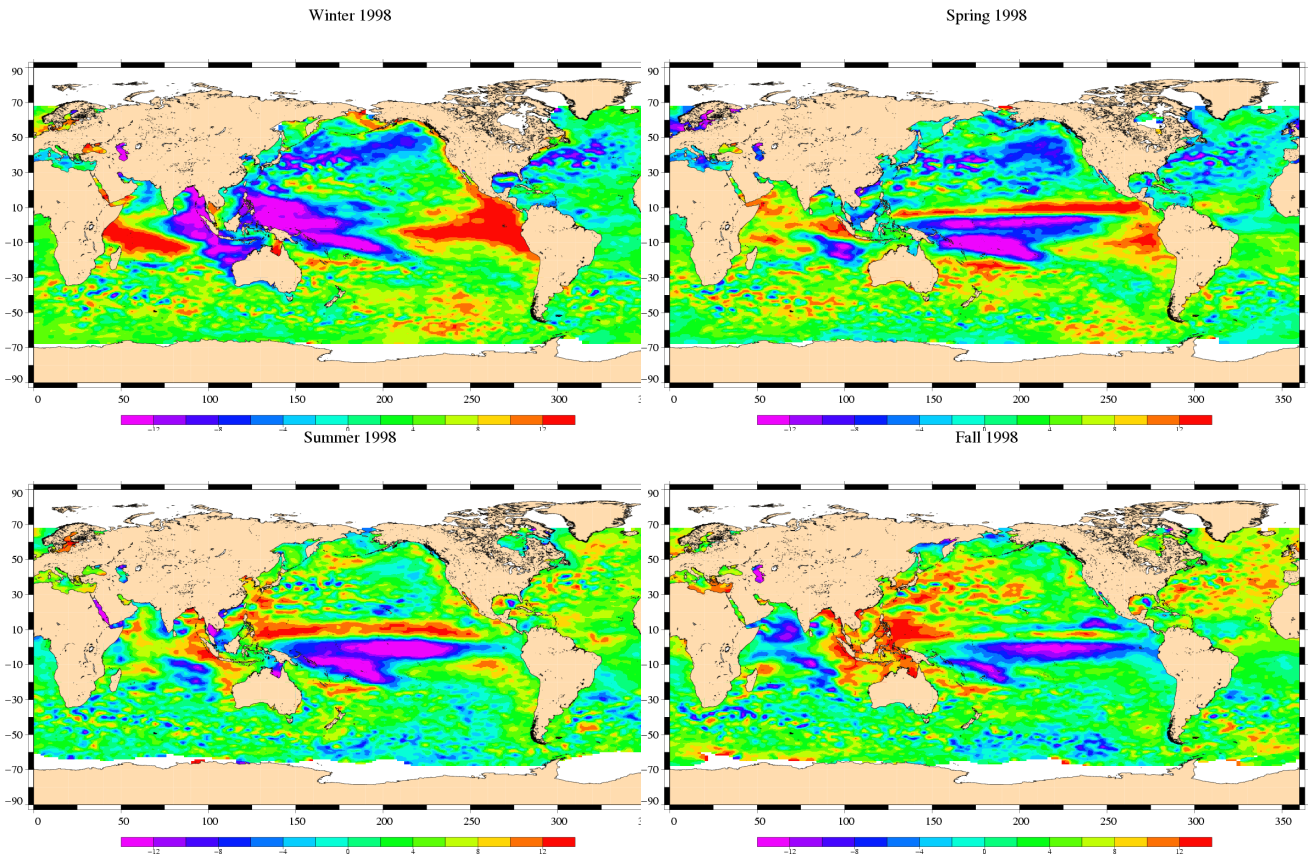


Figure 59: *Seasonal variations of Jason SLA (cm) for year 1998 relative to a MSS CLS 2001*

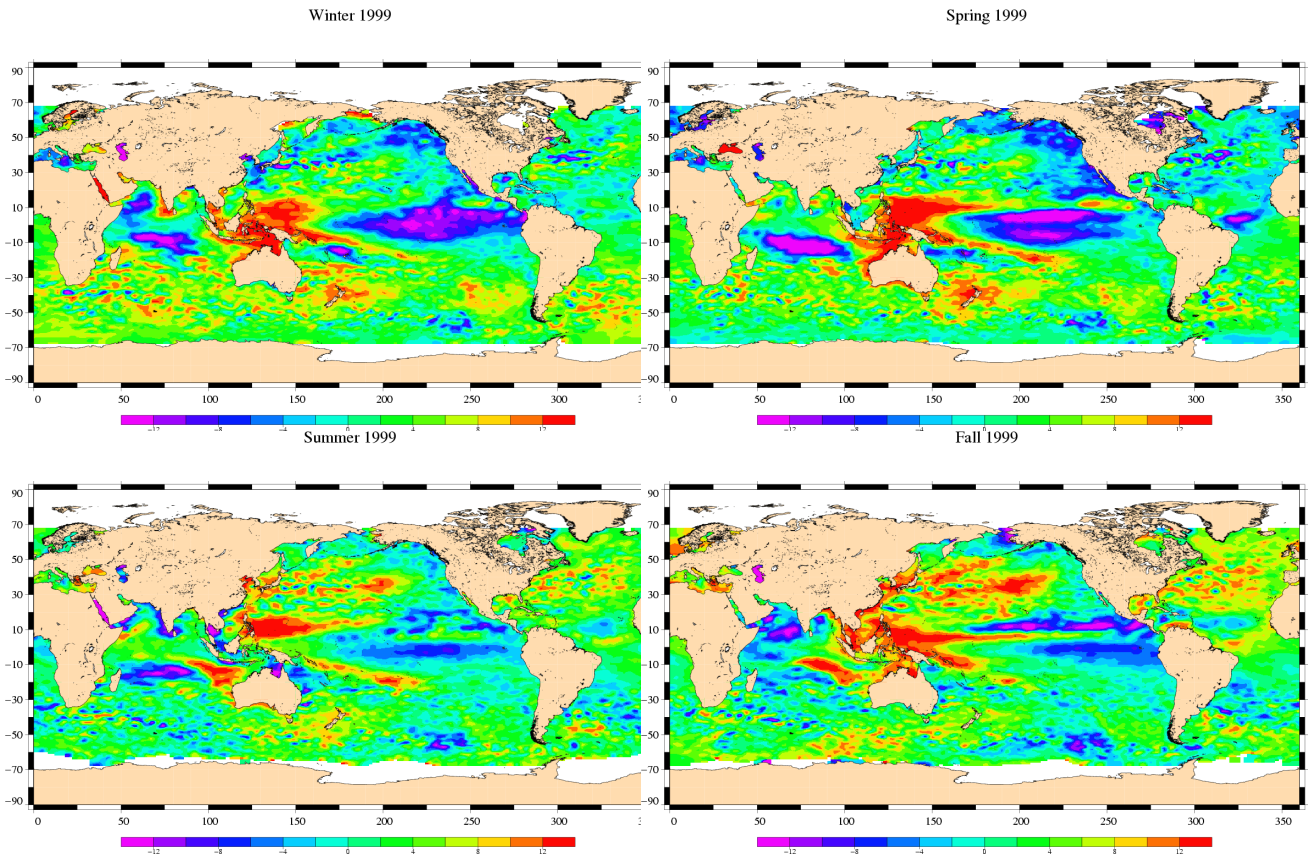


Figure 60: *Seasonal variations of Jason SLA (cm) for year 1999 relative to a MSS CLS 2001*

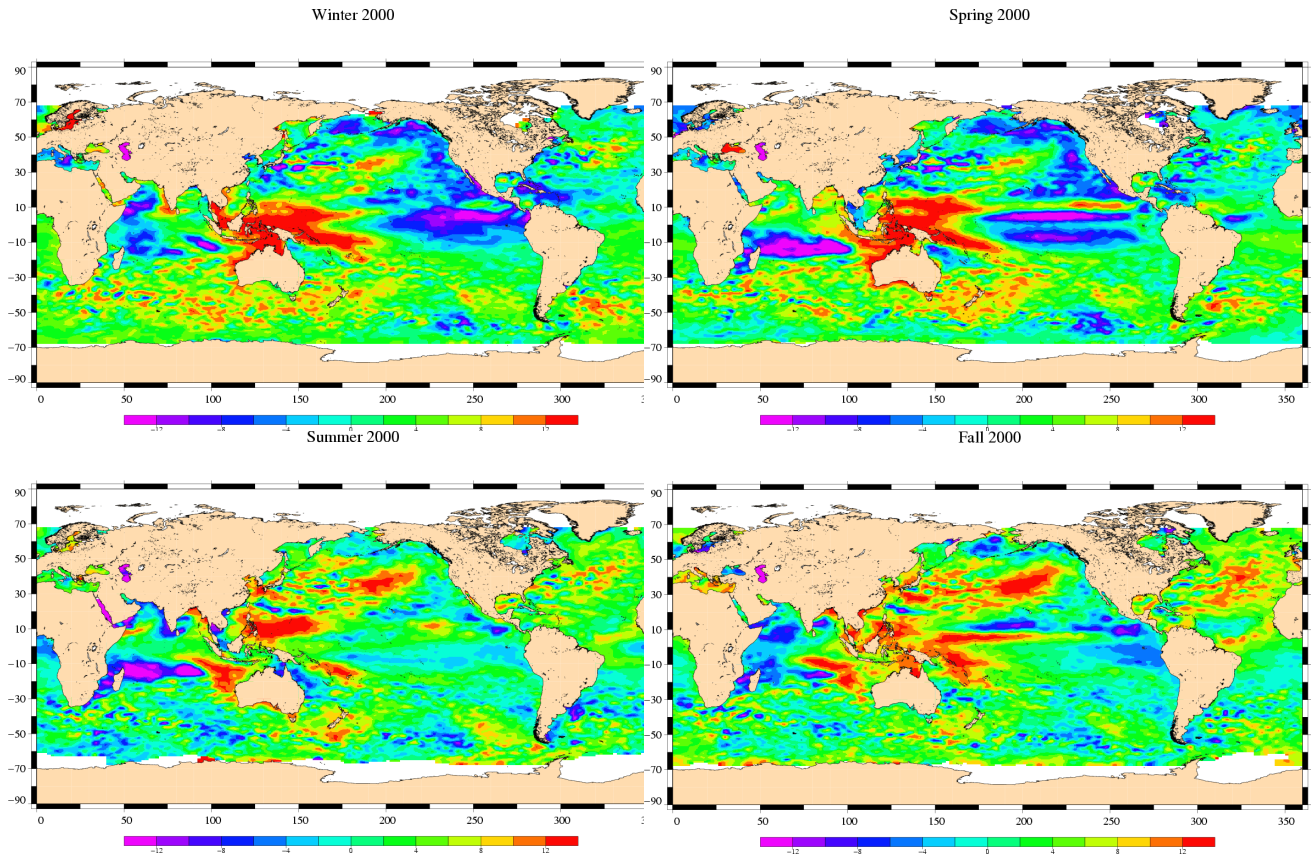


Figure 61: *Seasonal variations of Jason SLA (cm) for year 2000 relative to a MSS CLS 2001*

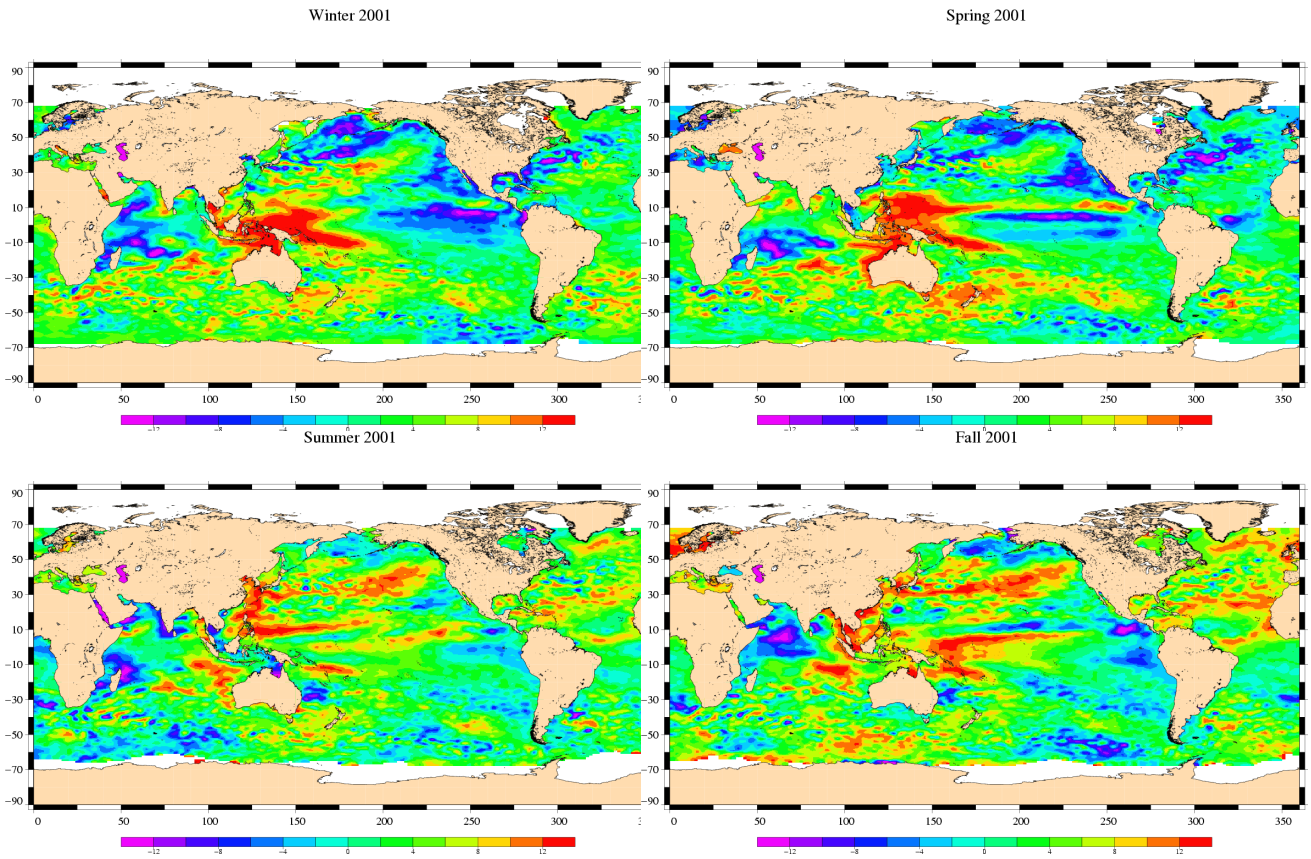


Figure 62: *Seasonal variations of Jason SLA (cm) for year 2001 relative to a MSS CLS 2001*

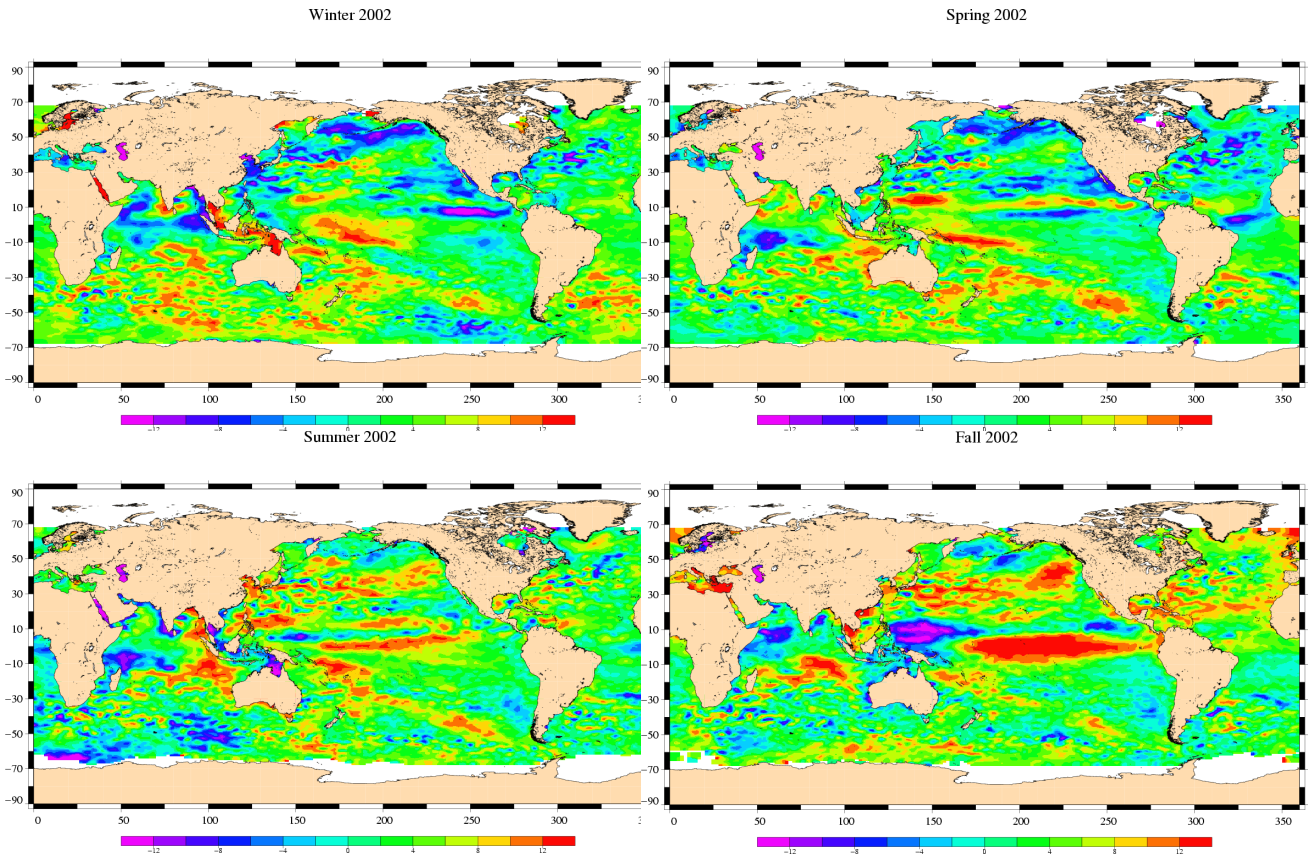


Figure 63: *Seasonal variations of Jason SLA (cm) for year 2002 relative to a MSS CLS 2001*

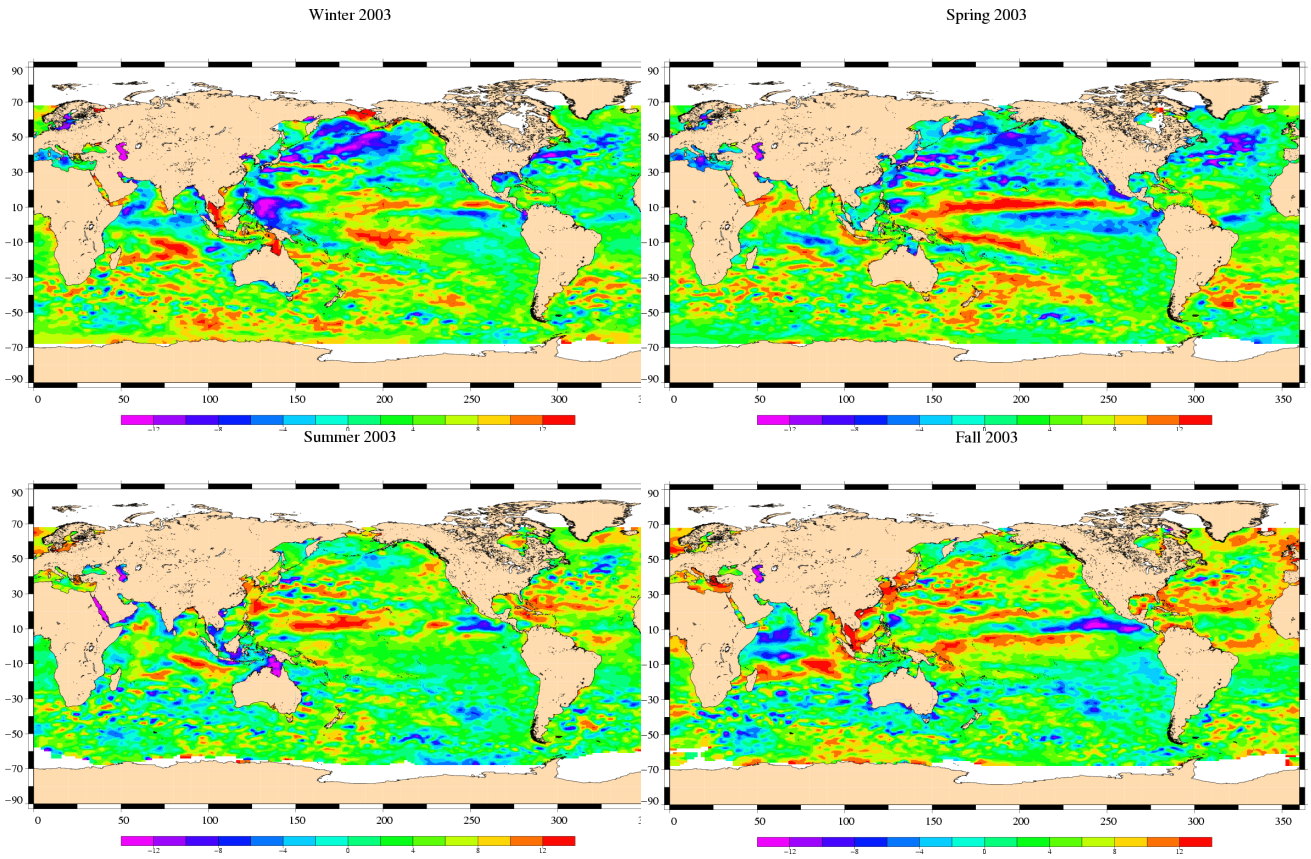


Figure 64: *Seasonal variations of Jason SLA (cm) for year 2003 relative to a MSS CLS 2001*

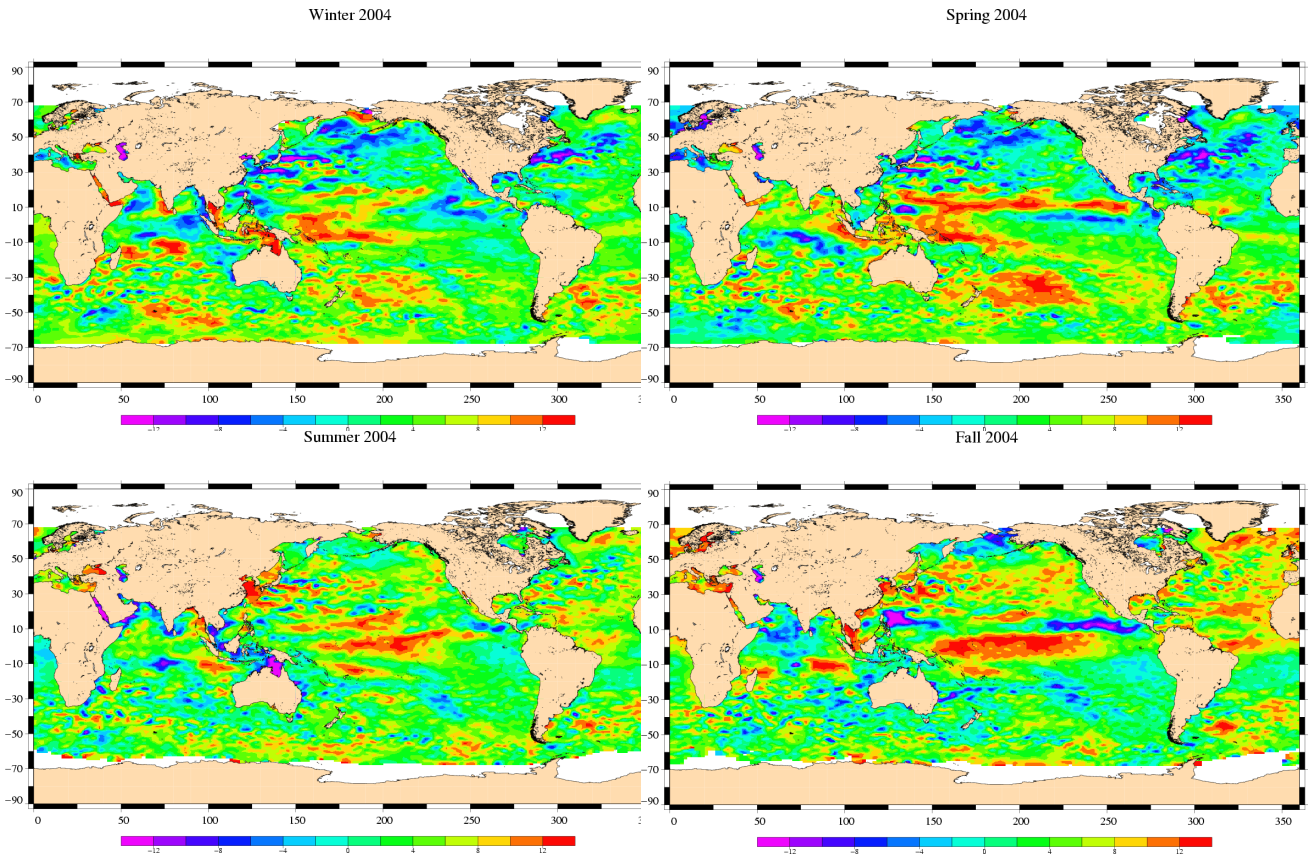


Figure 65: *Seasonal variations of Jason SLA (cm) for year 2004 relative to a MSS CLS 2001*

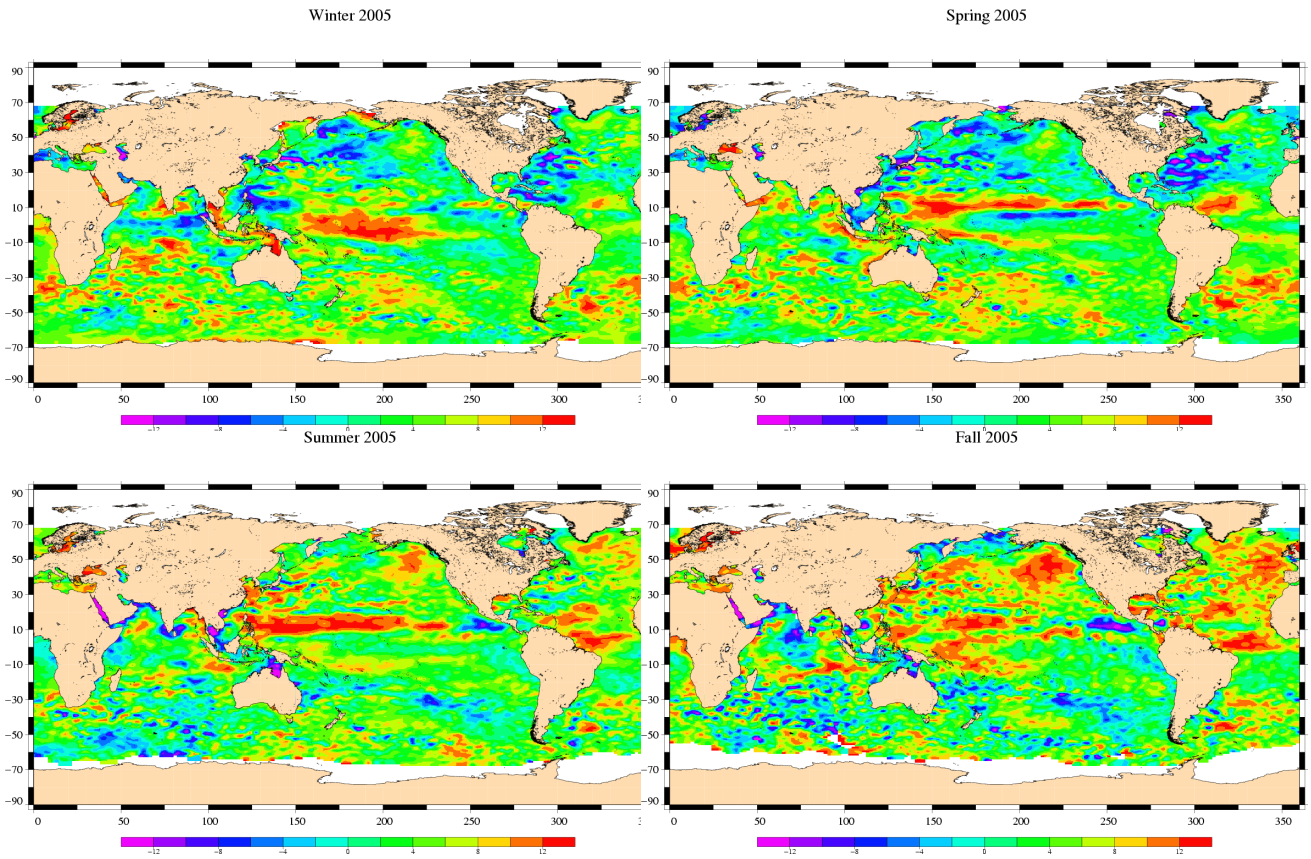


Figure 66: *Seasonal variations of Jason SLA (cm) for year 2005 relative to a MSS CLS 2001*

# 7 Mean Sea Level (MSL) and Sea Surface Temperature (SST) comparisons

This study has been carried out in order to monitor the MSL seen by all the operational altimeter missions. Long-term MSL change is a variable of considerable interest in the studies of global climate change. Then the objective here is on the one hand to survey the mean sea level trends and on the other hand to assess the consistency between all the MSL. Besides, the Reynolds SST is used to compare the MSL with an external data source. The mean SST is calculated the same way as the MSL.
The following missions have been used : TOPEX/Poseïdon (T/P), Jason-1 (J1), Geosat Follow-On (GFO) and Envisat. The MSL and SST time series have been plotted over global ocean. This allows us to correlate the MSL trends seen by each mission and to compare them with the SST.
In addition to these analysis, the maps of regional MSL change and SST change have been plotted for each mission over the Jason-1 period and the Envisat period. The differences of these maps have been performed; this is a way to display eventual local drifts.

## 7.1 SSH definition for each mission

The SSH formula is defined for all the satellites as below :

$$SSH = Orbit - Altimeter\ Range - \sum_{i=1}^{n} Correction_i$$

with :

$$\begin{aligned}
\sum_{i=1}^{n} Correction_i \;=\; & Dry\ troposhere\ correction : new\ S1\ and S2\ atmospheric\ tides\ applied \\
+\; & Combined\ atmospheric\ correction :\ MOG2D\ and\ inverse\ barometer \\
+\; & Radiometer\ wet\ troposhere\ correction \\
+\; & Filtered\ dual\ frequency\ ionospheric\ correction \\
+\; & Non\ parametric\ sea\ state\ bias\ correction \\
+\; & Geocentric\ ocean\ tide\ height,\ GOT\ 2000 :\ S1\ atmospheric\ tide\ is\ applied \\
+\; & Solid\ earth\ tide\ height \\
+\; & Geocentric\ pole\ tide\ height
\end{aligned}$$

Some additional corrections have been applied :

- For Jason-1 and Envisat the wet troposhere correction has been changed by the ECMWF model in order to remove the effects of abnormal changes or trends observed on the radiometer wet troposhere correction.
- For Envisat, the USO correction (Martini, 2003 [38]) has been applied.
- For T/P, the radiometer wet troposhere correction has been corrected from correction (Scharroo R., 2004 [51])

- For T/P, the relative bias between TOPEX and Poseidon and between TOPEX A and TOPEX B has been taken into account
- For T/P, the drift between the TOPEX and DORIS ionosphere corrections has been corrected for on Poseidon cycles.
- For Geosat Follow-On, the GIM model has been used for the ionospheric correction.

## 7.2 MSL and SST time series

### 7.2.1 MSL over global ocean

The MSL has been monitored for each satellite altimeter over global ocean in figure 67 over T/P period and Jason-1 period. The trends are similar for each satellite except for Envisat. The estimation of the Envisat MSL slope seems impacted by a strange behaviour on the first year as explained in Faugere et al. (2005, [21]). However, on the last two years, the Envisat slope is fully consistent with Jason-1 and T/P. The unexplained behavior of the first year of Envisat data is currently under investigation.

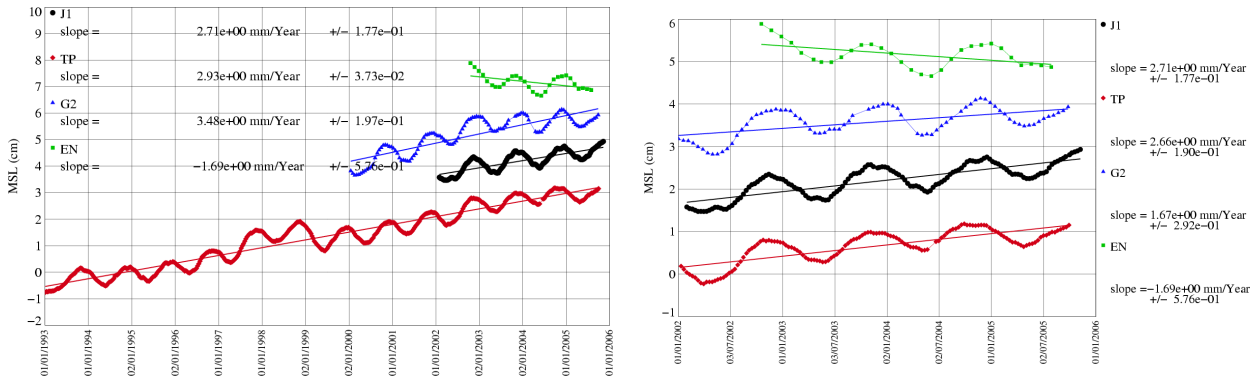


Figure 67: *MSL over global ocean for the T/P period on the left and the Jason-1 period on the right.*

In the following figure 68, MSL have been plotted after removing annual signal, semi-annual signal, and signals lower than 60 days. The T/P, Jason-1 and GFO MSL slopes over the Jason-1 period are still similar, respectively 2.75 mm/year, 2.3 mm/year and 1.8 mm/year with an adjustement formal error arround 0.2 mm/year. Notice that, for GFO, the slope computed over the global period is stronger, 3.2 mm/year. Beside, the orbit quality of Jason-1 early cycles is lower than usual. When those cycles are not taken into account, the Jason-1 slope increases by 0.3 mm/year to reach 2.6 mm/year. The conclusion is that the slope estimation is very sensitive. The formal error adjustement is only a mathematical error, not linked with the physical errors such as the orbit errors for instance.

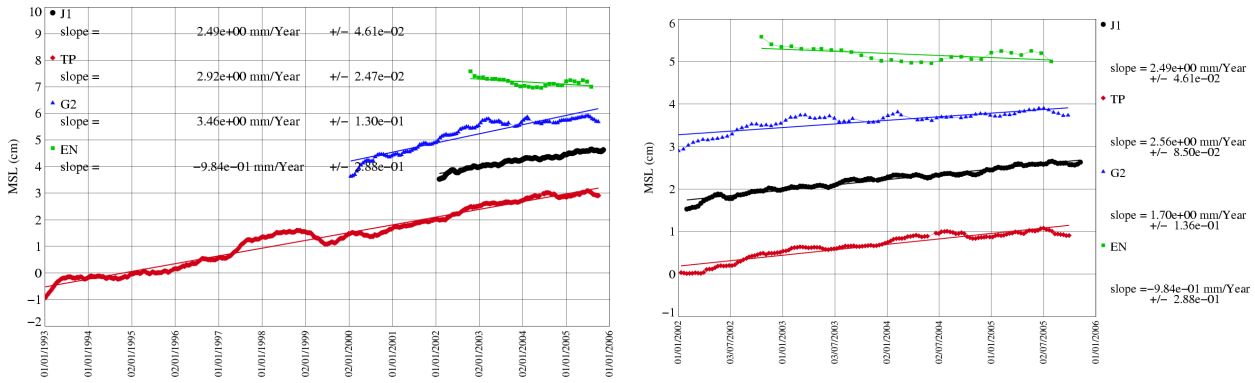


Figure 68: *MSL over global ocean for the T/P period on the left and the Jason-1 period on the right after removing annual, semi-annual and 60-day signals.*

### 7.2.2 SST over global ocean

In figure 69 on the left, the SST mean is compared to the T/P MSL. In the same figure on the right, annual signal, semi-annual signal, and signals lower than 60 days have been removed. Notice that the SST has been computed exactly over the T/P tracks. The SST increases by about 0.015 degree/year over the T/P period with a formal error close to 0.001 degree/year. The MSL and the SST don't have the same unit ("cm" and "degree"), thus to compare the 2 quantities, the SST scale is adjusted on the MSL scale so that the SST trend and the MSL trend are visually the same. This allows us to highlight that the SST dynamic is stronger than the MSL one. Inter-annual signal or climatic phenomena have a greater impact on the SST than on the MSL. Thus the SST trend estimation over a short period is not significant.

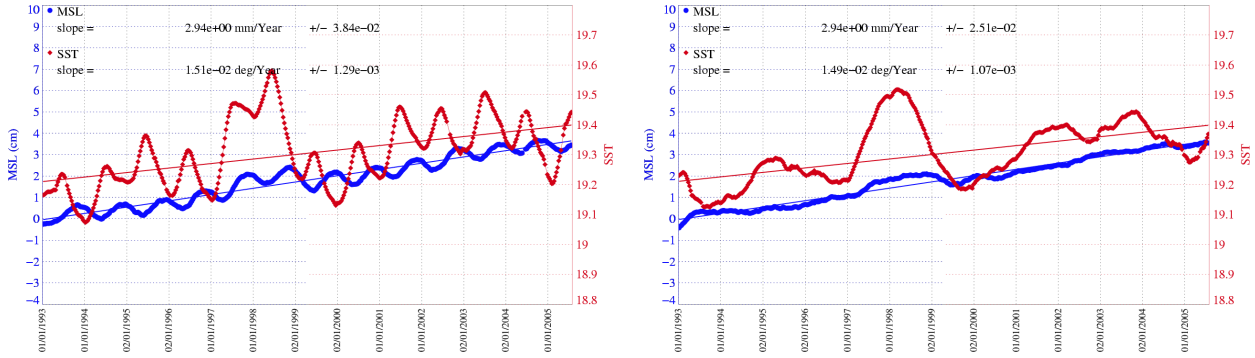


Figure 69: *MSL and SST over global ocean for the T/P period on the left, and after removing annual, semi-annual and 60-day signals on the left.*

## 7.3 Spatial MSL and SST slopes

### 7.3.1 Methodology

In order to monitor the MSL, the spatial MSL slopes have been calculated. The SLA grids (2x2 degree bins) have been computed cycle per cycle, and the slope has been computed on each grid point. As for time analysis, 60 day, semi-annual and annual signals have been removed before estimating the slopes. Then, the MSL slopes have been mapped for each mission. These maps are used to compare the MSL slopes between each altimeter mission. This allows us to detect potential local drifts.
Besides, the SST slopes have been computed the same way in order to correlate them with the MSL slopes.

### 7.3.2 Spatial MSL slopes over Jason-1 period

The MSL slopes have been plotted for Jason-1 (on the right) and T/P (on the left) over Jason-1 period in figure 70. The MSL trends seen by the two satellites are similar. However, differences greater than 4mm/year can be observed on the T/P-Jason-1 map (at the bottom).

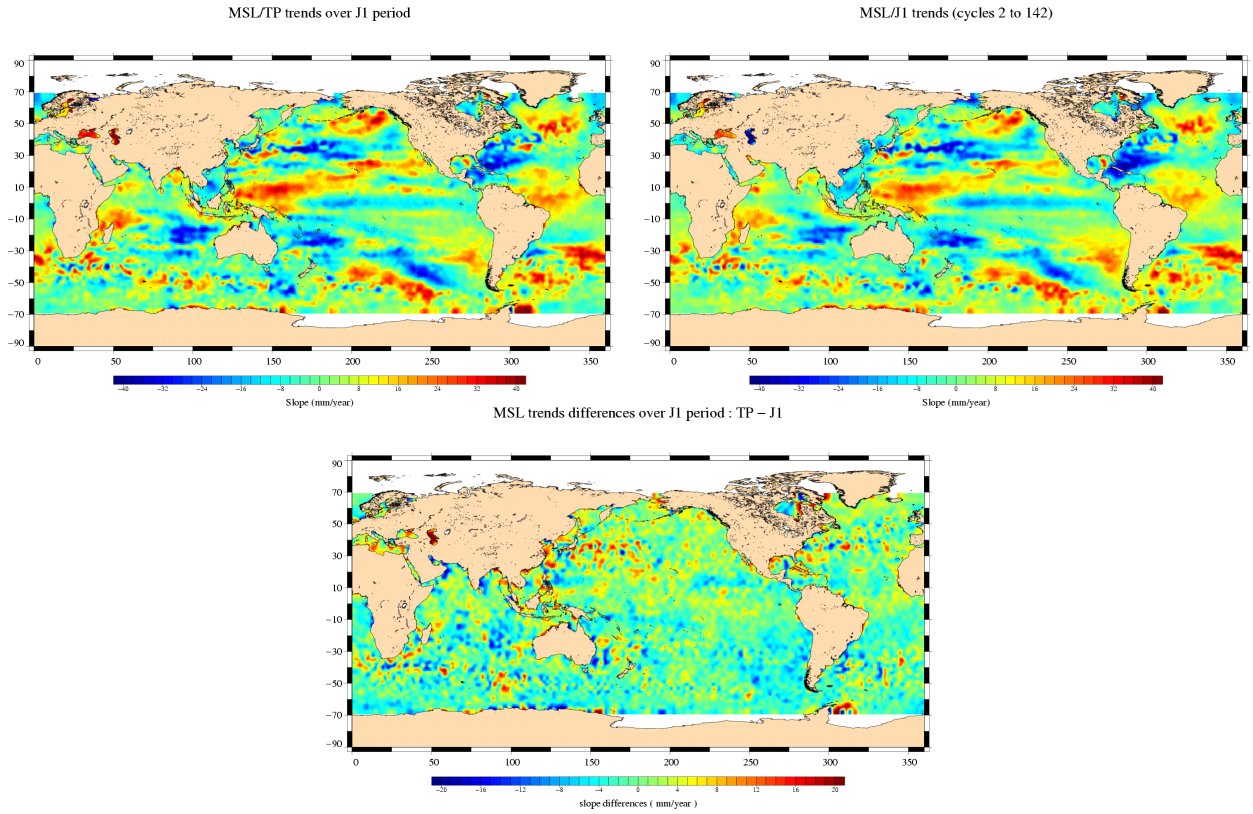


Figure 70: *MSL slopes over Jason-1 period for T/P (left) and Jason-1 (right), MSL slope differences between Jason-1 and T/P (bottom)*

### 7.3.3 Spatial MSL slopes over Envisat period

The same work has been performed over Envisat period using Envisat data in figure 71. The 3 maps are very similar.
In figure 72, the slope differences between each mission have been plotted. They allow us to observe differences in equatorial areas between Jason-1 and Envisat, and between T/P and Jason-1. Between Envisat and T/P, the difference has not the same geographical pattern. Investigations are on-going to understand the reasons of this observation.

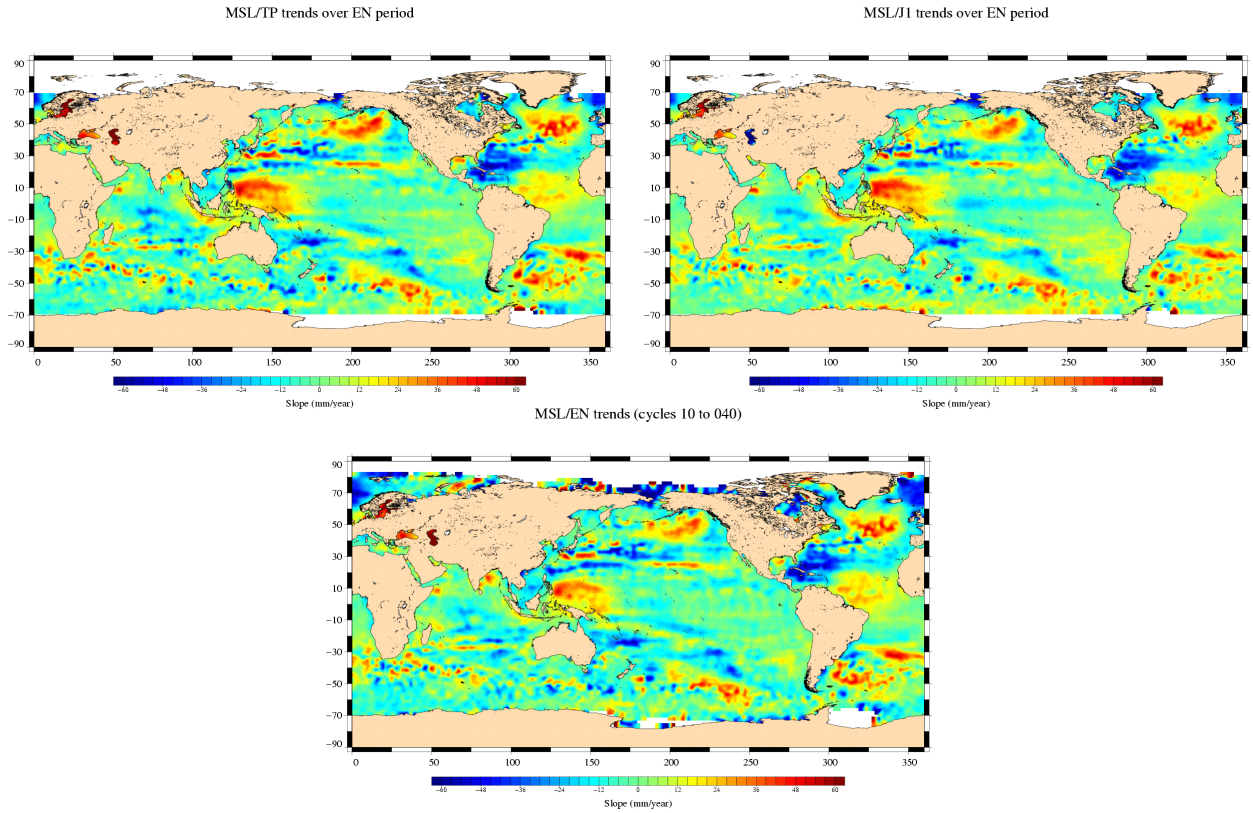


Figure 71: *MSL slopes over Envisat period for T/P (left), Jason-1 (right) and Envisat (bottom)*

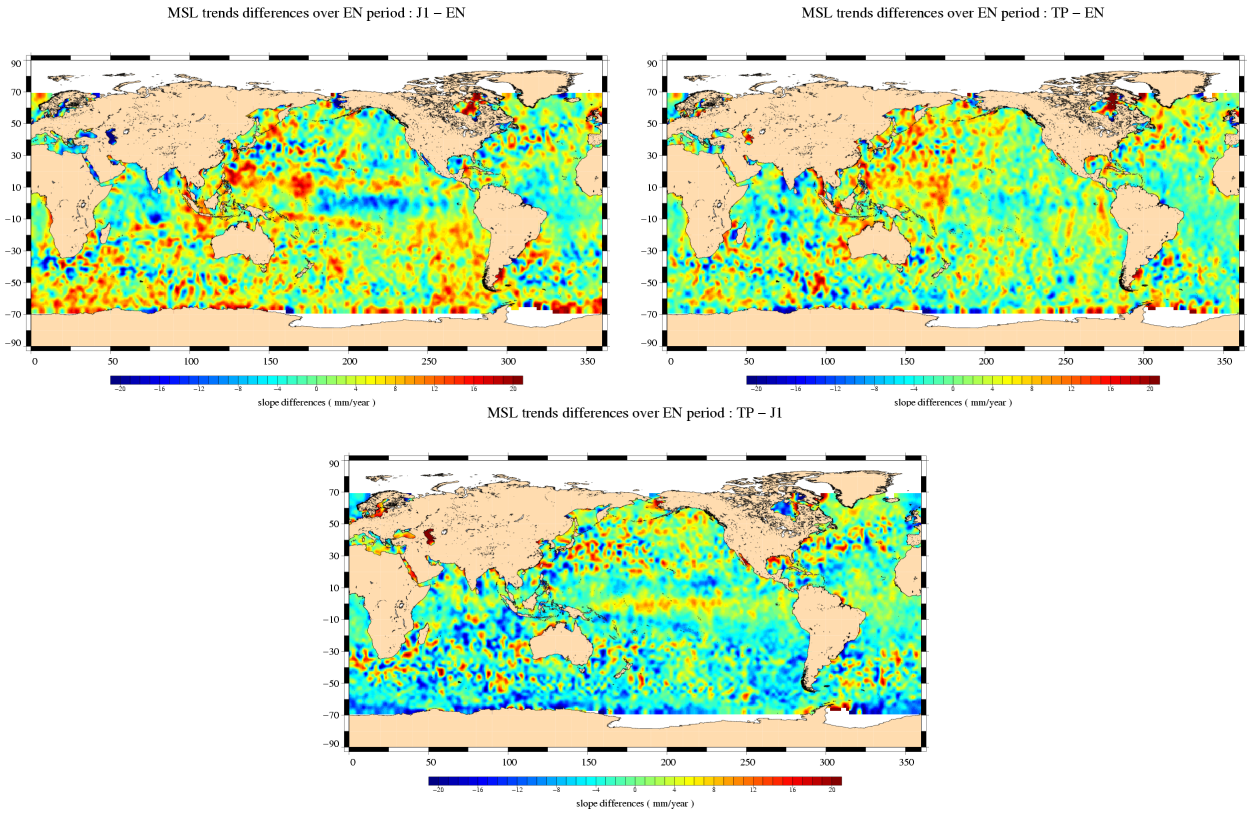


Figure 72: *MSL slopes differences over Envisat period between Jason-1 and Envisat (left), T/P and Envisat (right) and T/P and Jason-1 (bottom)*

### 7.3.4 Spatial SST and MSL slopes for T/P

The T/P MSL slopes are mapped in figure 73 on the left. In order to correlate the MSL and the SST, the SST slopes have been plotted in the same figure on the right.
13 years of T/P data have been used to estimate the slopes; this allows us to have a good estimation of the local MSL trends. The adjustment errors of the MSL and the SST slopes are mapped in figure 74.

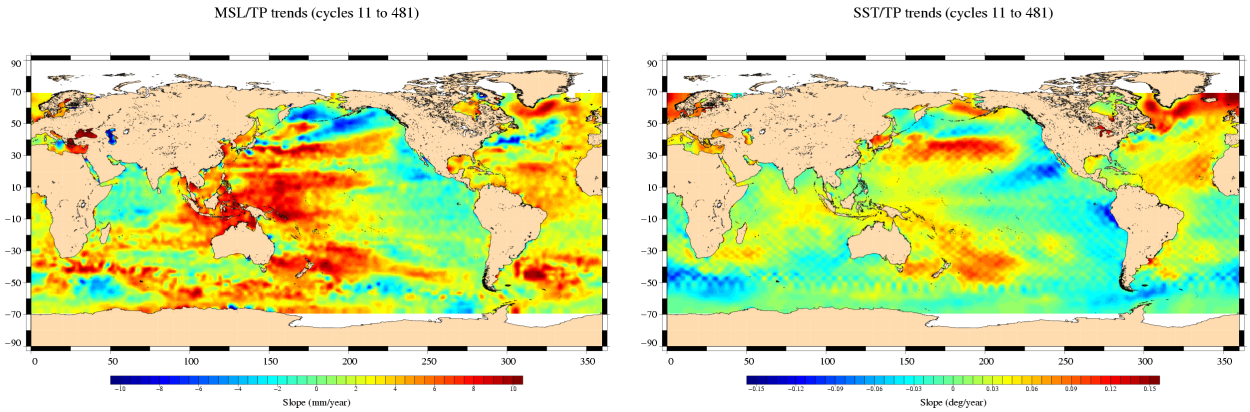


Figure 73: *T/P MSL and SST slopes over 13 years*

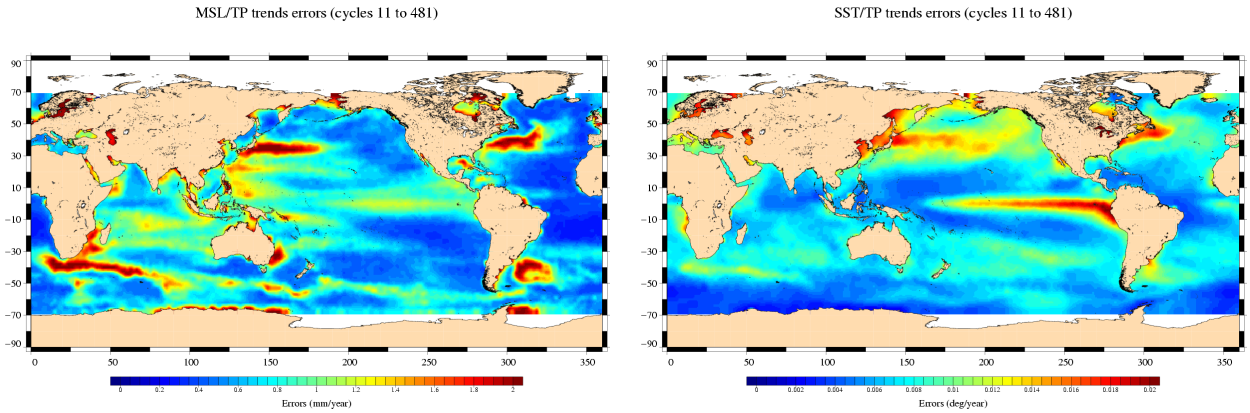


Figure 74: *Adjustment errors of T/P MSL and SST slopes over 13 years*

### 7.3.5 "El Niño" impact on SST and MSL slope estimations

The MSL and SST regional trends are largely impacted by inter-annual signal or oceanic phenomena such as "El Niño" for instance. The 4 maps in the figure 75 show the trend for the SST and the MSL before and after "El Niño". The first period ranges from 1992 and 1996 included, whereas the second period ranges from 1999 to 2004 included.
he MSL and SST regional trends are largely impacted by inter-annual signal or oceanic phenomena such as "El Niño" for instance. The 4 maps in the figure 75 show the trend for the SST and the MSL before and after "El Niño". The first period ranges from 1992 and 1996 included, whereas the second period ranges from 1999 to 2004 included.
MSL and SST trends are stronger for each period separetely than for the global period. In the Pacific ocean, the absolute values are greater than 20 mm/year for the MSL and 0.3 degree/year for the SST. SST and MSL maps show a strong correlation on the two period of time. But for both SST and MSL, the trends on the first period are very different from the trends of the second period. This is particularly true in tropical areas.
Finally, these maps highlight the importance of having long time series to evaluate the regional trends with a good accuracy.

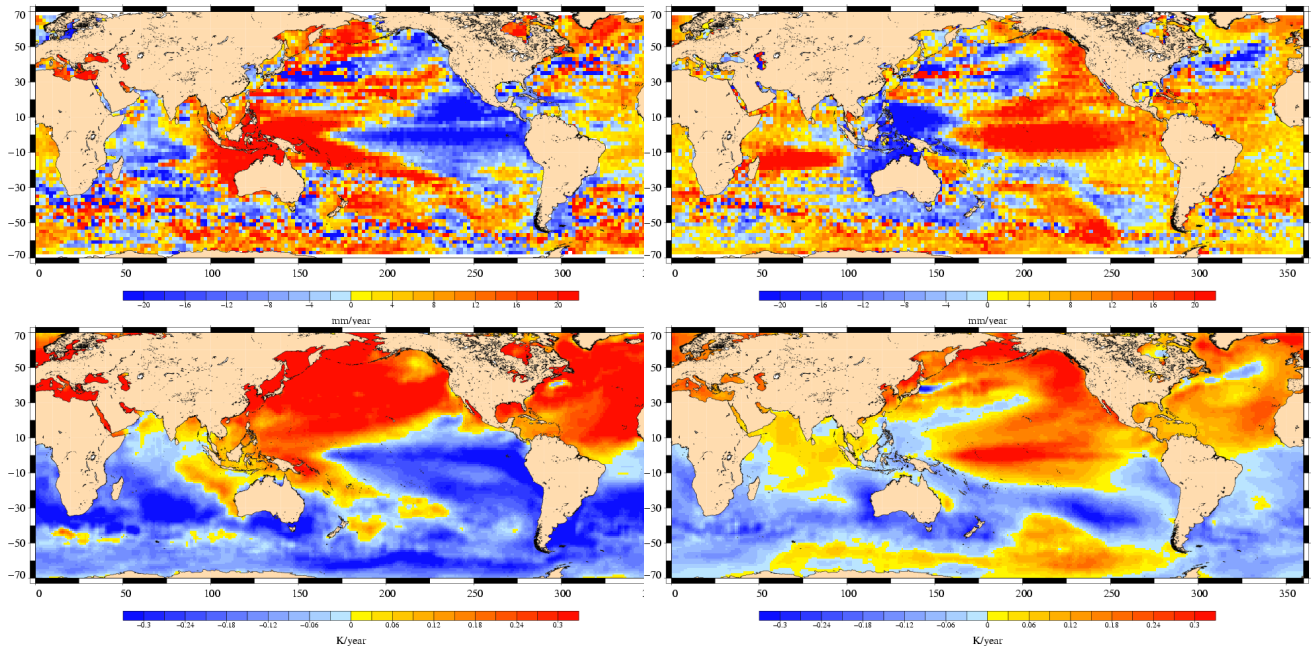


Figure 75: *Adjustment errors of T/P MSL and SST slopes over 13 years before and after "El Niño"*

# 8 New Standards

## 8.1 Statistical evaluation of Fes2004 tide model

### 8.1.1 Introduction

The purpose of this study is to assess the performances of the FES2004 tide model. The performance criteria are the variance of SSH differences at crossovers and the variance of along track Sea Level anomalies. The analysis has been done on Jason-1, Envisat and GFO. The results for Jason-1 satellite are similar to those which would have been obtained for TOPEX/Poseidon satellite, as both satellites are on the same ground track.
First, the FES04 model is compared to GOT00 model. Then, it is compared to older models, GOT99 and Fes99. Finally the impact of the new dynamic long period tide component is analyzed.

### 8.1.2 Comparison Between FES2004 and GOT00V2

In this part, the FES04 model is compared to GOT00 model on a two-year period on Jason-1 (31-104), Envisat (11-31) and GFO (98-140).

#### 8.1.2.1 SSH formulae

The parameters used to compute the sea surface height (SSH) for Jason-1 and Envisat are:

- radiometer wet troposphere correction
- ECMWF dry troposphere correction (rectangular grids)
- dual frequency ionospheric correction
- non parametric SSB
- MOG2D
- pole tide correction
- earth tide correction
- oceanic tide correction

The FES04 tide correction contains:

- the S1 and S2 atmospheric tide
- the dynamic long period tide

The original GOT00 tide correction contains:

- the S2 atmospheric tide

- the static long period tide

to be consistent, GOT00 has been computed as following:

$$\begin{aligned} GOT00_{used} &= original\ GOT00\ tide \\ &+ the\ S1\ atmospheric\ tide \\ &- static\ long\ period\ tide \\ &+ dynamic\ long\ period\ tide \end{aligned}$$

#### 8.1.2.2 Along track differences

Figure 76 shows the mean differences between FES04 and GOT00 on the 3 satellites. The differences are around 0 for Jason-1. On Envisat, the differences can locally overtake 1 cm. The strongest differences are in Indonesia and at high latitude. On GFO, the differences are weak at mid and low latitude, but have strong values above 60°. This behavior is not explained so far.

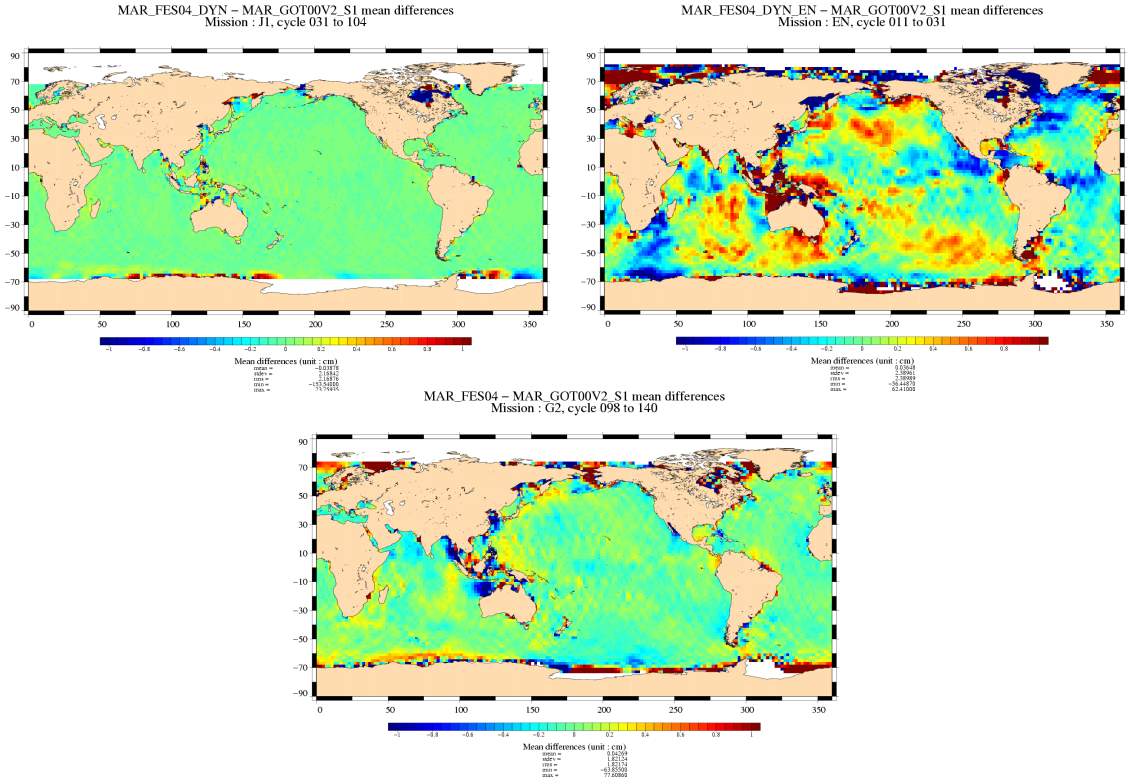


Figure 76: *Mean differences*

Figure 77 shows the variance of the difference between FES04 and GOT00 on the 3 satellites. The 3 maps are similar. High differences are found on low bathymetry areas and at high latitudes.

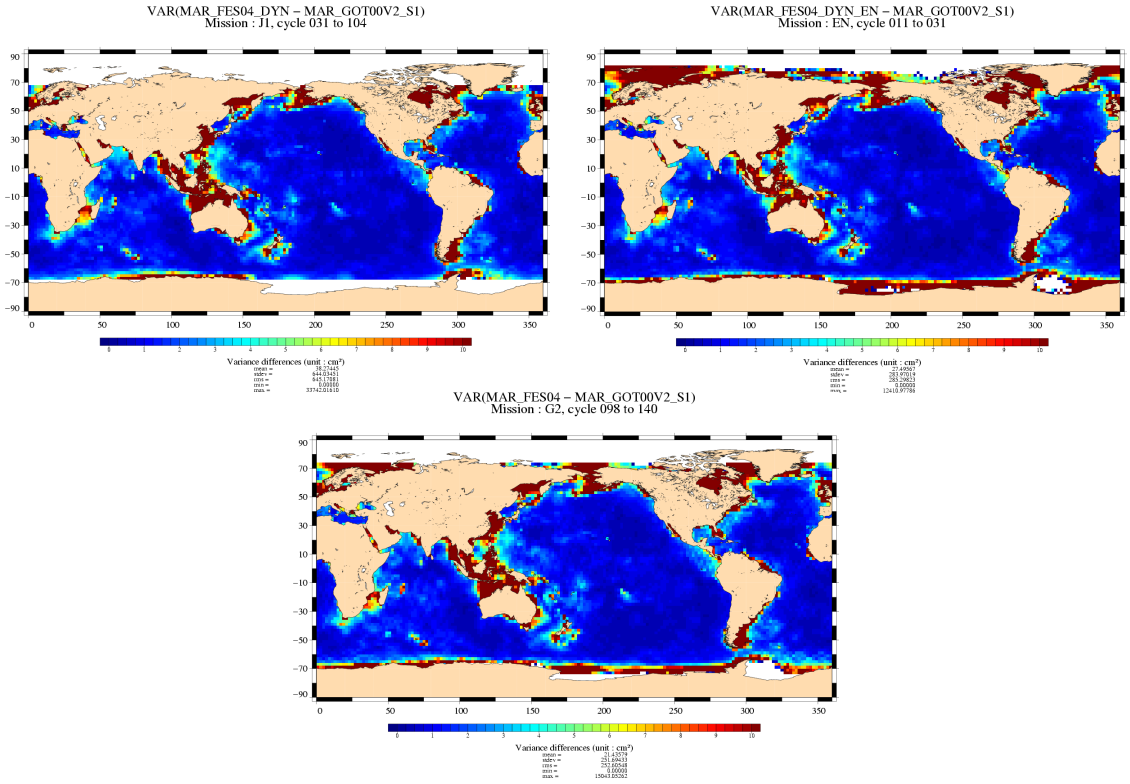


Figure 77: *Variance differences*

### 8.1.2.3 Performance at crossovers

Figures 78 and 79 show respectively the gain and the normalized gain at crossovers between FES04 and GOT00 on the 3 satellites. The blue color means that FES04 has a lower variance of SSH differences at crossover than GOT00. The red color means that FES04 has a larger variance of SSH differences at crossover than GOT00. For the 3 satellites, in open ocean at mid and low latitude, FES04 and GOT00 have approximately the same performances. In coastal regions and semi enclosed seas, at mid and low latitude, GOT00 better performs than FES04. It is especially true for Indonesia, China sea, Okhotsk Sea, Bering Sea or Hudson bay. This is due to the use of regional models in GOT00. At high latitude FES04 better performs than GOT00. This is particularly visible on Envisat because of its inclination.
The average variance differences over the period are summarized on tables 2, 3 and 4. These values confirm the pattern observed on the figures.

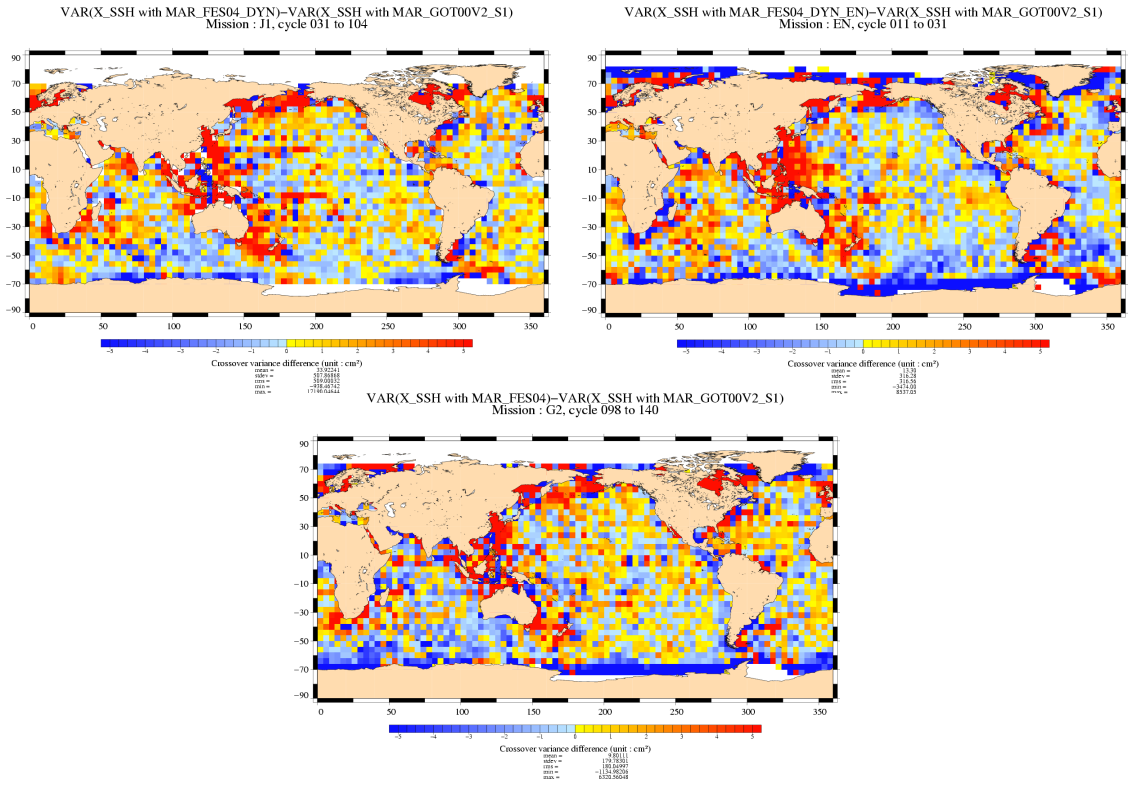


Figure 78: *Gain at crossovers*

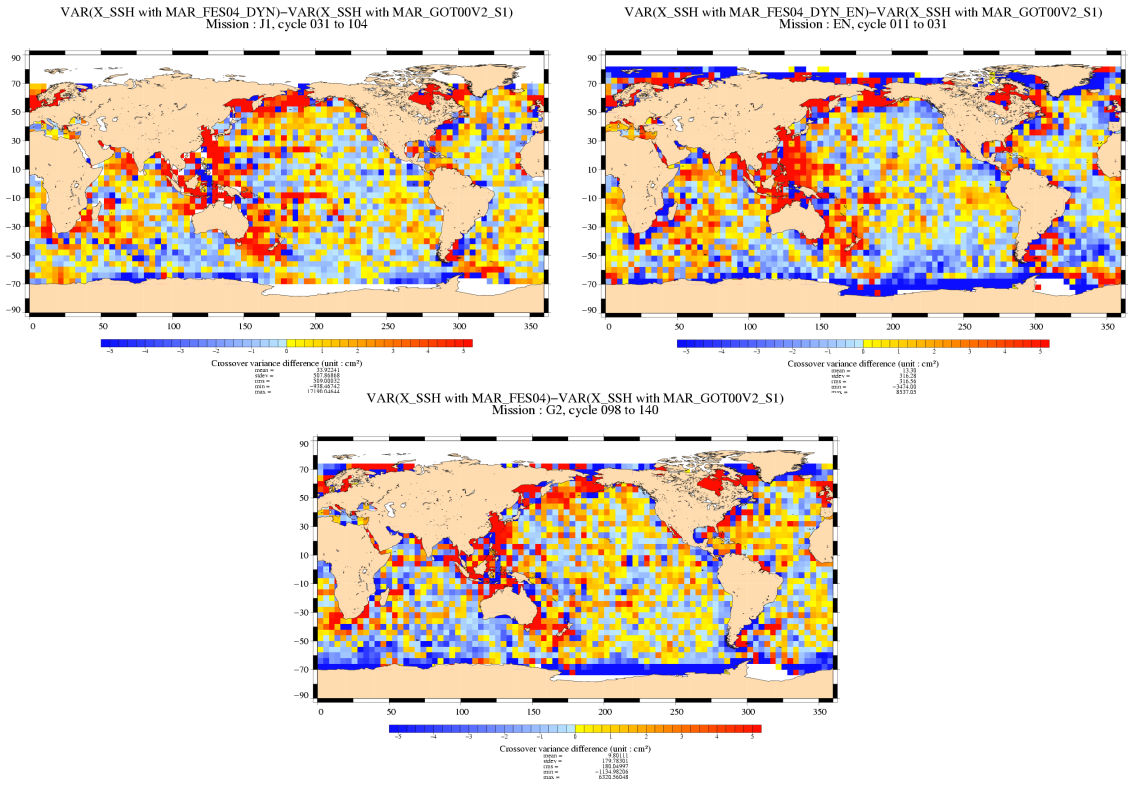


Figure 79: *Normalized gain at crossovers*

| Bathy \ Lat | No selection | $\|Lat\| < 50$ | $\|Lat\| > 50$ |
|---|---|---|---|
| No selection | 13.25 | – | – |
| Bathy < -1000 (m) | 0.15 | 0.41 | -0.05 |
| Bathy > -1000 (m) | 110.4 | 167.6 | 83.22 |

Table 2: *J*ASON var(X_SSH_FES04)-var(X_SSH_GOT00V2)

| Bathy \ Lat | No selection | $\|Lat\| < 50$ | $\|Lat\| > 50$ |
|---|---|---|---|
| No selection | -1.64 | – | – |
| Bathy < -1000 (m) | -1.80 | 0.008 | -4.50 |
| Bathy > -1000 (m) | 4.83 | 55.50 | -12.15 |

Table 3: *E*NVISAT var(X_SSH_FES04)-var(X_SSH_GOT00V2)

| Bathy \ Lat | No selection | $\|Lat\| < 50$ | $\|Lat\| > 50$ |
|---|---|---|---|
| No selection | 1.09 | – | – |
| Bathy < -1000 (m) | -0.01 | 0.31 | -2.34 |
| Bathy > -1000 (m) | 13.79 | 36 | 5.82 |

Table 4: *G*FO var(X_SSH_FES04)-var(X_SSH_GOT00V2)

#### 8.1.2.4 Along track performances

Figures 80 and 81 show respectively the gain and the normalized gain along track between FES04 and GOT00 on the 3 satellites. The blue color means that FES04 has a lower variance of SLA than GOT00. The red color means that FES04 has a larger variance.
The results obtained along track are similar to those obtained at crossovers. Some oceanic signals are however observed on Envisat and GFO notably around the equator.

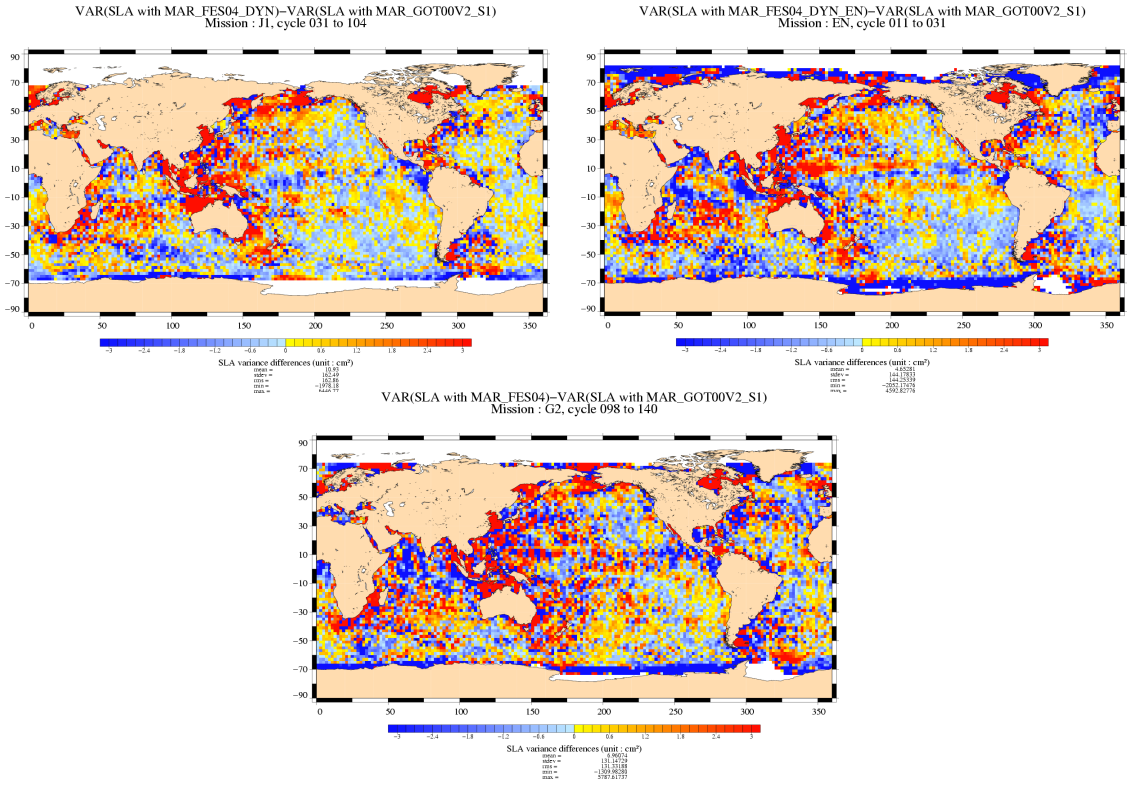


Figure 80: *Along track gain*

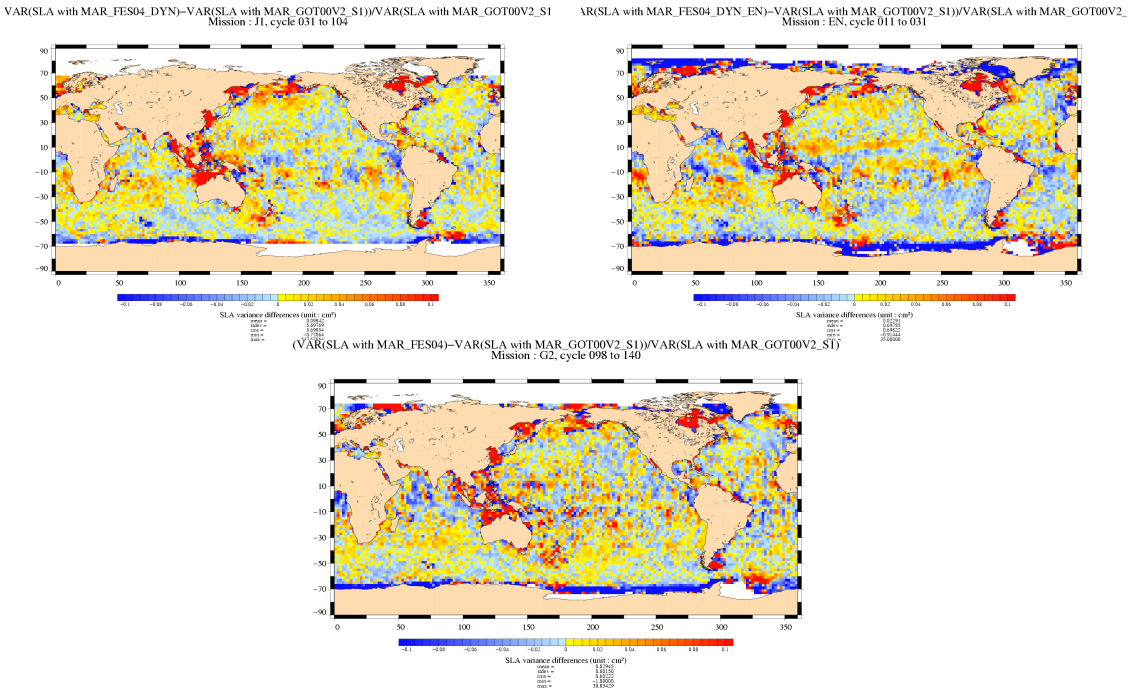


Figure 81: *Normalized gain at crossovers*

### 8.1.3 Comparison between FES2004, GOT99 and FES99

In this part, the FES04 model is compared to older models, GOT99 and FES99.
Note that FES04 and GOT00 include S1 and S2 atmospheric tide and dynamic long period tide.
FES04 is compared to GOT00 on Envisat (11-30) (a two-year period of data)

#### 8.1.3.1 SSH formulae

The parameters used to compute the sea surface height (SSH) for Envisat are:

- radiometer wet troposphere correction
- ECMWF dry troposphere correction (rectangular grids)
- dual frequency ionospheric correction
- non parametric SSB
- MOG2D
- pole tide correction
- earth tide correction
- oceanic tide correction

The FES04 tide correction contains:

- the S1 and S2 atmospheric tide
- the dynamic long period tide

The original FES02 tide correction contains:

- neither contains S1 nor S2 atmospheric tide
- contains the static long period tide

The original GOT99 tide correction contains:

- the S2 atmospheric tide
- the static long period tide

For this analysis, FES04 has been computed as following:

$$\begin{aligned} FES04 &= original\ FES04\ tide \\ &+ static\ long\ period\ tide \\ &- dynamic\ long\ period\ tide \end{aligned}$$

So FES04 is not fully consistent with FES02 and GOT99.

### 8.1.3.2 Along track differences

Figure 82 shows the mean differences FES04-FES02 and FES04-GOT99 on Envisat. The S2 signal is clearly visible on the first map. The FES04-GOT99 differences are very similar to the FES04-GOT00 differences.

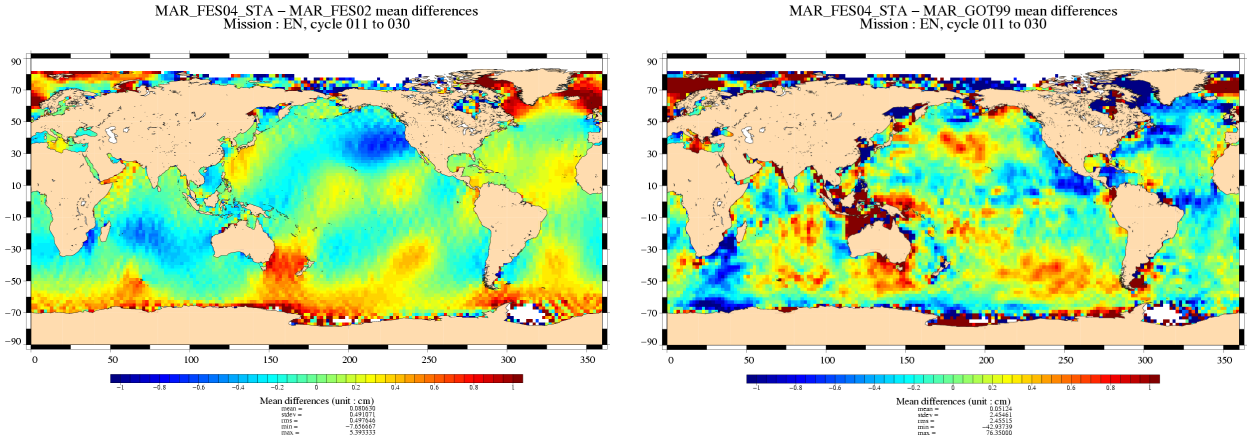


Figure 82: *Mean differences*

Figure 83 shows the variance of the differences FES04-FES02 and FES04-GOT99 on Envisat. As expected, the differences FES04 and FES02 are consistent. High differences are found on FES04-GOT99 in low bathymetry areas and at high latitudes.

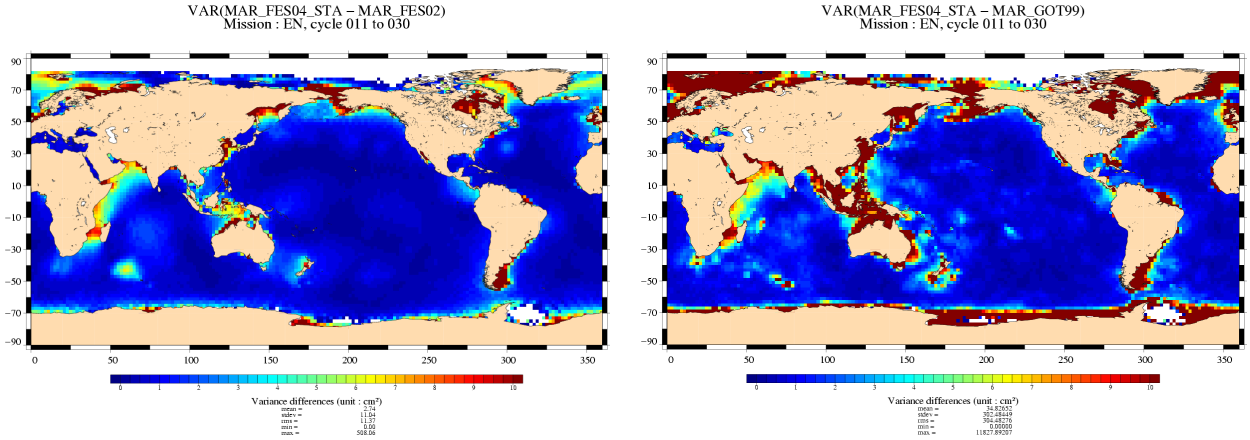


Figure 83: *Variance differences*

#### 8.1.3.3 Performance at crossovers

Figure 84 shows the gain at crossovers between FES04/FES99 FES04/GOT99 on Envisat. The blue color means that FES04 has a lower variance of SSH differences at crossover than FES99 or GOT99. FES04 has, in average, lower variance than FES99 and GOT99, especially in high latitude and low bathymetry areas. However, GOT99 has, locally, a lower variance: over Indonesia and in the Indian ocean for example.

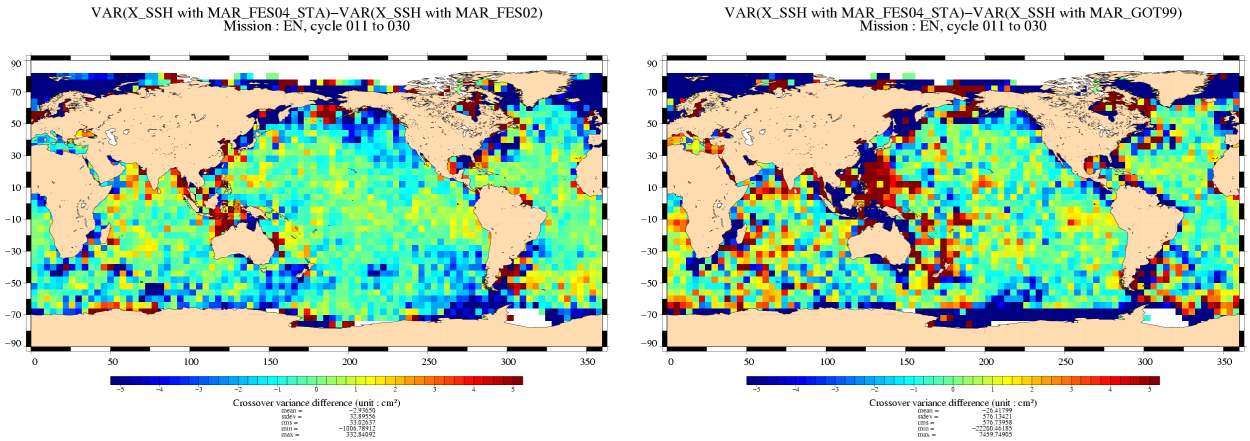


Figure 84: *Gain at crossovers*

#### 8.1.3.4 Along track performances

Figure 85 shows the gain along track between FES04 and GOT00 on the 3 satellites. The results obtained along track are similar to those obtained at crossovers. Some oceanic signals are however observed.

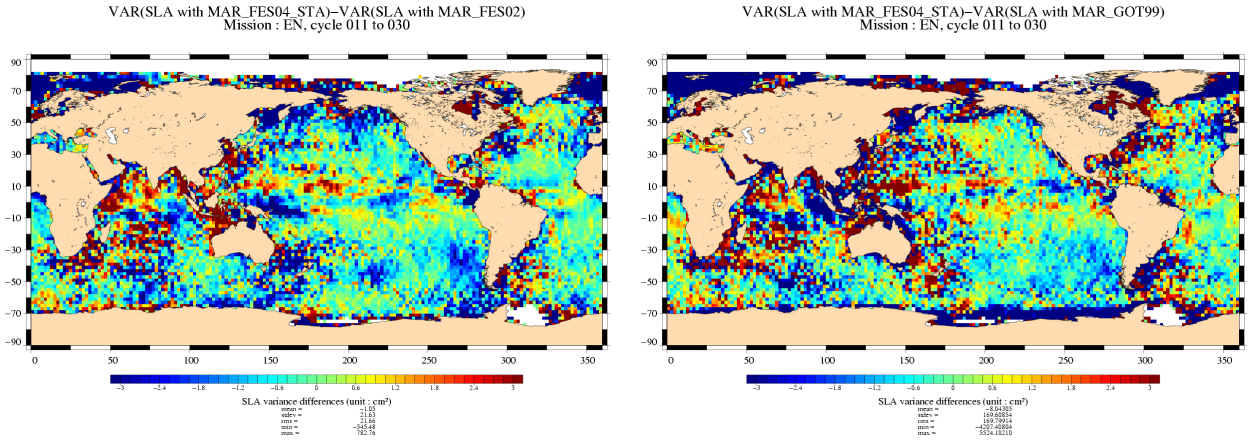


Figure 85: *Along track gain*

### 8.1.4 Impact of the dynamic long period tides

In this part, the impact of the new dynamic long period tide is analyzed on Envisat.
FES04 (dynamic) is compared to FES04 (static) on Jason-1 (1-101) (a three-year period of data)

#### 8.1.4.1 SSH formulae

The parameters used to compute the sea surface height (SSH) for Jason-1 are:

- radiometer wet troposphere correction
- ECMWF dry troposphere correction (rectangular grids)
- dual frequency ionospheric correction
- non parametric SSB
- MOG2D
- pole tide correction
- earth tide correction
- oceanic tide correction

#### 8.1.4.2 Along track differences

Figure 86 shows the mean difference Dynamic-Static long period tide. The differences are not very important, lower than 1cm.

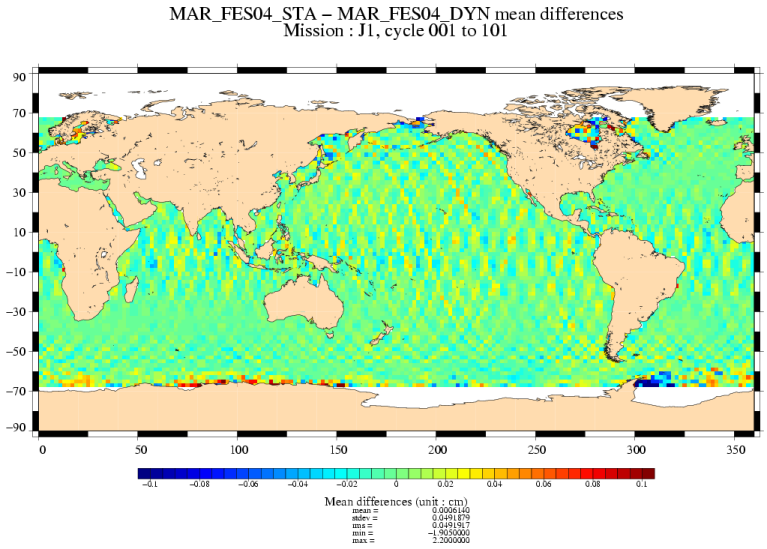


Figure 86: *Mean differences*

Figure 87 shows the variance of the difference Dynamic-Static long period tide.

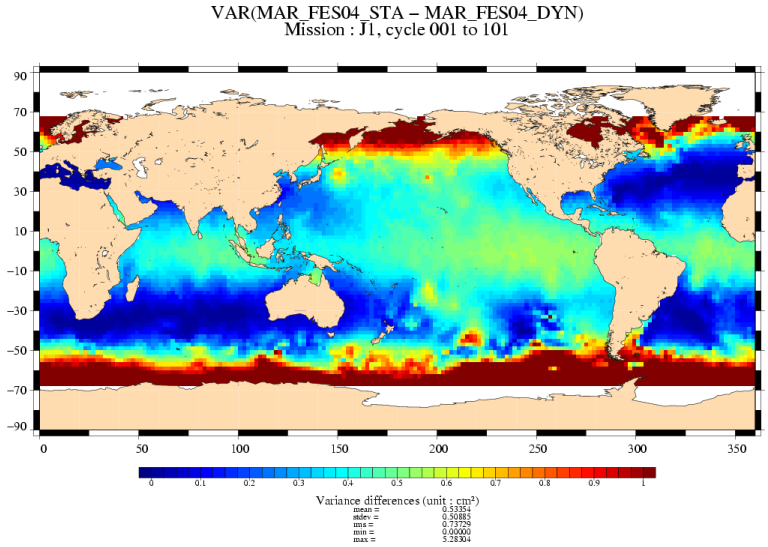


Figure 87: *Variance differences*

### 8.1.4.3 Performance at crossovers

Figure 88 shows the gain at crossovers between Static and dynamic. The red color means that the dynamic long period tide correction has a lower variance of SSH differences at crossover than the static long period tide correction. The differences are around 0 (-0.066 cm2). However, in the Pacific Ocean at mid latitude the dynamic long period tide has lower variance, and at latitude lower than 50˚S the static long period tide has lower variance.

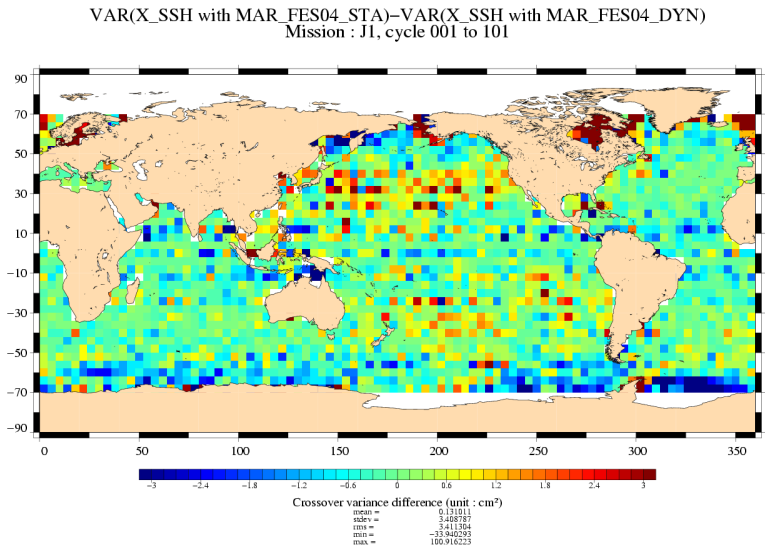


Figure 88: *Gain at crossovers*

#### 8.1.4.4 Along track performances

Figure 89 shows the gain along track between Static and dynamics. The results obtained along track are similar to those obtained at crossovers.

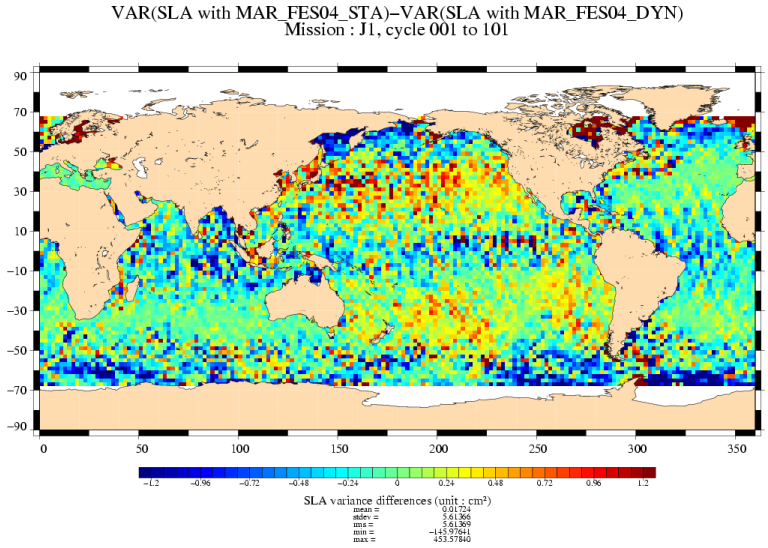


Figure 89: *Along track gain*

### 8.1.5 Conclusion

These 3 analyses allow us to choose a tide model for our products between FES04 and GOT00. In open ocean at mid and low latitudes the performances of the 2 models are very close. FES04 better performed at high latitudes which is strongly visible on Envisat and GFO, but less obvious on Jason-1. GOT00 is better in coastal areas thanks to the use of regional model.

FES04 assimilation technique is more physical than GOT00. GOT00 is strongly adjusted on altimetric data. So with equivalent performance, the best choice would be FES04. Moreover the dynamic long periods have been computed for FES04. However the fact that FES04 has, locally, lower performances than GOT00 is an argument leading to the choice of GOT00.

## 8.2 Impact of correction MOG2D versus only inverse barometer

As a first approximation, the so-called Inverse Barometer correction is conventionally used to correct altimeter data. This simple correction assumes a static ocean response to atmospheric pressure forcing. Neither dynamical effects at high frequency nor wind effects are taken into account in this correction.
In order to take account of dynamical effects and wind forcing, a new correction is computed from the MOG2D (Carrere and Lyard, 2003 [12]) barotropic model forced by pressure (without S1 and S2 constituents) and wind. Only the high frequency part of these model outputs are retained and combined to the low frequency inverse barometer.
A comparison between the 2 types of corrections was made for the Envisat period. The Figure 90 displays comparisons between the two types of correction. It shows that in comparison to the inverse barometer correction, the MOG2D correction reduces greatly the crossover variance and SLA variance in regions of high frequency variability (high latitudes and shallow water).

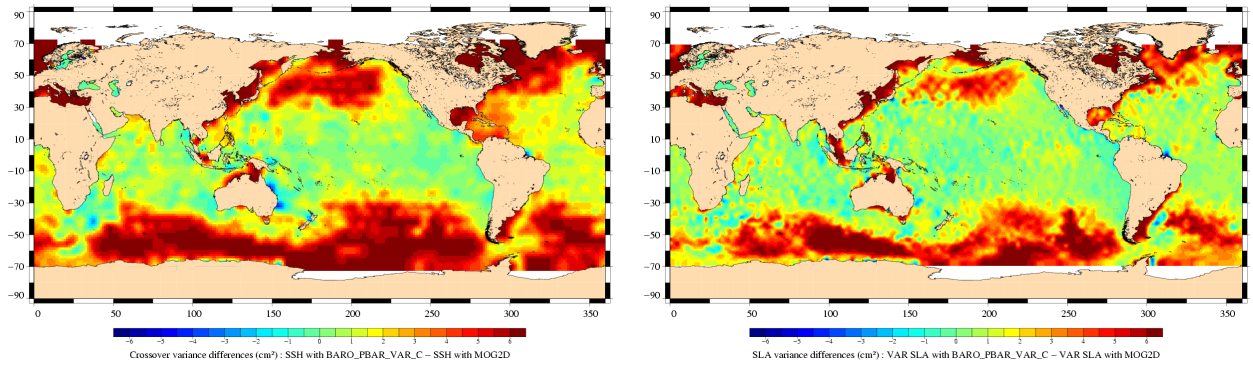


Figure 90: *Crossover variance difference (left) and SLA variance difference (right) when using correction MOG2D rather than inverse barometer correction*

## 8.3 Impact of new S1S2 wave model in dry troposphere

The S1 and S2 radiational tides are not well retrieved by ECMWF atmospheric fields (in particular because of poor temporal sampling). Following the QWG recommendation, the original S1 and S2 components are now filtered out from atmospheric and re-estimated using an S1/S2 model (Ponte and Ray, 2003 [46]) before computing the dry troposphere correction.
The figure 91 displays comparisons between the two dry tropospheric corrections for cycles 11to 361. The two corrections are very close.

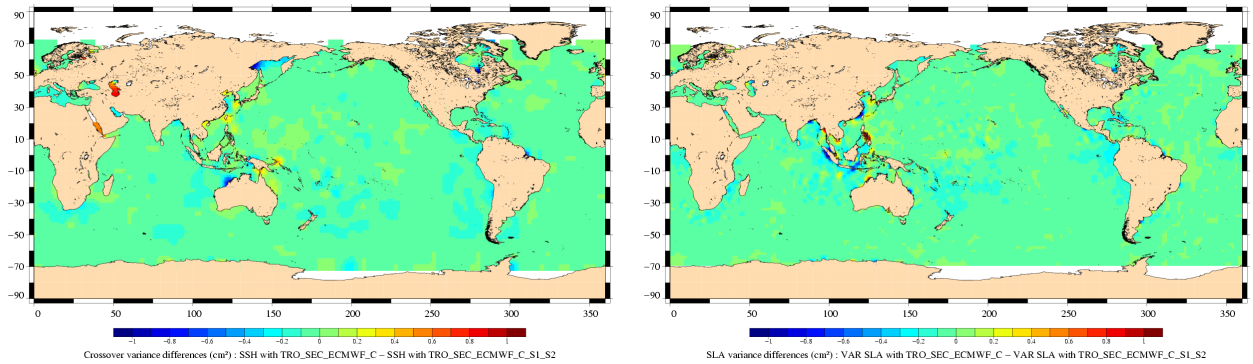


Figure 91: *Crossover variance difference (left) and SLA variance difference (right) when using dynamic S1S2 or only static S1S2 contributions for dry troposphere correction*

# 9 Conclusion

The TOPEX/Poseidon mission comes to an end after more than 13 years of loyal services. It is finished since 9th October 2005, following the loss of the pitch reaction wheel.

Originally planned as a 5 year mission it has become the longest earth-orbiting radar mission (see jointly NASA/CNES Press Release, 2006 [43]). During these 13 years, TOPEX/Poseidon data have contributed to :

- the first decade-long global descriptions of seasonal and yearly ocean current changes
- refine scientists' estimates of rising global sea level during the past decade
- provide a new understanding of the role tides play in mixing the deep ocean
- develop the most accurate ever global ocean tides' models
- provide the first global data set to test ocean general circulation model performance
- demonstrate global positioning system measurements in space could determine spacecraft positions with unprecedented accuracy, enabling rapid delivery of data

Since the beginning of the TOPEX/Poseidon mission, constant efforts have been made in all the TOPEX/ Poseidon system components to reach the major goals in terms of mesoscale study and SSH long term monitoring. Data quality and precision have been maintained thanks to instrumental survey, precise orbit determination, updated ground processing and careful data analysis. Calibration and validation activities, operated in line with the data production but also as a long term survey, represent a valuable contribution to the data quality maintenance and improvement.

The TOPEX/Poseidon mission thus provides an unprecedented long altimeter measurement series, allowing long term mean sea level trends determination and climate change studies. Continuity in data quality and precision is mandatory to achieve these goals.

During more than 13 years, continuous data quality assessment has proven to be essential to detect potential system errors or drifts and to maintain the TOPEX/Poseidon usefulness for oceanography. Now it also allows linking TOPEX/Poseidon measurements to the Jason-1 mission and this way to ensure the continuity of precise altimetry. The cross-calibration exercise has been performed during the Jason-1 verification phase. From that, is has been decided to move the TOPEX/Poseidon ground track westward at one half the nominal track intervals. This highly improved ocean sampling opens a new area of precise altimeter measurements, with large expected improvements for instance, in ocean studies, tide modeling, or coastal applications.

# References

[1] Ablain, M. and F. Mertz, TOPEX/Poseidon validation activities, 12 years of T/P data (GDR-Ms), March 2005.

[2] AVISO User Handbook. Merged Topex/Poseidon Products (GDR-Ms), AVINT-02-101-CN.

[3] AVISO/CALVAL. Validation du cycle 267. CLS.OC/NT/98.60. Version 267, 14 Janvier 2000.

[4] Berthias, J.P., Transition to ITRF2000, internet communication, 16 May 2001.

[5] Blusson, A, personal communication, March 2002.

[6] Callahan, P.S., New TOPEX Science Processing, internet communication to topex-poseidon@omnet.com, 2 September 1998.

[7] Callahan, P.S., Revised GDRs coming, internet communication to topexposeidon@omnet.com, 19 January 2000.

[8] Callahan, P.S., Change in Sigma0 and Reprocessing Cycles 277-284, internet communication to topex-poseidon@omnet.com, 3 August 2000.

[9] Callahan, P.S., Cycle 193 (Day 349) data, internet communication to topexposeidon@omnet.com. 20 January 1998.

[10] Callahan, P.S., TOPEX clock rollover, Internet communication to TOPEX/Poseidon@omnet.com, 29 April 2001.

[11] Callahan, P.S., TOPEX AGC/Sigma0 Errors, Internet communication to ostst@list.jpl.nasa.gov, 23 September 2005.

[12] Carrère, L., and F. Lyard, Modeling the barotropic response of the global ocean to atmospheric wind and pressure forcing - comparisons with observations. *Geophys. Res. Lett.*, **30(6), 1275, doi:10.1029/2002GL016473**, 2003.

[13] Chelton, D.B.. The Sea State Bias in altimeter estimates of sea level from collinear analysis of TOPEX data. *J. Geophys. Res.*, **99, 24995-25008**, 1994.

[14] Dorandeu, J., Impact sur le niveau moyen des mers d'un "biais en z" appliqué sur l'orbite. AVISO/CALVAL report. CLS.DOS/NT/98.89, 1998.

[15] Dorandeu, J., P.Y Le Traon, M.H. Calvez, P. Gaspar, F. Ogor. Validating TOPEX/Poseidon Data, AVISO/CALVAL yearly report. CLS/DOS/NT/97.042/2, 1997.

[16] Dorandeu, J., AVISO, "Side-B TOPEX Altimeter evaluation", AVI-NT011-317-CN, Edition 1.0, 1999.

[17] Dorandeu, J., M-H De Launay, F. Mertz and J. Stum, AVISO/CALVAL yearly report, 8 years of TOPEX/Poseidon data (M-GDRs), February 2001.

[18] Dorandeu, J., F. Mertz and J. Stum. Note on ERS-2 Sigma0 Variations since January 2000. CLS.DOS/NT/00.286, 2000.

[19] Dorandeu, J., and P-Y. Le Traon, Effects of Global Mean Atmospheric Pressure variations on Mean Sea Level Changes from TOPEX/Poseidon, *J. Atmos. Oceanic technology*, **1279-1283**, 1999.

[20] CERSAT Altimeter & Microwave Radiometer ERS Products User Manual. C2MUT-A-01-1F, version 2.2, 1996.

[21] Y.Faugere, J.Dorandeu, F.Lefevre, N.Picot and P.Femenias, 2005: Envisat ocean altimetry performance assessment and cross-calibration. Submitted in the special issue of SENSOR 'Satellite Altimetry: New Sensors and New Applications'

[22] Gaspar, P., F. Ogor, P-Y. Le Traon and O-Z. Zanife, Estimating the Sea State Bias of the TOPEX and POSEIDON altimeters from crossover differences, *J. Geophys. Res.*, **99, C12, 24981-24994**, 1994.

[23] Gaspar, P., S. Labroue and F. Ogor. Improving nonparametric estimates of the sea state bias in radar altimeter measurements of sea level, *J. Atmos. Oceanic Technology*, **19, 1690-1707**, October 2002.

[24] Hancock, D.W., Alt-B bad measurements, Internet communication to TOPEX Side-B CAL/VAL group, 19 August 1999.

[25] Hancock, D.W., Alt-B bad measurements, Internet personal communication, 23 August 1999.

[26] Hancock, D.W., TOPEX Altimeter Performance 1997 Day 349 during ASTRA Outage, internet communication cited in [9], 20 January 1998.

[27] Hayne, G.S., and D.W. Hancock III, Observations from Long-Term Performance Monitoring of the TOPEX Radar Altimeter. TOPEX/Poseidon/Jason-1 Science Working Team Meeting, Keystone, Colorado, 1998.

[28] Hayne, G.S. and D.W. Hancock III, TOPEX Side B Calibration Table Adjustments, 7 November 2000.

[29] Hayne, G.S. and D.W. Hancock III, Observations from long-term Performance Monitoring of the TOPEX Radar Altimeter, TOPEX/Poseidon/Jason-1 Science Working Team Meeting, Keystone, Colorado, 1998.

[30] Hayne, G. S. and D.W. Hancock III, The TOPEX Sigma0 Calibration Table and its Updates, 14 March 1997.

[31] Hayne, G. S. and D.W. Hancock III, TOPEX Sigma0 Calibration Table History for all Side A Data, 27 July 1999. Available on the internet at http://topex.wff.nasa.gov/Sigma0Cal_A_All.pdf

[32] Hayne, G. S. and D.W. Hancock III, TOPEX Side B Calibration Table Adjustments : March 2002 Update, 08 March 2002. Available on internet at http://topex.wff.nasa.gov/mar_02_update_sig0_cal_tbl.pdf

[33] Hayne, G.S., TOPEX Side-B Sigma0, etc, personal communication, 15 June 2000.

[34] Keihm, S.J., V. Zlotniki and C.S. Ruf, TOPEX Microwave Radiometer Performance Evaluation, 1992-1998. *IEEE Trans. Geosci. Remote Sensing*, **Vol. 38, pp. 1396-1386**, May 2000.

[35] Labroue S., P. Gaspar and J. Dorandeu, Qualification des corrections ionosphériques et du biais électromagnétique pendant la phase tandem TP/JASON, Contrat SALP n°731/CNES/00/8435/00 - CLS Lot 2, 2002.

[36] Le Traon, P.-Y., J. Stum, J. Dorandeu, P. Gaspar and P. Vincent. Global statistical analysis of TOPEX and POSEIDON data. *J.Geophys. Res.*, **99 : 24619-24631**, 1994.

[37] Le Traon, P.-Y., P. Gaspar, J. Dorandeu, F. Ogor. Amélioration des performances des altimètres TOPEX/POSEIDON et ERS. Contrat 856/CNES/95/1523/01, 1996.

[38] Martini A., 2003: Envisat RA-2 Range instrumental correction : USO clock period variation and associated auxiliary file, Technical Note ENVI-GSEG-EOPG-TN-03-0009 Available at http://earth.esa.int/pcs/envisat/ra2/articles/USO_clock_corr_aux_file.pdfhttp://earth.esa.int/pcs/envisat/ra2/auxdata/

[39] Mertz, F., J. Dorandeu and J. Stum, Long term monitoring of the OPR altimeter data quality. Report of IFREMER contract n°01/2.210 374, January 2002.

[40] Mertz, F., N. Tran, S. Labroue, J. Dorandeu, V. Marrieu, J. Savaresse, ERS2 OPR data quality assessment (Long-term monitoring and particular investigations), Annual report 2004 of task 2 of IFREMER Contract No 04/2.210.714., CLS.DOS/NT/04.277, January 2005.

[41] Mertz F., J. Dorandeu, J. Stum, Validation and long-term monitoring of reprocessed (version 6) phase C ERS-1 OPR data. CLS.DOS/NT/02.539, March 2002.

[42] Morel, L., C. Boucher, P. Willis, J.P. Berthias. Terrestrial Reference Frame Differences for TOPEX POSEIDON, SWT Jason, Keystone, USA, 1998.

[43] NASA/CNES Press Release. NASA's TOPEX/Poseidon Oceanography Mission Ends. Release 05-478, 5th January 2006.

[44] Obligis, E., L. Eymard and N. Tran, ERS2/MWR drift evaluation and correction, CLS.DOS/NT/03.688, 2003.

[45] Ray, R.D., A global ocean tide model from Topex/poseidon altimetry. *NASA Tech Memo*, **55pp.**, 1999.

[46] Ray, R.D. and R.M. Ponte, Barometric tides from ECMWF operational analyses. *Annales G*, **99, 24995-25008**, 1994.

[47] Queuffeulou P., P. Long-term comparison of ERS, TOPEX and Poseidon altimeter wind and wave measurements, 1998.

[48] Ruf, C.S., 2002. TMR Drift Correction to 18 GHz Brightness Temperatures, Revisited. Report to TOPEX Project, June 2002.

[49] Ruf, C.S. Detection of calibration drifts in spaceborne microwave radiometers using a vicarious cold reference. *IEEE Trans. Geosci. Remote Sensing*, **vol 38, pp 44-52**, Jan 2000.

[50] Stum, J., A comparison of brightness temperatures and water vapor path delays measured by the TOPEX, ERS-1 and ERS-2 microwave radiometers, *J. Atmos. Oceanic Technology*, **Vol 15, 987-994**, 1998.

[51] Scharroo R., J. L. Lillibridge, and W. H. F. Smith, Cross-Calibration and Long-term Monitoring of the Microwave Radiometers of ERS, TOPEX, GFO, Jason-1, and Envisat, **Marine Geodesy, 27:279-297**, 2004.

[52] TOPEX/POSEIDON daily status, internet communication for cycle 285, 12 Juny 2000.

[53] TOPEX/POSEIDON daily status, internet communication for cycle 304, 14 December 2000.

[54] TOPEX/POSEIDON daily status, internet communication for cycle 324, 2 July 2001.

[55] TOPEX/POSEIDON daily status, internet communication for cycle 332, 24 September 2001.

[56] TOPEX/POSEIDON MGDR Quality Assessment Report, Cycle 475, October 2005.

[57] TOPEX/POSEIDON MGDR Quality Assessment Report, Cycle 476, October 2005.